Radiation from particles in crystal undulators with allowance for a polarization of the medium

R. O. Avakyan, L. A. Gevorgyan, K. A. Ispiryan,[a)] and R. K. Ispiryan
Erevan Physics Institute, 375036 Erevan, Armenia

(Submitted 20 August 1998)
Pis'ma Zh. Éksp. Teor. Fiz. **68**, No. 6, 437–441 (25 September 1998)

The radiation from relativistic particles channeled in a microscopic undulator created by applying transverse ultrasonic vibrations to a single crystal is investigated. The results of numerical investigations are presented for real crystal undulators. The calculations show the radiation spectra in the particle and photon energy ranges where narrowing of the spectrum occurs when the particle energy is close to a definite threshold energy. © *1998 American Institute of Physics.* [S0021-3640(98)00118-2]

PACS numbers: 61.85.+p, 43.35.Ty

Papers on undulator radiation[1–4] have predicted that at certain particle energies the influence of the medium will lead to narrowing of the radiation spectrum in the x-ray and harder frequency ranges. It was shown[3,4] that by varying the parameters of the medium or the undulator it is possible to obtain quasi-monochromatic beams of photons with energies $\hbar\omega \simeq 10-200$ keV using electrons with energies $E=3-15$ GeV. A similar phenomenon has been predicted[5–7] for radiation from channeled particles. It has been shown[7] that spectrum narrowing will be appreciable for $E \leqslant 10$ MeV and $\hbar\omega \leqslant 1$ keV, making the effect difficult to observe. Despite the fact that the experimental investigations of the radiation from particles in undulators filled with a medium (see, for example, Ref. 8) as well as during channeling in single crystals were initiated a long time ago, to date the predicted narrowing of the spectrum has still not been observed.

For obtaining intense x- and γ-ray beams, the radiation from particles in crystal undulators (CUs) with the shortest possible periods $l=v/f=0.1-100$ μm, obtained using transverse ultrasonuc waves with frequency f and propagation velocity v in the crystal, has been studied in the dipole approximation.[9] The advantage of the radiation produced in CUs as compared with the radiation produced in ordinary undulators is that decreasing the period by several orders of magnitude makes it possible, at a given energy, to obtain photons with higher energies $\hbar\omega$ and, as compared with radiation from channeled particles, higher intensities because in CUs the vibrational amplitude A is much larger than the interplanar spacing d_p of the CU crystal. Such radiation was recently studied[10] in the dipole approximation, and it was shown that stimulated emission can be obtained. We note that the theoretical possibility of increasing the intensity of radiation from channeled particles by using ultrasound has been examined in Refs. 11–18. References 14–18 examine the case where the values of l are close to the period l_{ch} of the

particle motion during channeling. Only amplification of parametric x radiation by means of ultrasound has been observed to date.[19]

Since interest in methods for obtaining intense x-ray beams using electrons[b)] with $E>5$ MeV has increased recently and since the polarization of the medium was neglected in Refs. 9 and 10, in the present letter we investigate the radiation produced in a CU taking the narrowing of the spectrum into account. It is shown for CUs based on certain single crystals that the use of particles with energies $E=500-1000$ MeV will make it possible to obtain quasi-monochromatic beams and to investigate experimentally the narrowing at $\hbar\omega\approx 10-100$ keV.

Let a particle moving along the Z axis enter a CU whose crystallographic planes, perturbed by a transverse ultrasonic wave propagating along the Z axis, have a sinusoidal form with amplitude A and period l. If the angle of entry of a particle into the crystal relative to the bent crystallographic planes is less than the corresponding critical angles for channeling, and if the minimum radius of curvature $R_{\min}=l^2/4\pi^2A$ of an averaged particle trajectory or of the crystallographic planes is greater than the Tsyganov critical radius R_{Ts} (see, for example, Ref. 20), then, in neglect of multiple scattering, a positive particle will on average execute during planar channeling a vibrational motion with amplitude A and frequency $\Omega=2\pi c/l$. We note that the consequences of the above-noted condition $R_{\min}>R_{\mathrm{Ts}}$ for positive particles were studied in Ref. 10. In the present letter, besides $A\gg d_p$ and $l\gg l_{\mathrm{ch}}$, it is assumed that the transit time of an ultrarelativistic particle through the CU is much shorter than the period of the ultrasonic wave. We investigate the narrowing of the spectrum in the frequency range in which the first harmonic of the radiation is dominant..

It is well known that when the undulator parameter $q=2\pi\gamma A/l\geqslant 1$, and the longitudinal oscillations cannot be neglected, the longitudinal particle motion can be characterized by an effective Lorentz factor $\gamma_z=\gamma/\sqrt{1+q^2/2}$. Using the results of Refs. 1–4 it is easy to show that because of the presence of the medium, radiation arises in the CU only when the particle energy $E=\gamma mc^2$ exceeds a threshold energy $E_n=\gamma_n mc^2$,

$$\gamma_n=\gamma_0/\sqrt{1-\eta^2}, \tag{1}$$

where $\gamma_0=\omega_p/\Omega$, $\eta=\sqrt{2}\pi A/\lambda_p$, $\lambda_p=2\pi c/\omega_p$, and ω_p is the plasma frequency of the CU. It follows from Eq. (1) that $\eta<1$ and $A<\lambda_p/\sqrt{2}\pi$. Setting $\gamma=k\gamma_n$ $(k\geqslant 1)$, we obtain $\gamma_z=\gamma(1-\eta^2)^{1/2}/(1+\eta^2(k^2-1))^{1/2}$.

The physics of this phenomenon is as follows. In the laboratory frame a particle undergoes translational–vibrational motion with frequency Ω. In a reference frame moving with the particle we have an oscillating dipole at rest which emits a wave with frequency $\Omega\gamma_z$. Since the plasma frequency $\omega_p=\sqrt{2\pi ne^2/m}$ remains unchanged in the latter frame, the plasma has the property that waves with frequency $\Omega\gamma_z<\omega_p$ do not propagate and that particles with $\gamma<\gamma_n$ (or $\gamma_z<\gamma_0$) do not radiate.

The frequency and angle of emission θ of the radiation are related by

$$\omega=2\Omega\Big/\left(\gamma_z^{-2}+\frac{\omega_p^2}{\omega^2}+\theta^2\right). \tag{2}$$

Hence it follows for a vacuum undulator $(\omega_p=0)$ that photons all with the same frequency, lying in the interval $0\leqslant\omega\leqslant 2\omega_c$, where $\omega_c=\Omega\gamma_z^2$, can be emitted at each angle

TABLE I.

	Parameters						
Crystals	ρ (g/cm^3)	v (km/s)	$\hbar\omega_p$ (eV)	E_n (MeV)	l (μm)	f (MHz)	$k\eta$
Quartz	2.65	5.7	33.1	523	37.7	151	0.23
Silicon	2.33	8.43	31.1	556	42.9	196	0.22
Diamond	3.5	11.65	38.8	451	27.5	421	0.27

θ. For an undulator filled with a medium ($\omega_p \neq 0$), photons with two different values of ω in the range $(1-\delta)\omega_c \leqslant \omega \leqslant (1+\delta)\omega_c$ can be emitted at each angle θ (compound Doppler effect), where $\delta^2 = 1 - \gamma_0^2/\gamma_z^2 = (k^2-1)(1+\eta^2)/k^2$. Using δ and the dimensionless frequency $x = \omega/\omega_c$ $(1-\delta \leqslant x \leqslant 1+\delta)$, we can rewrite expression (2) in the form

$$\theta = (\delta^2 - (x-1)^2)^{1/2}/\gamma x. \tag{3}$$

Therefore photons with the maximum and minimum frequencies are emitted at angles $\theta = 0$, while photons with $x = 1$ are emitted at the angle $\theta = \delta/\gamma_z$. Thus, the frequency and angular distributions become narrower by a factor of δ around $x = 1$ or $\omega = \omega_c$.

The spectral distribution of the number of photons per unit particle travel distance is given by the expression

$$\frac{d^2N}{dxdz} = B\left[\left(x + \frac{1-\delta^2}{x} - 1\right)^2 + 1\right], \tag{4}$$

where $B = \pi\alpha\eta^2/2l(1-\delta^2)$ and $\alpha = 1/137$. The width of the spectral distribution, with allowance for the finiteness of the length L and the spread $\Delta l/l$ in the values of the undulator period, is determined by the expression

$$\frac{\Delta\omega}{\omega} = \frac{l}{L} + \left[2\left(\frac{\Delta\gamma}{\gamma} + \frac{\Delta l}{l}\right)\right]^{1/2}, \tag{5}$$

where $\Delta\gamma = \gamma - \gamma_0$ if $\gamma_z > \gamma_0$ and $\Delta\gamma$ equals the width of the spread in γ if $\gamma_z = \gamma_0$.

Integrating (2) over the admissible range, we obtain in the case $\delta \ll 1$ the following expression for the number of photons emitted in a CU of length L:

$$N = 2\pi\alpha \frac{\eta^2 k^2}{1 + (k^2-1)\eta^2} \frac{L}{l} \delta. \tag{6}$$

In the dipole approximation, $k\eta < 1$, the contribution of the high harmonics is small, while $N \sim A^2$. However, N stops increasing with A when $k\eta \geqslant 1$.

Table I gives the values of the density, the sound velocity, and the plasma frequency of some crystals which are convenient for preparing CUs (quartz, silicon, and diamond) as well as the values of E_n, l, f, and $k\eta$ that are required in order to obtain quasimonochromatic photon beams with $\omega = \omega_c = 33$ keV and $A = 2$ nm. We note that channeling radiation has been observed in piezoelectric quartz,[21] and diamond and silicon are the best radiators for obtaining radiation from channeled particles. As one can see from the table, in all cases $k\eta < 1$, because the value of A is moderate. Since $E_n \sim \omega_c$, $l \sim \omega_c$, and $f \sim 1/\omega_c$, it is unreasonable to employ the crystals listed in the table at

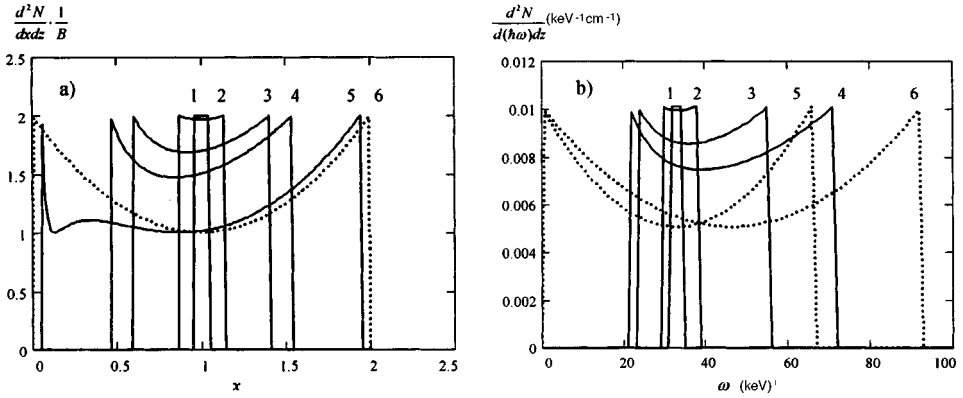

FIG. 1. Spectral distribution of the radiation from particles channeled in a quartz CU with period $l=27.7$ μm and amplitude $A=20$ nm, with (solid curves) and without (dotted curves) allowance for a polarization of the medium: a) $d^2N/dx/dz/B$ versus x at energies 1.001, 1.01, 1.1, 1.2, and 4.0 times higher than the energies $E_n=523.1$ MeV (curves *1–5*, respectively) and at any relativistic energy (curve *6*); b) $d^2N/d(\hbar\omega)/dz$ (keV^{-1} cm^{-1}) versus $\hbar\omega$ (keV) for energies $E=523.6$, 528.3, 575.4, and 627.7 MeV (curves *1–4*) and for energies $E=523.6$ and 627.7 MeV (curves *5* and *6*).

$\omega_c \leqslant 10$ keV and $\omega_c \geqslant 10$ MeV, since in the first case very high values of f are required, with the attendant difficulties in obtaining high ultrasonic powers, while in the second case the very large values of l will lead to a small number of periods in a CU of limited length.

As an illustration, Fig. 1 shows $(d^2N/dx)/(dz/B)$ versus x for a quartz CU with the parameters presented in Table I for different values of the particle energy (solid curves). For comparison, the same dependence (identical for all values of the energies) is shown for a hypothetical vacuum ($\omega_p=0$ or $\delta=1$) undulator with the same values of l and A (dashed curve). One can see that the quasi-monochromaticity deteriorates as the energy increases and that at high frequencies the vacuum undulator and CU spectra increasingly resemble each other. Figure 1b shows the directly measured curves of $d^2N/d(\hbar\omega)/dz$ versus $\hbar\omega$ for CU and vacuum undulators. We note that at $x=1$ or $\omega=\omega_c=\Omega\gamma_z^2$ the height of the CU spectra is twice that of the spectra in the same microundulators with $\omega_p=0$. When the existing macroundulators with $l_{\text{macro}}\sim 1$ cm are used, one can obtain emission spectra in the frequency range of Fig. 1b at particle energies $\sqrt{l_{\text{macro}}/l}\sim 60$ times higher than the energy in Fig. 1b, since for undulators $\omega\sim\gamma^2/l$.

When comparing the possible applications of the radiation studied here and other types of radiation the following must be taken into account: i) Since deflection of electrons in bent crystals is not observed,[20] channeled electrons do not undulate in a CU and are unsuitable for obtaining radiation in a CU; ii) suitable positrons undergo multiple scattering, as a result of which it is not sensible to use CUs thicker than the dechanneling length, which is smaller in bent crystals than in unbent crystals; and, iii) there are difficulties in obtaining intense ultrasonic oscillations with frequencies greater than 100 MHz. Despite these drawbacks, by using positrons with $E\simeq 525$ MeV and a quartz CU with $L\simeq 1$ mm (with allowance for dechanneling) it is possible to obtain (see Fig. 1b) $N\sim 3\times 10^{-3}$ photons per electron for $\hbar\omega_c\simeq 33$ keV, $\Delta\omega/\omega\simeq 0.1$, which are two orders and one order of magnitude greater than that obtainable with parametric x radiation (PXR)

and transition x radiation (TXR) from electrons with $E \simeq 500$. Such an intensity can be obtained by using channeled-particle radiation (CPR) with particle energy $E \simeq 50$ MeV, since $l_{ch} \ll l$. However, it should be kept in mind that by increasing the positron energy slightly to $E = 650$ MeV it is possible to obtain a beam (see Fig. 1b) whose width is much greater than the width in the case of PXR, TXR, and CPR. This will make it possible to obtain at the same time several quasi-monochromatic photon beams with $\hbar\omega \sim 5-100$ keV, just as in the case of ordinary wigglers and undulators with much higher electron energies $E \geqslant 10$ GeV.

In conclusion, there is no doubt that it is of great scientific interest to investigate the radiation produced in CUs by particles with relatively high ($E > 1$ GeV) and low ($E < 1$ GeV) energies, where narrowing of the spectrum does not and does occur, respectively. The practical value of this radiation for obtaining intense quasi-monochromatic x-ray and hard-photon beams with a wide spectrum must still be proved experimentally despite the estimates presented above and other more optimistic estimates.[9,10] Nonetheless, we note that the investigated narrowing of the spectral and angular distributions of the radiation may be important for the generation of stimulated emission,[10] as has been shown for gas-filled free-electron lasers.[22]

[a)]e-mail: ispirian@vx1.yerphi.am

[b)]See *Proceedings of the Symposium on the Radiation from Electrons in Periodic Media, RREPS-97*, Tomsk, 1997, to be published in Nucl. Inst. Methods (1998), as well as the proceedings of the conferences in Holzau and Tabarze, Germany, 1998.

[1] L. A. Gevorgyan and N. A. Korkhmazyan, Preprint EFI-272(66)-77, Erevan Physics Institute, Erevan (1977).
[2] L. A. Gevorgian and N. A. Korkhmazian, Phys. Lett. A **74**, 453 (1979).
[3] L. A. Gevorgyan and N. A. Korkhmazyan, Zh. Éksp. Teor. Fiz. **76**, 1226 (1979) [Sov. Phys. JETP **49**, 622 (1979)].
[4] L. A. Gevorgyan and P. M. Pogosyan, Izv. Akad. Nauk Arm. SSR, Fiz. **19**, 239 (1984).
[5] V. A. Bazylev and N. K. Zhevago, Preprint IAÉ-2865, I. V. Kurchatov Institute of Atomic Energy, Moscow (1977).
[6] V. A. Bazilev and N. K. Zhevago, Phys. Lett. B **84**, 182 (1979).
[7] V. A. Bazylev and N. K. Zhevago, Usp. Fiz. Nauk **137**, 606 (1982) [Sov. Phys. Usp. **25**, 565 (1982)].
[8] R. H. Pantel *et al.*, Nucl. Instrum. Methods Phys. Res. A **250**, 312 (1986).
[9] V. V. Kaplin, S. V. Plotnikov, and S. A. Vorob'ev, Zh. Tekh. Fiz. **50** (5), 1079 (1980) [Sov. Phys. Tech. Phys. **25**, 650 (1980)].
[10] A. V. Korol, A. V. Solovyov, and W. Greiner, J. Phys. G: Nucl. Part. Phys. **24**, L45 (1998).
[11] V. V. Kaplin *et al.*, *Abstracts of the 10th Conference on the Application of Charged-Particle Beams for Studying the Composition and Properties of Materials*, Moscow State University, 1979, p. 28.
[12] V. G. Barishevsky *et al.*, Phys. Lett. A **77**, 61 (1980).
[13] H. Ikezi *et al.*, Phys. Rev. B **30**, 1567 (1984).
[14] A. R. Mkrtchian *et al.*, Phys. Lett. A **115**, 410 (1986).
[15] A. R. Mkrtchyan *et al.*, Zh. Éksp. Teor. Fiz. **93**, 432 (1987) [Sov. Phys. JETP **66**, 248 (1987)].
[16] A. R. Mkrtchian *et al.*, Phys. Lett. A **126**, 528 (1988).
[17] A. Ts. Amatuni and S. S. Elbakyan, Zh. Éksp. Teor. Fiz. **94**, 297 (1988) [Sov. Phys. JETP **67**, 1903 (1988)].
[18] A. R. Avakian and C. Yang, Radiation Effects Express **2**, 195 (1989).
[19] A. R. Mkrtchian *et al.*, Phys. Lett. A **152**, 297 (1991).
[20] R. A. Carrigan Jr., in *Relativistic Channeling*,edited by R. A. Carrigan and J. A. Ellison, Plenum, New York, 1987, p. 339.
[21] R. O. Avakian *et al.*, Nucl. Instrum. Methods Phys. Res. B **48**, 266 (1990).
[22] L. Gevorgian, *Abstracts of the 17th International Free Electron Laser Conference*, August 21–25, 1995, New York.

Translated by M. E. Alferieff

Theory of sonoluminescence in single bubbles: flexoelectric energy contribution

N. García

Laboratorio de Física de Sistemas Pequeños y Nanotecnología, CSIC, 28006 Madrid, Spain

A. Hasmy

Laboratorio de Física de Sistemas Pequeños y Nanotecnología, CSIC, 28006 Madrid, Spain; Laboratorio de Física Estadística de Sistemas Desordenados, Centro de Física, IVIC, Apartado 21827, Caracas 1020A, Venezuela

(Submitted 10 August, 1998)
Pis'ma Zh. Éksp. Teor. Fiz. **68**, No. 6, 442–448 (25 September 1998)

An equation of motion for a cavitating gas bubble immersed in a liquid is introduced which includes a flexoelectric energy term. This energy is deduced from the electric field produced by the bubble wall acceleration (pressure gradient) in the fluid (the flexoelectric effect). We show that under conditions of sonoluminescence, this electric field reaches values typical of the electric breakdown field in water. Our theoretical results are consistent with the duration of light emission, minimum bubble radius, and energy release as measured in sonoluminescence experiments in water. © *1998 American Institute of Physics.* [S0021-3640(98)00218-7]

PACS numbers: 78.60.Mq

A short and intense flash of light is emitted when ultrasound-driven air (or other gas) bubbles immersed in a liquid collapse. This phenomenon, discovered 60 years ago,[1] is called *sonoluminescence* (SL). Renewed interest now exists because a crucial experiment[2] showed repetitive emissions from a single, stable cavitating gas bubble in water. Usually, SL experiments address a range of parameter values where the emission is stable, since it has been shown[3] that the existence of SL and its stability depend on the region of parameter space. Various interesting measurements have been reported in the literature, namely, the evolution of the bubble radius R,[2–5] the spectrum of the emitted light,[6] and the effect of noble gas doping in a single bubble.[7,8] Measurements indicate that the energy released amounts to $\sim 10^{-12}$ J (Ref. 6) and that the duration of light emission ranges from 40 ps to over 350 ps.[8]

From the theoretical point of view, the pioneering work for the equation of motion of a cavitating bubble is due to Rayleigh.[9] Subsequently the Rayleigh equation has been generalized by taking into account the compressibility, surface tension, and viscosity of the fluid. Additionally, an acoustic pressure term has been added to describe bubble cavitation experiments under the action of this acoustic field. All these considerations lead to the Rayleigh–Plesset (RP) equation.[10] Even though this equation has been used

with success to describe the evolution of the radius of a cavitating bubble, it fails when one tries to reproduce in detail the evolution of the radius of SL experiments in the region where light emission occurs (i.e., near the bubble collapse); neither the SL phenomenon nor the light emission mechanism is explained by this theory. Recently, García and Levanyuk[11] proposed a new hypothesis which takes into account the fact that in SL experiments high pressure gradients produce high electric fields due to the flexoelectric effect.[12] This effect has been invoked previously to explain the polarization of water by shock waves.[13] The estimated time of the shock action is 1 ps, while the relaxation time of the water polarization at 25 °C is 9 ps,[14] and the mechanism of polarization in the shock wave can be quite different from the dipole orientation mechanism which dominates for intervals longer than the relaxation time. In the SL case the typical time for buildup of large pressure gradients is 10^{-9} s, a time much longer than the breakdown time.

In this letter we show that, as was predicted by García and Levanyuk,[11] for parameter values in the region for which SL has been observed experimentally, the collapsing region of the bubble produces electric fields of the same order as the electric breakdown field E_{bd} in water (which has an electronic character, being $\sim 10^7$ V/m under static conditions[15] and $\sim 10^8$ V/m under dynamic conditions.[16]) Furthermore, as we will show below, when the flexoelectric potential energy is taken into accounted, the evolution of the bubble radius in this collapsing region agrees with a recent experiment; in particular, the minimum radius R_m agrees with the values measured in many experiments ($0.7\ \mu$m).[4,5] Calculations of the energy release and of the duration of the emission are also consistent with experimental results.[5,8]

Including up to first-order corrections due to the compressibility of the liquid (as proposed by Herring[17]), energy conservation for the bubble reads:

$$2\pi\rho_w R^3\left(1-\frac{4}{3}\frac{\dot{R}}{c_w}\right)\dot{R}^2+U = \int_{R_0}^{R}\left[P_g-P_a-P_0+\frac{R}{c_w}\frac{d}{dt}(P_g-P_a)-\frac{2}{R}(\sigma+2\nu\dot{R})\right]4\pi R^2 dR, \tag{1}$$

where $\dot{R}$ and $\ddot{R}$ are the velocity and the acceleration of the bubble wall; σ and ν are the surface tension and kinematic viscosity of the fluid; ρ_w and c_w are the density of the water and the sound velocity in it; P_g and P_0 are the gas and ambient pressures; the acoustic field is given by $P_a(t)=P_a'\sin(w_a t)$, where w_a is the acoustic frequency. For the gas pressure P_g, we consider the van der Waals adiabatic equation of state:

$$P_g=\frac{P_0 R_0^{3\gamma}}{(R^3-a^3)^{\gamma}}, \tag{2}$$

where γ is the ratio of specific heats (for air, γ is 7/5), R_0 is the initial radius of the bubble (which corresponds to the equilibrium radius when $P_a'=0$), and a is the van der Waals hard core (for air, $a=R_0/8.5$). The integral in Eq. (1) corresponds to the total work done by the system. The term in the integrand that contains the derivative of the pressure with respect to the time t corresponds to a zeroth-order correction for the compressibility of the liquid. Standing on the left-hand side are a kinetic energy term (dimin-

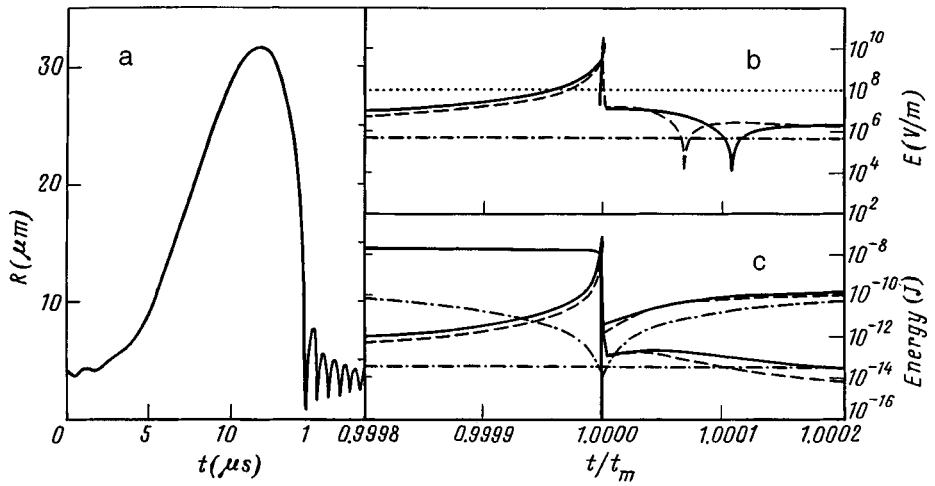

FIG. 1. Solution of the RP equation (where U is neglected), for $P'_a=1.45$ atm, $w_a/2\pi=40$ kHz and $R_0=4\,\mu$m (solid curves). (a) Bubble radius R, (b) electric field E and (c) kinetic energy (black curves) and flexoelectric energy U (gray curves), as functions of time t. For $P'_a=1.45$ atm, $w_a/2\pi=40$ kHz and $R_0=4\,\mu$m (solid curves); $P'_a=1.375$ atm, $w_a/2\pi=26.5$ kHz and $R_0=3.25\,\mu$m (dashed curves), and $P'_a=1.075$ atm, $w_a/2\pi=26.5$ kHz and $R_0=10.5\,\mu$m (dot-and-dash curves). In (b) the horizontal dotted line corresponds to $E_{\rm bd}$. In all our calculations we considered a viscosity $\nu=0.001$ kg·m/s and a surface tension $\sigma=0.07275$ N/m, as extracted from a handbook.

ished by a term corresponding to the first-oder correction for the compressibility of the liquid) and a potential energy term U. The standard RP equation neglects U and is obtained by differentiating Eq. (1) with respect to the bubble radius R. Figure 1a shows a typical bubble radius evolution curve obtained from the RP equation with parameter values for which SL has been observed experimentally.[5] In all our calculations we used a fourth-order Runge–Kutta method with a time step $dt=10^{-12}$ s.

As was proposed in Ref. 11, in the vicinity of the bubble wall the electric field E (due to the polarization of the water) is related to the pressure gradient ∇p by the equation[11,18]

$$E_R=f\nabla p=f\rho_w\ddot{R}, \tag{3}$$

where f is the flexoelectric coefficient (for water, f has been estimated to be approximately 10^{-7} V·m^2/N (Ref. 11). In Fig. 1b we show the resulting electric fields E for two cases where SL has been observed experimentally (the dashed and solid lines correspond to the parameter regions of Refs. 4 and 5, respectively). The dot-and-dash curve corresponds to the parameter region of an experiment in which no SL was observed.[4] Note that only in the two first cases does the electric field exceed the typical electric breakdown field $E_{\rm bd}$ of water (which is denoted by the horizontal dotted line), and this occurs prior to $t/t_m=1$, i.e., before the bubble reaches its minimum radius R_m at the time $t=t_m$.

The acceleration at any distance $r>R$ from the bubble center is

$$\ddot{r}=\frac{\ddot{R}R^2+2R\dot{R}^2}{r^2}-\frac{2R^4\dot{R}^2}{r^5}, \tag{4}$$

and the potential electric energy in volume units is $U_v(r)=(\epsilon_0\varepsilon/2)\,E(r)^2$. Therefore, the energy U reads:

$$U(R,\dot{R},\ddot{R})=\int_R^\infty U_v 4\pi r^2 dr=2\pi f^2\rho_w^2\epsilon_0\varepsilon R^3\left(\ddot{R}^2+3\frac{\dot{R}^2}{R}\ddot{R}+\frac{18}{7}\frac{\dot{R}^4}{R^2}\right), \tag{5}$$

where ϵ_0 and ε are the permittivity of free space and the dielectric constant of the water.

We computed the RP equation (Eq. (1) for $U=0$) and Eq. (5) to estimate the flexoelectric energy U, taking $f=10^{-7}$ V·m^2/N. We found that in the parameter regions for which SL has been observed experimentally (the same parameters as in Fig. 1b), the potential energy U (the dashed and solid gray curves in Fig. 1c) reaches values of the same order as the kinetic energy (the dashed and solid black curves in Fig. 1c) in the vicinity of the collapsing region $(t/t_m\sim 1)$, where very high accelerations ($\sim 10^{13}$ m/s^2) take place, in contrast to the non-SL case (dot-and-dash curves). This indicates that under SL conditions the energy U should not be neglected as in the RP equation. In the bubble rebound $(t>t_m)$, the work term due to the gas compression dominates over other terms due to the liquid. The bubble responds by increasing its radius up to the next maximum. In general, for $t>t_m$, the bubble evolution takes place with a small amount of kinetic energy and a negligible flexoelectric energy, because both the velocity and the acceleration are much smaller in the oscillating regime than they are just before the first rebound, and the electric field does not exceed the breakdown field $E_{\rm bd}$ until the first rebound of the next cycle.

When considering $U\neq 0$, the highest derivative order in Eq. (1) is contained in U (see Eq. (5)). For this reason, at each iteration we computed R, $\dot{R}$, and $\ddot{R}$ from (1). After that, the resulting quantities are inserted into (5) to compute U for the next iteration. This procedure avoids numerical problems (for example, numerical indeterminacies for $f\to 0$). Note that we do not differentiate the equation of motion with respect to R as is done to obtain the RP equation; in this way energy conservation is absolutely ensured (even in the collapsing region). Because here $\dot{R}$ is calculated from the quadratic velocity term (corresponding to the kinetic energy in (1)), an inconvenience appears in the choice of the velocity sign. In our case, since U is negligible both for $t<t_M$ (t_M is the time at which the bubble radius reaches its maximum — the time limiting the bubble expansion and contraction) and for $t>t_m$ (this is after the first rebound of the bubble), we computed the various dynamical quantities of these regimes in the standard manner of solving the RP equation (neglecting U), while in the bubble contraction region we considered the negative solution for the velocity when computing Eq. (1). Furthermore, in order to take into account the energy emission mechanism when E exceeds $E_{\rm bd}$, we subtracted U (which is the energy stored in water by its polarization) to the total energy accumulated in the system at each time when $E>E_{\rm bd}$ (here, we considered $E_{\rm bd}=10^8$ V/m). After that, the algorithm continues by going on to the next iteration in the calculation of Eq. (1). In this paper the released energy U_r is taken equal to the value of U, but the results are almost the same if one considers an energy release U_r slightly smaller than U.[19]

In Fig. 2 we compare the $R(t)$ results obtained from the RP equation ($f=0$, dot-and-dash curve) with two cases that result when values $U\neq 0$ are considered in Eq. (1), for $f=5\cdot 10^{-8}$ V·m^2/N (dashed curve) and 10^{-7} V·m^2/N (solid curve). Note that the minimum radius R_m increases with f, while for $f=0$ the value of R_m is very close to the

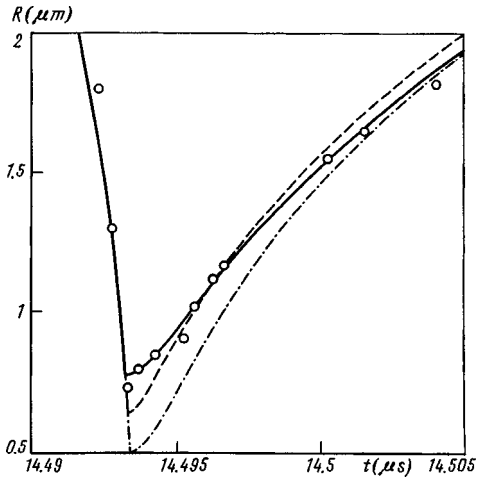

FIG. 2. $R(t)$ curves for $P_a'=1.45$ atm, $w_a/2\pi=40$ kHz and $R_0=4\mu$m, and for $f=0$ (dot-and-dash curve), $f=5\cdot10^{-8}$ (dashed curve) and $f=10^{-7}$ (solid curve) $\mathrm{V\cdot m^2/N}$. The circles correspond to the experiments of Ref. 5.

radius of the air hard core ($R_0/8.5\sim0.47$ μm). The circle symbols in Fig. 2 correspond to the experimental data that we extracted from the collapsing region in Fig. 4 of Ref. 5 The agreement between the theoretical curve for $f=10^{-7}$ $\mathrm{V\cdot m^2/N}$ and the experimental ones is quite good, in contrast to the RP case. We recall that in different SL experiments R_m came out to be ~0.7 μm as on our theoretical curve. For $f=10^{-7}$ $\mathrm{V\cdot m^2/N}$ the electric field E exceeds E_{bd} for the first time at a radius R_{bd} (~1.01 μm) greater than R_m and at a time $t_{\mathrm{bd}}<t_m$. At $t=t_{\mathrm{bd}}$ the velocity $\dot{R}_{\mathrm{bd}}$ is equal to 1159 m/s. For an estimation of the Mach number M relative to the speed of sound c_g of the gas bubble ($\mathrm{M}=\dot{R}/c_g$), it should be noted that c_g depends on R, since the gas density ρ_g increases as $\rho_{g_0}(R_0/R)^3$ (ρ_{g_0} is the air density at room temperature and ambient pressure, equal to 1.161 $\mathrm{kg/m^3}$); i.e., for $R\sim1.01$ μm one has $\rho_g\approx70$ $\mathrm{kg/m^3}$ (that is, $62\rho_{g_0}$ or $0.07\rho_w$). Considering the formula for c_g in an ideal gas and the expression for the gas temperature deduced from the van der Waals theory,[19] at this gas density we find that $c_g\approx803$ m/s ($c_g\approx2.5c_{g_0}$). Therefore, at the beginning of the electric breakdown the Mach number $\mathrm{M}\approx1.44$, which is close to the value of the Mach number at $R=R_m$, since in this region it turns out that c_g and $\dot{R}$ increase in a similar way.

An interesting point is that, when considering a breakdown field equal to 10^7 V/m and $f=5\cdot10^{-8}$ $\mathrm{V\cdot m^2/N}$ (parameters for which also the experimental curve is reproduced), at the moment that the first electrical breakdown occurs (i.e., at radius R_{bd}), the Mach number $\mathrm{M}=0.96$.[19] This means that the electric breakdown phenomenon may take place before the bubble wall becomes supersonic. Additionally, in the different cases discussed here, at the radius R_{bd} the gas temperature comes out to be approximately 800 K. In other words, this electrical phenomenon may take place earlier than other possible effects invoked in the literature to explain the SL phenomenon, like those associated with thermal effects,[20,21] those corresponding to an incoming shock wave that passes through the center of the bubble,[21] or other based on an electrical discharge in which numerous

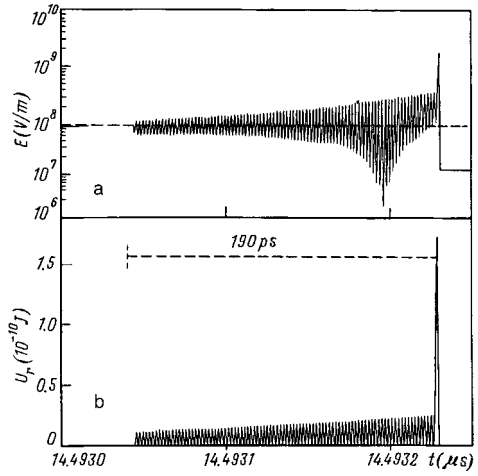

FIG. 3. For same parameters as in Fig. 2 and $f=10^{-7}$. Time distributions of the electric field $E(t)$ (a) and of the energy release $U_r(t)$ (b). For the same parameters as in Fig. 2 and $f=10^{-7}$ V·m^2/N. In part (a) the horizontal dashed line indicates the value adoped for $E_{\rm bd}$.

small, charged liquid jets penetrate the interior of the bubble during its collapse.[22]

The top panel in Fig. 3 shows the evolution of the electric field $E(t)$ (solid line) around the collapsing region for $f=10^{-7}$ V·m^2/N and $E_{\rm bd}=10^8$ V/m (as indicated by the horizontal dashed line). As a consequence of the energy released, the $E(t)$ curve exhibits many jumps going from values where the quantity $E_{\rm bd}$ is exceeded to values where it is not. Indeed, on account of the motion of the bubble radius and the energy emission, the system is electrically charged and discharged. The corresponding time distribution of the energy released is illustrated in the bottom panel of Fig. 3. As expected, the jumps are also evidenced in the $U_r(t)$ curve. Note that this emission exists for approximately 190 ps, and the quantity of energy released in each burst increases with time from approximately 10^{-11} to 10^{-10} J. In general, the increase of $U_r(t)$ with t is smooth, except at the end of the emission, which reveals that the abrupt change of energy conditions is a prelude for the rebound of the bubble. The total energy released is 10^{-9} J per cycle, a value much bigger than the 10^{-12} J measured in SL experiments.[6] This suggests that the efficiency of the light emission in experiments is much less than unity ($\sim 10^{-3}$), and it may be that the remainder of the energy is released in other ways.

With our model we do not intend to exclude other phenomena at the time of energy release, i.e., a more complicated relaxation mechanism at the time of electrical breakdown or other simultaneous physical phenomena produced by supersonic motions. Even if the electrical breakdown phenomenon in water is of electronic character, it is difficult to clarify what happens when the energy is released, since water has a fast relaxation of the molecule orientation, which is not incorporated in our model. On the other hand, it is possible that just at the first moment when the energy starts to be released, the system may respond with other mechanisms that are not described by the standard hydrodynamic equations. Of course, the mechanism responsible for the relaxation may interfere strongly in the bubble motion, preventing (or maybe allowing) supersonic bubble-wall motion, but this is an open question which should be considered as a problem for further development

of our model. Unfortunately, from the experimental point of view, velocity measurements are very poor, since they are obtained by measuring the slope between very few points near the minimum radius.[5] In any case, it should be noted that the experimental maximum velocity reached by the bubble wall has been estimated to be 1200–1600 m/s,[5] which corresponds to a Mach number of 4–6 relative to the speed of sound at room temperature and ambient pressure, while the real Mach number (in terms of the sound velocity at the actual density of the gas bubble) is slightly greater than 1. For very small radius (close to the hard core) the sound velocity of the bubble has a value very close to that of the liquid.

In conclusion, we have presented an equation of motion for a gas bubble with the energy emission taken into account. We have shown that by a calculation of the electric field one can establish that the electric breakdown field can serve as a criterion for SL, since the electric field exceeds the typical electric breakdown field in water only in those cases where SL has been observed experimentally. A very important point is that consideration of the flexoelectric energy in the equation of motion leads to a minimum radius value that fits quite nicely with the experimental data of Refs. 4 and 5, in contrast to the RP equation, where the resulting minimum radius is a quantity very close to the radius gas hard core. The values obtained for the duration of the light emission and the quantity of energy released are consistent with experiments. The breakdown may occur in the water as well in the gas inside the bubble; besides, polarization of the gas may explain the effects of noble gas doping[7,8] in terms of the influence of the concentration gradients, which also produce polarization, and the influence of minute noble gas impurities on the breakdown voltage, an effect which has been known since long ago as the Penning effect.[23] An asphericity of the bubble or a breakdown starting in a local region (rather than at the same time in all the system) will lead to light emission with a ''dipolar component'' in the angular distribution of the intensity. Large magnetic fields should also modify the SL conditions because they influence the electronic motion and consequently the breakdown conditions.

We thank A. P. Levanyuk, E. Medina and P. A. Serena for helpful discussions. This study was supported by Spanish agencies and the EC through the ESPRIT projects. One of us (A. H.) would like to acknowledge financial support from the EC through the HCM program.

[1] N. Marinesco and J. J. Trillat, Proc. R. Acad. Sci. **196**, 858 (1933); H. Frenzel and H. Schultes, Z. Phys. Chem. **27B**, 421 (1934).
[2] D. F. Gaitan, L. A. Crum, R. A. Roy, and C. C. Church, J. Acoust. Soc. Am. **91**, 3166 (1992).
[3] R. G. Holt and D. F. Gaitan, Phys. Rev. Lett. **77**, 3791 (1996).
[4] B. P. Barber and S. J. Putterman, Phys. Rev. Lett. **69**, 3839 (1992).
[5] K. Weninger, B. P. Barber, and S. J. Putterman, Phys. Rev. Lett. **78**, 1799 (1997).
[6] R. Hiller, S. J. Putterman, and B. P. Barber, Phys. Rev. Lett. **69**, 1182 (1992).
[7] R. Hiller, K. Weninger, S. J. Putterman, and B. P. Barber, Science **266**, 248 (1994).
[8] R. Hiller, S. J. Putterman, and K. Weninger, Phys. Rev. Lett. **80**, 1090 (1998).
[9] L. Rayleigh, Philos. Mag. **34**, 94 (1917).
[10] M. Plesset, J. Appl. Mech. **16**, 277 (1949); B. Noltingk and E. Neppiras, Proc. Phys. Soc. London, Sect. B **63**, 674 (1950).
[11] N. García and A. P. Levanyuk, JETP Lett. **64**, 907 (1996).
[12] A. K. Tagantsev, Usp. Fiz. Nauk **152**, 423 (1987) [Sov. Phys. Usp. **30**, 588 (1987)].
[13] P. Harris and H.-N. Presles, J. Chem. Phys. **77**, 5157 (1982).
[14] J. B. Hasted, Prog. Dielectr. **3**, 103 (1961).
[15] Y. Toriyama and U. Shinohara, Phys. Rev. **51**, 680 (1937).

[16] C. A. Sacchi, J. Opt. Soc. Am. B **8**, 337 (1991).
[17] C. Herring, OSRD Rep. No. 236 (1941); A. Prosperetti and A. Lezzi, J. Fluid Mech. **168**, 457 (1986).
[18] Ya. I. Frenkel', Zh. Fiz. Khim. **14**, 305 (1940); G. L. Natanson, Dokl. Akad. Nauk SSSR **59**, 83 (1948); M. Degrois and P. Baldo, Ultrasonics **12**, 25 (1974); M. A. Margulis, Zh. Fiz. Khim. **59**, 1497 (1985) [Russ. J. Phys. Chem. **59**, 882 (1985)]; Ultrasonics **30**, 152 (1992).
[19] A. Hasmy and N. García (to be published).
[20] E. B. Flint and K. S. Suslick, Science **253**, 1397 (1991); V. Kamath and A. Prosperetti, J. Acoust. Soc. Am. **94**, 248 (1993); L. A. Crum and T. J. Matula, Science **276**, 1348 (1997).
[21] C. C. Wu and P. H. Roberts, Phys. Rev. Lett. **70**, 3424 (1994); W. C. Moss, D. B. Clarke, and D. A. Young, Science **276**, 1398 (1997).
[22] T. Lepoint, D. De Pauw, F. Lepoint-Mullie *et al.*, J. Acoust. Soc. Am. **101**, 2012 (1997).
[23] F. M. Penning, Naturwissenschaften **15**, 818 (1927); Physica (Utrecht) **1**, 1007 (1934).

Published in English in the original Russian journal. Edited by Steve Torstveit.

On a characteristic feature of grazing-incidence nuclear monochromators for synchrotron radiation

M. A. Andreeva
M. V. Lomonosov Moscow State University, 119899 Moscow, Russia

(Submitted 18 August 1998)
Pis'ma Zh. Éksp. Teor. Fiz. **68**, No. 6, 449–453 (25 September 1998)

It is shown theoretically that the optimum resonance monochromatization of synchrotron radiation by means of grazing-incidence antireflection mirrors is obtained not at the maximum possible enrichment (~100%) but rather with a low enrichment in the Mössbauer isotope (the natural abundance in the case of iron). This possibility is due to the fact that the conditions of interferometric suppression of electron reflection in the range of total external reflection angles is uniquely sensitive to small variations of the film or substrate density. © *1998 American Institute of Physics.* [S0021-3640(98)00318-1]

PACS numbers: 41.60.Ap

The unique brightness of synchrotron radiation (SR) as well as various of other important properties of this radiation, such as unidirectionality, virtually complete linear polarization, small beam size, and pulse structure, make such radiation extremely attractive for purposes of Mössbauer optics and spectroscopy. However, despite the substantial progress made in recent years in this direction, mainly by using temporal filtering of the nuclear-resonance response, the separation of an extremely narrow Mössbauer spectral component at x-ray wavelengths (from 1.1×10^{-7} eV for ^{169}Tm, with a transition energy of 8.4 keV, to 6.7×10^{-11} eV for ^{181}Ta, with a transition energy of 6.2 keV; the width of the recoilless 14.4-keV line of ^{57}Fe is 4.7×10^{-9} eV; the Mössbauer transition energy of the isotopes ^{67}Zn and ^{107}Ag, with record low resonance widths, is much too high, and these isotopes are not as yet being considered) from the essentially white SR spectrum presents a serious problem. We note that the limiting energy width that can be discriminated by ultrahigh-resolution x-ray crystal monochromators at the present time is $\sim10^{-3}$ eV.[1]

There exist two ideas for extracting the nuclear-resonance component from a white SR spectrum: 1) using purely nuclear maxima of the Bragg reflection from crystals enriched with a Mössbauer isotope,[2–6] and 2) using grazing-incidence antireflection (GIAR) films.[7] The first idea has passed all stages of a careful study and has recently been brilliantly implemented.[8] The second idea, despite all the difficulties in its implementation, has substantial advantages. In the first place, it is difficult to obtain single crystals enriched with a Mössbauer isotope, and such crystals cannot be grown from all Mössbauer isotopes. At present α-$^{57}Fe_2O_3$, $^{57}FeBO_3$, α-$^{57}Fe_3BO_6$, and YIG (with ^{57}Fe) single crystals have been investigated, and this is apparently the entire list of possible

crystals. In the second place, purely nuclear Bragg-reflection maxima are by their very nature due to the presence of hyperfine splitting of the nuclear levels, which complicates the spectrum and the polarization properties of the filtered radiation. Special conditions were produced in Ref. 8 to obtain a single reflection line: a $^{57}FeBO_3$ single crystal was heated to the Néel temperature (75.35 °C) and placed in a 10 mT magnetic field. In the process the lines of the magnetic hyperfine structure virtually ''collapsed,'' but the quadrupole doublet remained, and one of its lines gave a purely nuclear reflection (333). Thus, the result obtained in Ref. 8 was almost a miracle of experimental technique.

Grazing-incidence optics is very convenient for micron-size SR beams. Since there are virtually no restrictions in choosing the components and thicknesses of the films, the parameters of the hyperfine interactions in them can be varied over wide limits (without the stringent temperature limitation of Ref. 8). However, the corresponding practical results obtained thus far for the isotopes ^{119}Sn and ^{57}Fe are not very convincing.[9–12] Suppression of electronic reflection by more than two orders of magnitude has been achieved (by comparison, the suppression effect achieved in Ref. 8 on a $^{57}FeBO_3$ single crystal is 10^{-10}), and moreover the nuclear reflection spectrum is strongly broadened (up to 100 natural resonance widths) and has a quite complicated shape with a dip near exact resonance. Some of the problems are due to the imperfection of the technology used to prepare ultrathin films (problems of density uniformity of the films, reducing surface roughness to a minimum, obtaining prescribed thicknesses to within 0.1 nm, and so on). However, as will be shown in the present work, the initial approach, using enriched films in analogy with enriched crystals, is completely unjustified.

The idea of grazing-incidence antireflection films, which is presented in Ref. 7, is well known in optics and is based on the use of multibeam interference in ultrathin films. If for a certain grazing angle θ the wave reflected once from the film surface has the same amplitude as and is in antiphase with the outgoing total wave formed as a result of multiple re-reflection in the film, then the total coefficient of reflection of such a film is zero. To obtain complete suppression of reflection the thickness d and density of the film and substrate must satisfy stringent conditions. An important point is that for prescribed values of the density and photoabsorption in the film and substrate, the thicknesses at which antireflection is possible for some angle θ form a discrete series of values. This follows from the need to satisfy two conditions simultaneously: amplitude and phase matching. In Ref. 13 an elegant graphical method was introduced to determine the required parameters of the antireflection film. There are a number of works devoted to the analysis of possible materials for films and substrates, to the investigation of more complicated multilayer systems, and to the question of the stability of the solution in the presence of weak nonuniformities of the film thickness, interfacial roughness, and divergence of the incident radiation beam, for two different types of solutions — IM (impedance-matched) and DS (damping stabilized).[9,11,13–15] The question of what effect the concentration of the resonant isotope in the film might have on the optimal resonance monochromatization of the incident radiation has still not been analyzed. It has been conjectured that the higher the concentration of the resonant isotope, the better the film will reflect in the resonant frequency range.

Figure 1 displays on a logarithmic scale the reflection spectra at interference antireflection minima of the DS type for a resonant $^{57}Fe/Ta$ film (left-hand panel) and of the IM type for a Zr film on a resonant ^{57}Fe substrate (right-hand panel). The calculations were

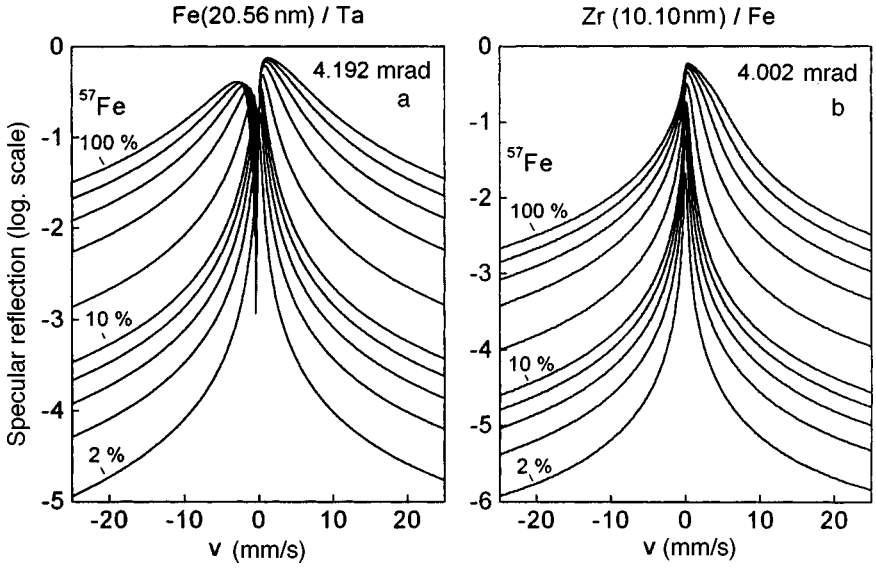

FIG. 1. Theoretical resonance reflection spectra (on a logarithmic scale) for the case of a resonant ^{57}Fe film on a Ta substrate (a) and a Zr film on a ^{57}Fe substrate (b). The calculations were performed for different degree of enrichment of the film or substrate with the resonant isotope: $Q=100$, 80, 60, 40, 20, 10, 8, 6, 4, and 2%. In the left-hand panel the grazing angle $\theta=4.192$ mrad corresponds to a DS-type reflection minimum, and the computed thickness of the ''antireflection'' ^{57}Fe film is 20.56 nm. In the right-hand panel the grazing angle $\theta=4.002$ mrad corresponds to an IM-type reflection minimum, and the computed thickness of the ''antireflection'' Zr film is 10.10 nm.

performed using the well-known formula for reflection from a film (see, for example, Ref. 7). The working parameters are ($\lambda=0.086$ nm): susceptibility of the Zr film $\chi_f=(-10.82+0.4i)\times10^{-6}$, susceptibility of the Ta substrate $\chi_s=(-26.5+3.42i)\times10^{-6}$, susceptibility of the ^{57}Fe film or substrate $\chi=(-14.5+0.7i)\times10^{-6}$, and the resonant correction to it in the form

$$\chi_{\rm res}=Q\frac{-9.0\ {\rm mm/s}}{v-v_{\rm res}+i\Gamma/2}\times10^{-6};$$

where $v-v_{\rm res}$ is the Doppler shift of the energy relative to resonance. For simplicity, the hyperfine splitting was not introduced, but to be realistic the width of the resonance was assumed to be three times greater than the natural width: $\Gamma=0.3$ mm/s. It is evident from the plots that as the enrichment is decreased by almost two orders of magnitude, the intensity at the maximum of the resonance line decreases very little, while at the same time the intensity of the ''tails'' of the resonance lines decreases by 3 or 4 orders of magnitude, so that the monochromatization effect is enhanced substantially. In Fig. 2 some of the spectra from Fig. 1 are normalized and presented in an ordinary (linear) scale to permit comparison of the shape of the resonance lines of the reflected radiation. This figure requires no discussion. As the enrichment decreases, the resonance reflection line becomes essentially unbroadened. It is obvious that the computed and observed[9–12,14] exotic shape of the resonance line at the antireflection minima is a consequence of the ''supersaturation'' of the film with the resonant isotope.

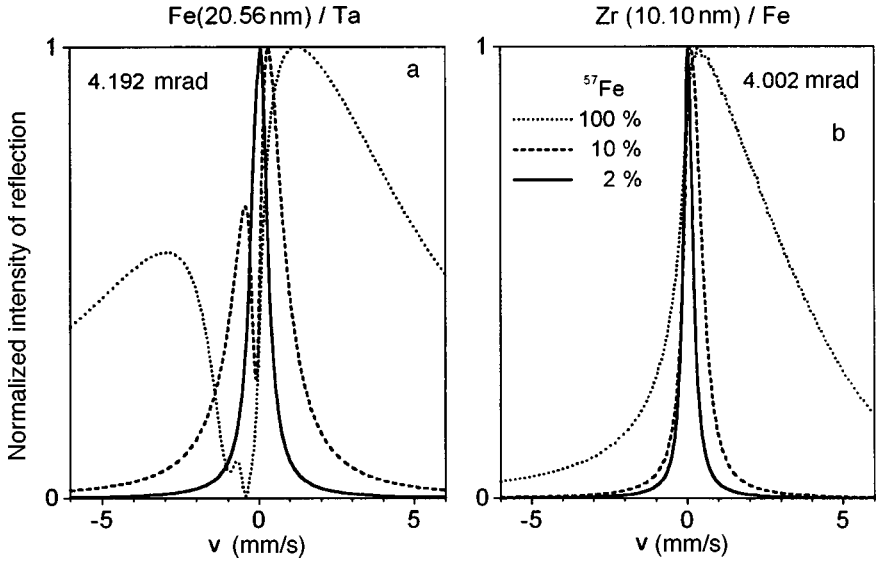

FIG. 2. Normalized intensities of the same resonance lines as in Fig. 1 in the standard scale. The scale along the *x* axis is substantially magnified compared with Fig. 1. The designations of the lines presented in part b are the same as in part a.

To be fair, we note that for IM type solutions the effect noted is less pronounced and the reflection lines as a whole are narrower.

The computed regularities can be easily explained. In the case of purely nuclear Bragg-reflection maxima, the nuclear-reflection signal is formed against a zero background, and the more resonant nuclei present in the sample, the higher the reflection intensity will be. Under total external reflection conditions (the DS-type maxima are closest to these conditions), the suppression of electron reflection is an interferometric effect, which is extremely sensitive to very small variations of the thickness and density of the film (this circumstance creates substantial technological difficulties in fabricating such antireflection coatings). A large amount of isotopes is not required to destroy the conditions of interferometric quenching in the resonant frequency range and to restore almost complete external reflection (''burying'' of the interference minimum on the reflection curve). Thus, the observed resonance maximum in the reflection spectrum is formed as a result of not only scattering by nuclei but also the interaction with the entire electronic subsystem of the film. This can be interpreted as a manifestation of the collective character of the interaction of the radiation with the film under total external reflection conditions (other striking manifestations of the collective character of the interaction are acceleration of the decay of the nuclear state (speed-up effect) under total external reflection conditions,[16,17] appearance of an interference maximum near the critical angle for the integrated delayed reflection intensity,[16–19] appearance of a resonance dependence for the yield of secondary photoelectrons,[20,21] and others).

In summary, a new result of the above analysis of the characteristic features of nuclear monochromatization by ultrathin films under grazing-incidence conditions is the possibility of effective monochromatization by weakly enriched resonance films. Consid-

ering the enormous cost of Mössbauer isotopes, this is a very useful result.

I thank Dr. B. G. Semenov for some stimulating discussions.

This work was supported by the Russian Fund for Fundamental Research (Grant 97-02-17686).

[1] A. I. Chumakov, J. Metge, A. Q. R. Baron *et al.*, Nucl. Instrum. Methods Phys. Res. A **383**, 642 (1996).
[2] G. V. Smirnov, V. V. Sklyarevskiĭ, R. A. Voskanyan, and A. N. Artem'ev, JETP Lett. **9**, 70 (1969).
[3] V. A. Belyakov and Yu. M. Aĭvazyan, JETP Lett. **7**, 368 (1968).
[4] M. A. Andreeva and R. N. Kuz'min, Kristallografiya **14**, 708 (1969) [Sov. Phys. Crystallogr. **14**, 605 (1969)]; Dokl. Akad. Nauk SSSR **185**, 1282 (1969) [Sov. Phys. Dokl. **14**, 298 (1969)].
[5] A. I. Chechin, N. V. Andronov, M. V. Zelepukihn *et al.*, JETP Lett. **37**, 633 (1983).
[6] E. Gerdau, R. Rüffer, H. Winkler *et al.*, Phys. Rev. Lett. **54**, 835 (1985).
[7] J. P. Hannon, G. T. Trammell, M. Mueller *et al.*, Phys. Rev. Lett. **43**, 636 (1979).
[8] G. V. Smirnov, U. van Bürck, A. I. Chumakov *et al.*, Phys. Rev. B **55**, 5811 (1997).
[9] H. Homma, H. Kentjana, E. E. Alp *et al.*, J. Appl. Phys. **72**, 5668 (1992).
[10] E. E. Alp, E. E. Mooney, T. M. Toellner *et al.*, Phys. Rev. Lett. **70**, 3351 (1993).
[11] R. Röhlsberger, E. Gerdau, M. Harsdorff *et al.*, Europhys. Lett. **18**, 561 (1992).
[12] R. Röhlsberger, E. Gerdau, E. Lüken *et al.*, Z. Phys. B **92**, 489 (1993).
[13] J. P. Hannon, N. V. Hung, G. T. Trammell *et al.*, Phys. Rev. B **32**, 5068 (1985); ibid., 5081 (1985).
[14] J. P. Hannon, G. T. Trammell, M. Mueller *et al.*, Phys. Rev. B **32**, 6363 (1985); ibid., 6374 (1985).
[15] E. Gerdau, M. Grote, and R. Röhlsberger, Hyperfine Interact. **58**, 2433 (1990).
[16] A. M. Andreeva, Phys. Lett. A **210**, 359 (1996).
[17] M. A. Andreeva, S. M. Irkaev, K. A. Prokhorov *et al.*, Poverkhnost', in press.
[18] A. Q. R. Baron, J. Arthur, S. L. Ruby *et al.*, Phys. Rev. B **50**, 10354 (1994).
[19] T. S. Toellner, W. Sturhahn, R. Röhlsberger *et al.*, Phys. Rev. Lett. **74**, 3475 (1995).
[20] M. A. Andreeva, S. M. Irkaev, and S. M. Semenov, Zh. Éksp. Teor. Fiz. **105**, 1767 (1994) [JETP **78**, 956 (1994)].
[21] M. A. Andreeva, S. M. Irkaev, and V. G. Semenov, Hyperfine Interact. **97/98**, 605 (1996).

Translated by M. E. Alferieff

Characteristic features of the x-ray spectra of a plasma produced by heating CO_2 clusters by intense femtosecond laser pulses with $\lambda = 0.8$ and 0.4 μm

S. Dobosz, M. Schmidt, M. Perdrix, P. Meynadier, O. Gobert, and D. Normand

Centre d'Etudes de Saclay, Commissariat à l'Energie Atomique, 91191 Gif-sur-Yvette Cedex, France

A. Ya. Faenov, A. I. Magunov, T. A. Pikuz, and I. Yu. Skobelev

Center for Data on the Spectra of Multiply Charged Ions, All-Russia Scientific Research Institute of Engineering Physics and Radio Engineering Measurements, 141570 Mendeleevo, Russia

N. E. Andreev

High Energy Density Research Center, Joint Institute for High Temperatures, Russian Academy of Sciences, 127412 Moscow, Russia

(Submitted 12 August 1998)
Pis'ma Zh. Éksp. Teor. Fiz. **68**, No. 6, 454–459 (25 September 1998)

The x-ray spectra of a plasma produced by heating CO_2 clusters with intense femtosecond laser pulses with $\lambda = 0.8$ μm and $\lambda = 0.4$ μm are investigated. Spatially resolved x-ray spectra of the cluster plasma are obtained. The observed characteristic features of the x-ray emission spectra show unequivocally that such a plasma contains quite a large relative number of ions ($\simeq 10^{-2}$–10^{-3}) with energies of 0.1–1 MeV. The contour of the O VIII Ly_α line is found to have characteristic features that are especially conspicuous when the clusters are heated with second-harmonic pulses. These features cannot be explained by any mechanisms known to the authors. © *1998 American Institute of Physics.* [S0021-3640(98)00418-6]

PACS numbers: 52.50.Jm

1. In the last few years a new class of targets, falling between solid-state and rarefied gas targets, has been actively used in investigations of the interaction of subpicosecond laser pulses with matter. These are so-called cluster targets, i.e., gas beams that contain 100–1000 nm size clusters consisting of a substantial number (10^3–10^7) of molecules and having solid-state densities. On the one hand such targets possess all practical advantages of gases (easy control, simple replacement, good replication, and so on) and on the other hand they make it possible to investigate all processes characteristic for high material density. In the last few years the self-focusing of short laser pulses in plasmas, the production of hollow ions, high-harmonic generation,[1–5] and the production of high-energy ions (all the way up to 1 MeV) in plasmas[6,7] have been discovered using such cluster targets.

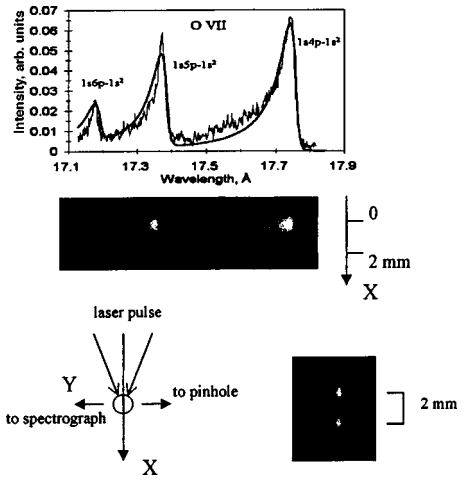

FIG. 1. Emission spectra of a plasma produced by the interaction of a femtosecond laser pulse at the fundamental frequency ($\lambda = 0.8\ \mu$m) with CO_2 clusters. The gas pressure in the valve was 15 atm.

It should be noted that the picture of the interaction of short laser pulses with clusters is still far from clear. For example, there now exist several models which give different explanations of the ionization of cluster targets.[1,8,9] Similarly, the mechanism leading to the generation of fast ions in such a plasma has not been definitively determined.

In the present letter it is shown that x-ray spectroscopic methods of investigation can be used successfully for the systematic acquisition of a large volume of experimental information about the plasma of cluster targets. Specifically, the characteristic features which we have detected in the x-ray emission spectra unequivocally show that such plasma contains quite a large relative number of ions ($\simeq 10^{-2}-10^{-3}$) with energies of 0.1–1 MeV.

2. The experiments were performed on the laser unit at Center d'Etudes de Saclay (France). A titanium–sapphire laser with 60 fs pulses with energy 70 mJ at the fundamental frequency ($\lambda_{las} = 0.8\ \mu$m) or 20 mJ in the second harmonic was used to heat the plasma. Focusing of the radiation with a parabolic mirror gave a radiation flux density up to 10^{18} W/cm^2. The cluster target was produced by adiabatic expansion into vacuum of a small amount of CO_2 gas emerging from a gas valve through a pulsed nozzel 0.3 mm in diameter. The gas pressure in the valve was 10–40 atm.

The x radiation of the plasma was detected simultaneously with three spectrographs with spherically curved mica crystals.[10] The radii of curvature of the crystals were $R = 100$ mm and $R = 150$ mm and the spectral resolution was $\lambda/\Delta\lambda = 2000-4000$ with spatial resolution $\delta x \sim 15-25\ \mu$m. The spectral ranges 17–17.8 Å, 15.8–16 Å, and 18.5–19.2 Å containing the $1snp\ ^1P_1-1s^2$ ($n \geqslant 3$) lines of He-like O VII and the $np\ ^2P-1s\ ^2S$ ($n = 2, 3$) lines of H-like O VIII, were observed. An example of the spectrograms and densitometer traces obtained by heating clusters with laser pulses of the first harmonic ($\lambda = 0.8\ \mu$m) are shown in Fig. 1.

3. A characteristic feature of the emission spectra of a CO_2 plasma can be seen in

Fig. 1 (we note that similar spectra were observed using $\lambda = 0.8$ and 0.4 μm radiation for heating). This feature is due to the presence of a strong asymmetry of the profiles of the spectral lines of H- and He-like oxygen ions. Such an asymmetric line shape, not previously observed in experiments with laser plasmas, cannot be due to thermal Doppler or Stark broadening of the spectral lines in plasma. We propose below a simple model that explains the observed shape of the spectral lines. The basic features of the model are: a) line broadening due to macroscopic motion (expansion) of the plasma, and b) appearance of asymmetry of the shapes of the lines of oxygen ions as a result of the photoionizational absorption on H- and He-like carbon ions present in the CO_2 plasma.

4. If it is assumed that ion acceleration occurs only at the moment when the laser radiation acts, then for $t \gg \tau_{las}$ (τ_{las} is the duration of the laser pulse) an ion with velocity v will be located at a distance $y = vt$ from the plasma center, i.e., spatial separation of ions moving with different velocities will occur. In this connection we shall examine the following model of an expanding plasma. Let the y axis determine the direction toward the detection spectrograph (see Fig. 1). Let $N_i^*(y)$ be the density of ions in the excited state i which are located at a distance y from the plasma center (i.e., the focusing point of the laser pulse), and let $v(y)$ be their velocity of directed motion; accordingly, $v(y)$ is a linear function $v(y) = by$, where $b =$ const. Consider a spectral line due to a radiative transition $i \to k$ with frequency ω_{ik}, and let the line shape at $y = 0$ (i.e., for ions which are on average at rest) be given by the symmetric function $S_{ik}(|\omega - \omega_{ik}|)$. Let us also assume that the plasma possesses absorbing properties and that the mechanism of absorption is wideband, i.e., the absorption coefficient $k(y)$ is independent of ω in a narrow frequency band $\Delta\omega/\omega \ll 1$. Since the spectrograph detects the total radiation from all ions, the observed profile will be determined by the expression

$$F_{ik}^{obs}(\omega - \omega_{ik}) = \frac{\int_{-\infty}^{+\infty} \exp\left\{-\int_y^{\infty} k(x)dx\right\} N_i^*(y) A_{ik} S_{ik}\left(\omega - \omega_{ik}\left(1 + \frac{by}{c}\right)\right) dy}{\int_{-\infty}^{+\infty} \exp\left\{-\int_y^{\infty} k(dx)\right\} N_i^*(y) A_{ik} dy}, \quad (1)$$

where the factor $(1 + by/c)$ in the argument of S_{ik} derives from the Doppler frequency shift. One can see from expression (1) that the presence of the factor $\exp[-\int_y^{\infty} k dx]$ in the integrand results in the appearance of an asymmetry of the observed profile even if the functions $k(y)$, $N_i^*(y)$, and $S_{ik}(\omega - \omega_{ik})$ are themselves symmetric. Expression (1) makes it possible to describe the observed spectra qualitatively correctly even with very rough assumptions about the form of the functions $N_i^*(y)$, $k(y)$, and $S_{ik}(\omega - \omega_{ik})$. In the calculations whose results are shown by the thick lines in Fig. 1, it was assumed that $S_{ik}(\omega - \omega_{ik})$ is a δ function, while the absorption coefficient $k(y)$ and the populations $N_i^*(y)$ of the excited levels are proportional to the density $N_0(y)$ of ground-state ions, for which we employed the model function $N_0/(1 + (y/y_0)^2)$, which is characteristic for cylindrical expansion of a plasma. In this case the observed line profiles depend only on two parameters: $\alpha = by_0/c$ and the optical thickness τ_{ik} of the plasma. The best agreement between the computed and observed spectra (see Fig. 1) was obtained with $\alpha = 10^{-3}$ and $\tau_{ik} = 9$.

5. It can be shown (see Ref. 11 for details) that under the conditions of the present experiment photoionization absorption, i.e., absorption accompanying bound–free tran-

sitions, is responsible for the wide-band absorption of x-ray photons. This process can be efficient enough only if the ground state of the ion is subject to photoionization, since the populations of the excited levels of the ions in a plasma are, as a rule, low. The threshold character of photoionization absorption (only photons with energy greater than the ionization energy of an ion are subject to absorption) is the reason why this mechanism ordinarily has no effect on plasma emission spectra.

Another situation can arise in plasma with a complex chemical composition. In this case the spectral lines of ions of one chemical element can photoionize ions of a different element; here the concentration of the latter ions in the plasma can be substantial. For example, in our CO_2 plasma the lines of He-like O VII can photoionize H-like C VI. The plasma optical thickness τ_{ik} associated with such a process can be estimated[11] as $\tau_{ik} \simeq 1-7$, which should lead to a modification of the emission spectra of the CO_2 plasma.

6. Since in our experiments the spectral line broadening was due to the directed motion of plasma, analysis of the line profiles, generally speaking, can be used to measure the distribution $N(v)$ of ions over the expansion velocity. Although in the case of a CO_2 plasma direct measurements of $N(v)$ are impossible because of the existence of photoionization absorption, the use of model functions for values of the parameters α and τ_{ik} giving good agreement with experiment makes it possible to estimate the distribution $N(v)$. Our plasma contained ions with expansion velocities up to $v \approx 3.6 \times 10^8$ cm/s (i.e., with energies ≈ 1 MeV), and the relative number of such ions was $\approx 7 \times 10^{-3}$.

7. Let us examine the possible mechanisms that could lead to the production of such fast ions in a femtosecond laser plasma. We note that ion acceleration can occur as a result of various processes associated with the appearance of strong electric fields in the plasma. Possible mechanisms that have been discussed include the Coulomb explosion of molecules and clusters[7] and the ''hydrodynamic'' acceleration of ions accompanying the expansion of clusters under the influence of the electron kinetic energy.[12]. The ponderomotive acceleration of ions by high-frequency pressure forces due directly to the intense laser radiation in the plasma near the critical density N_c was discussed in Refs. 13 and 14 for quite long nanosecond-range laser pulses, for which τ_{las} is substantially greater than the acceleration time. Estimates of the maximum ion energy for different acceleration mechanisms show (see Ref. 11 for a more detailed discussion) that under the conditions of our experiment neither a Coulomb explosion of molecules or clusters nor hydrodynamic acceleration of ions with a Maxwellian electron distribution function can lead to the appearance of an appreciable number of ≈ 1 MeV ions.

The action of a superintense field of ultrashort laser pulses on a plasma opens up an interesting possibility for ponderomotive acceleration of ions up to high energies.[15] Let us consider a model of a plasma produced by the action of radiation on a clusterized gas, where the intercluster plasma density (which is formed from the uncondensed gas) is lower than the critical value, while the density of the plasma clusters is much higher than the critical value. A ponderomotive force in standing waves formed as a result of reflection from clusters will act on the ions of the intercluster plasma by means of the charge-separation field for the duration of the laser pulse. In this period of time ions with charge Z_i and mass M_i acquire the velocity

$$v_i \simeq (Z_i/M_i) F_p \tau_{\text{las}} \simeq (Z_i/M_i)(m_e v_E^2/4 l_E)\tau_{\text{las}}, \qquad (2)$$

where $F_p = m_e v_E^2/4l_E = e^2 E_{las}^2/4m_e\omega_0^2 l_E$ is the ponderomotive force acting on an electron in the standing wave of a laser field with electric field intensity E_{las} (which can exceed the electric field intensity of the laser field incident on the plasma), frequency ω_0, and characteristic scale $l_E \simeq c/2\omega_0$. Formula (2) is valid for laser pulse durations less than the acceleration time l_E/v_i but greater than the period of the electronic plasma oscillations. For simplicity it was also assumed that the amplitude v_E of the velocity of the electron oscillations in the laser field does not exceed the speed of light. The maximum energy of the accelerated ions is, according to Eq. (2),

$$M_i v_i^2/2 \simeq (Z_i/8) m_e c^2 (Z_i m_e/M_i)(v_E/c)^4 (\omega_0 \tau_{las})^2. \quad (3)$$

The condition for acceleration to be nonstationary is

$$\omega_0 \tau_{las} < 2(M_i Z m_e)^{1/2} c/v_E = \omega_0 \tau^*. \quad (4)$$

For longer laser pulses, in which case the condition inverse to (4) holds ($\tau_{las} > \tau^*$), the maximum ion energy is determined by the total ponderomotive potential drop and equals

$$M_i v_i^2/2 \simeq (Z_i/4) m_e c^2 (v_E/c)^2. \quad (5)$$

For laser pulse duration corresponding to a transition from nonstationary to stationary acceleration ($\tau_{las} \simeq \tau^*$) the two formulas (3) and (5) give practically the same energy. Under the conditions of the experiment that we are discussing ($Z_i = 8$, $\tau_{las} \simeq 60$ fs), with $v_E/c \simeq 1$, we have $\tau_{las} \simeq \tau^*$, and according to Eqs. (3) and (5) the maximum energy of the accelerated ions is $\simeq 1$ MeV, which agrees with the results of x-ray spectroscopic measurements. We also note that for an uncondensed (intercluster) gas density $n_a \simeq 3 \times 10^{19}$ cm^{-3} ($P = 1$ atm) the number of ions in the intercluster plasma will be only 2–2.5 times less than the number of ions in the clusters. Then the number of electrons is sufficient to maintain the charge-separation field which allows the ponderomotive force to act on the ions. The number of accelerated ions, which is determined by their density in the region of the standing wave, will also be sufficiently large for the conditions under study, when the distance between the clusters is of the order of half the wavelength of the laser radiation.

8. The experiments performed showed that the spatial structure of a plasma produced by the heating of clusters can have the form of either two luminescing points or a channel. This depends mainly not on the frequency of the heating radiation but rather on the gas pressure in the valve and thereby on the size of the clusters obtained and the average density of matter in the interaction region — a plasma channel arises for a higher gas densities and two spatially separated luminescing regions arise for lower gas densities.

9. The strongest difference between the emission spectra of a plasma produced by pulses of the first and second harmonics is observed in the region of the Ly_α resonance line of the H-like O VIII ion, i.e., for $\lambda \simeq 19$ Å (see Fig. 2). Just as in the spectra examined above, the line shape is likewise sharply asymmetric and has a wide short-wavelength wing, but in contrast to all other lines several maxima are clearly seen on this wing, their number and position depending on λ_{las} (one or two additional maxima for $\lambda_{las} = 0.8$ μm and five or six for $\lambda_{las} = 0.4$ μm). The experiments performed showed that the position of these maxima are reproduced very well and that they cannot be an instrumental effect associated with the reflection properties of the crystal. Theoretical estimates

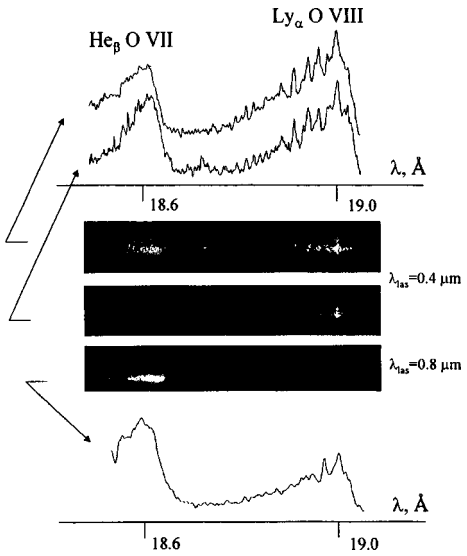

FIG. 2. Plasma emission spectra in the region $\lambda = 18.5-19.2$ Å with the plasma heated by pulses of the first (bottom spectrum and densitometer trace) and second (top two spectra) harmonics.

show that these maxima cannot be due to any of the following: laser or plasma satellites, transitions in hollow ions, high harmonics of the warming radiation, or the result of Zeeman splitting in ultrahigh quasistatic fields.

10. In summary, this study has achieved the following reults:

– spatially resolved x-ray spectra of a cluster plasma were obtained;

– photoionizational absorption was found to influence the shape of the spectral lines;

– ions accelerated to 1 MeV as a result of the interaction of a femtosecond laser pulse with the clusters were detected by x-ray-spectroscopic methods, and an acceleration mechanism was proposed;

– characteristic features of the shape of the O VIII Ly$_\alpha$ line, which are especially conspicuous when the clusters are heated with second-harmonic pulses and cannot be explained by any mechanisms known to the authors, were observed.

This work was supported in part by Grants 98-02-1623 and 96-02-16111 from the Russian Fund for Fundamental Research.

[1] B. D. Thompson, A. McPherson, K. Boyer, and C. K. Rhodes, J. Phys. B **27**, 4391 (1994).
[2] A. B. Borisov, A. McPherson, B. D. Thompson *et al.*, J. Phys. B **28**, 2143 (1995).
[3] A. B. Borisov, J. W. Longworth, A. McPherson *et al.*, J. Phys. B **29**, 247 (1996).
[4] A. B. Borisov, A. McPherson, K. Boyer, and C. K. Rhodes, J. Phys. B **29**, L113 (1996).
[5] T. Donnelly, T. Ditmire, N. Neuman *et al.*, Phys. Rev. Lett. **76**, 14 (1996).
[6] T. Ditmire *et al.*, Phys. Rev. Lett. **78**, 2732 (1997).
[7] M. Lezius, S. Dobosz, D. Normand, and M. Schmidt, Phys. Rev. Lett. **80**, 261 (1998).
[8] C. Rose-Petruck, K. Schaefer, and C. P. J. Barry, in *Application of Laser Plasma Radiation II*, Proc. Soc. Photo-Opt. Instrum. Eng. (SPIE) **2523**, 272 (1995).
[9] E. M. Snyder, S. A. Buzza, and A. W. Castleman Jr., Phys. Rev. Lett. **77**, 3347 (1996).

[10] I. Yu. Skobelev, A. Ya. Faenov, B. A. Bryunetkin *et al.*, Zh. Éksp. Teor. Fiz. **108**, 1263 (1995) [JETP **81**, 692 (1995)].
[11] S. Dobosz, M Schmidt, M. Perdrix *et al.*, JETP (1998), in press.
[12] A. V. Gurevich and L. P. Pitaevskiĭ, in *Reviews of Plasma Physics*, Vol. 10, edited by M. A. Leontovich, Consultants Bureau, New York (1986) [Russian original, Atomizdat, Moscow, 1980, p. 3].
[13] V. P. Silin, JETP Lett. **21**, 152 (1975).
[14] N. E. Andreev, Yu. A. Zakharenkov, N. N. Zorev *et al.*, Zh. Éksp. Teor. Fiz. **76**, 976 (1979) [Sov. Phys. JETP **49**, 492 (1979)].
[15] C. S. Sarkisov, V. Yu. Bychenkov, V. T. Tikhonchuk *et al.*, JETP Lett. **66**, 828 (1997).

Translated by M. E. Alferieff

Collective effects in a system of Pearl vortices and the magnetization of a thin superconducting film

A. N. Artemov[a)]

Donetsk Physicotechnical Institute, Ukrainian National Academy of Sciences, 340114 Donetsk, Ukraine

(Submitted 31 July 1998)
Pis'ma Zh. Éksp. Teor. Fiz. **68**, No. 6, 460–465 (25 September 1998)

The magnetization curves of a thin superconducting monolayer are calculated. It is found that for sufficiently high fields and temperatures the magnetization of a monolayer exhibits the same features as the reversible magnetization of layered superconductors in high fields. It is shown that these features are due to instability with respect to the dissociation of pairs of Pearl vortices into a gas of free vortices and to collective effects in a system of free vortices.
 [S0021-3640(98)00518-0]

PACS numbers: 74.76.Bz, 74.25.Ha

Experimental investigations of the magnetization of high-T_c superconductors in a magnetic field directed along the c axis have shown that there exists a wide range of fields and temperatures in which the magnetization is reversible. The temperature and field dependences of a magnetic sample in this range exhibit a variety of characteristic features which have been observed both in bismuth-based superconductors with a distinct layered structure[1–4] and in the less anisotropic yttrium- and mercury-based superconductors.[5] The reversible magnetization curves of these superconductors intersect at one point at a certain temperature T^*, while below T^* they show a linear temperature dependence.

The theoretical interpretations of the behavior of the magnetization are based on the idea of a layered structure of superconductors. The free energy of a system of Abrikosov vortices formed from two-dimensional (2D) vortices, including the contribution of harmonic oscillations of 2D vortices near their equilibrium positions, is obtained in Ref. 6. A different approach is developed in Ref. 7, where the renormalization-group method is used to analyze the effect of critical fluctuations of the order parameter of a layered superconductor near the second critical field H_{c2} on the thermodynamic properties of the superconductor. In Ref. 8 the thermodynamics of a superconductor is constructed in a model where the superconducting layers are represented as reservoirs containing an equilibrium number of 2D vortices and antivortices. At least qualitative agreement with experimental results is obtained in all of these works.

In the present letter the thermodynamic properties of a system of Pearl vortices in a thin superconducting film are studied, and it is shown that the equilibrium magnetization of the system can possess the same features as that of layered superconductors.

To describe the thermodynamics of the system we shall follow Ref. 9. The free energy density F of a system of Pearl vortices in an external magnetic field is a function of temperature T and magnetic induction $B=S^{-1}\int d\mathbf{x}h(\mathbf{x})=\varphi_0(\rho_+-\rho_-)$, where $h(\mathbf{x})$ is the z component of the microscopic magnetic field in the film, $\rho_\pm=N_\pm/S$ is the density of vortices directed along and opposite to the field, ϕ_0 is a magnetic flux quantum, and S is the area of the film. The thermodynamic or internal field H_i in a superconductor is determined by the expression[10]

$$\frac{\partial F}{\partial B}=\frac{H_i}{4\pi}. \tag{1}$$

For a long cylinder in a longitudinal field, H_i coincides with the external field H_e. To study the magnetization of a thin film we cannot use either this approximation or the infinite-film approximation, where $B=H_e$ and the magnetic moment is zero. We shall assume that the sample is an oblate ellipsoid of revolution with minor axis d and diameter $D\gg d$ and that the external field is directed along the minor axis. In this case the field H_i and the induction B are related with the external field H_e by the relation[11]

$$(1-n)H_i=H_e-nB, \tag{2}$$

where $n=1-d/\pi D$ is the demagnetization factor in the direction of the field.

We define the density of the Gibbs potential as[9]

$$G(H_e,T)=F-\frac{BH_i}{4\pi}-\frac{1}{8\pi}\frac{nB^2}{1-n}. \tag{3}$$

In the limit of a long cylinder $n\to 0$ this expression acquires the standard form. The grand partition function of the system of vortices in the sample has the form

$$\Xi=e^{-\beta G}=\sum_{N_+,N_-}\frac{\epsilon^{\mu_+N_++\mu-N_-}}{N_+!N_-!}\left(\int\frac{d^2x}{\pi\xi^2}\right)^{N_++N_-}$$
$$\times\exp\left\{-(N_++N_-)\beta E_0-\frac{\beta}{2}\sum_{ij}U(\mathbf{x}_i-\mathbf{x}_j)-\beta V\delta G\right\}, \tag{4}$$

where $\beta=1/T$, E_0 is the energy of the vortex core, $U(\mathbf{x}_i-\mathbf{x}_j)$ is the interaction energy of Pearl vortices, and δG is the last term in expression (3). The interaction energy of Pearl vortices can be calculated in the ring approximation.[12] This approximation takes into account the contribution of collective effects to the free energy of the system. The corresponding calculations are performed in Ref. 9.

In an external magnetic field the number N_+ of vortices oriented along the field is different from the number N_- oriented opposite to the field. This imbalance has the effect that diagrams which depend on the difference N_+-N_- and which vanish in the absence of a field appear in the expansion of the free energy. Such diagrams must also be taken into account in the calculations. Their contribution to the energy is proportional to the average interaction energy $U(q=0)=S^{-2}\int d\mathbf{x}_i d\mathbf{x}_j U(\mathbf{x}_i-\mathbf{x}_j)$. In an infinite film this expression diverges and the integration must be bounded by the dimensions of the sample. This part of the free energy can be obtained by averaging the expression for the interaction energy over the sample volume directly in the argument of the exponential in Eq. (4). It gives the magnetic flux energy in the sample

$$\frac{1}{2}\sum_{ij}\int \frac{d\mathbf{r}_i}{V}\frac{d\mathbf{r}_j}{V}U(\mathbf{x}_i-\mathbf{x}_j)=V\frac{\phi^2(\rho_+-\rho_-)^2}{8\pi}\frac{1}{1-n}=V\frac{B^2}{8\pi}\frac{1}{1-n}. \tag{5}$$

Here $\mathbf{r}=(\mathbf{x},z)$ and the integration extends over the sample volume. The contribution of terms with the minimum wave vector $q_{\min}\sim 1/D$, which is associated with the nonzero topological charge of a system of vortices in a magnetic field, to the free energy is thereby singled out. This has no effect on the result of summing the ring diagrams, since $q_{\min}$ does not contribute to their sum.

Introducing the dimensionless variables $\pi\xi^2\rho_\pm=n_\pm$ and $\pi\xi^2H_{i(e)}/\phi_0=h_{i(e)}$, we obtain for the dimensionless potential $g=\beta G\pi\xi^2 d$ the expression

$$g=n_+(\ln n_+-1)+n_-(\ln n_--1)+p(n_++n_-)[1-\ln 4p(n_++n_-)]+p(n_++n_-)e_0$$
$$+\frac{1}{4\Lambda^2}W[16p\Lambda^2(N_++n_-)]+4pk^2\frac{(n_+-n_-)^2}{1-n}-8pk^2h_i(n_+-n_-). \tag{6}$$

All lengths are presented in units of the coherence length ξ, $p=\phi_0^2/16\pi^2\Lambda T$, $\Lambda=\lambda^2/2d$ is the effective Pearl length, $k=\lambda/\xi$, $pe_0=\beta E_0$, and

$$W[x]=\frac{1}{2}\ln\frac{x}{4}+\sqrt{|1-x|}\begin{cases}\tan^{-1}\dfrac{1}{\sqrt{x-1}}-\dfrac{\pi}{2}, & x\geqslant 1\\[2ex] \dfrac{1}{2}\ln\dfrac{1+\sqrt{1-x}}{1-\sqrt{1-x}}, & x\leqslant 1.\end{cases}$$

Differentiating Eq. (6) with respect to $n_\pm$, we obtain the equilibrium equation

$$\ln n_\pm - p\ln(n_++n_-)+4pW'[16p\Lambda(n_++n_-)]\pm 8pk^2\frac{(n_+-n_--h_e)}{1-n}=p(\ln 4p-e_0). \tag{7}$$

Subtracting one of the equations in (7) from the other, we obtain a relation between the equilibrium densities of vortices and the magnetic moment of the sample:

$$\ln\frac{n_+}{n_-}=-16pk^2\frac{n_+-n_--h_e}{1-n}=-16pk^2m. \tag{8}$$

In ordinary units the expression for the moment $4\pi M=(B-H_e)/(1-n)$ can be written as

$$4\pi M=m\frac{\phi_0}{\pi\xi^2}.$$

The equilibrium characteristics of a system of Pearl vortices in the sample as a function of temperature for different values of the external field are shown in Fig. 1. These dependences were obtained by solving Eqs. (7) numerically with the following numerical values of the parameters: $\Lambda(0)/\xi(0)=500$, $k=50$, $n=0.99$, $e_0=3$, and $T_{c0}/T_{KT}=1.2$. It was also assumed that the London and correlation lengths of the superconductor have the model temperature dependence:

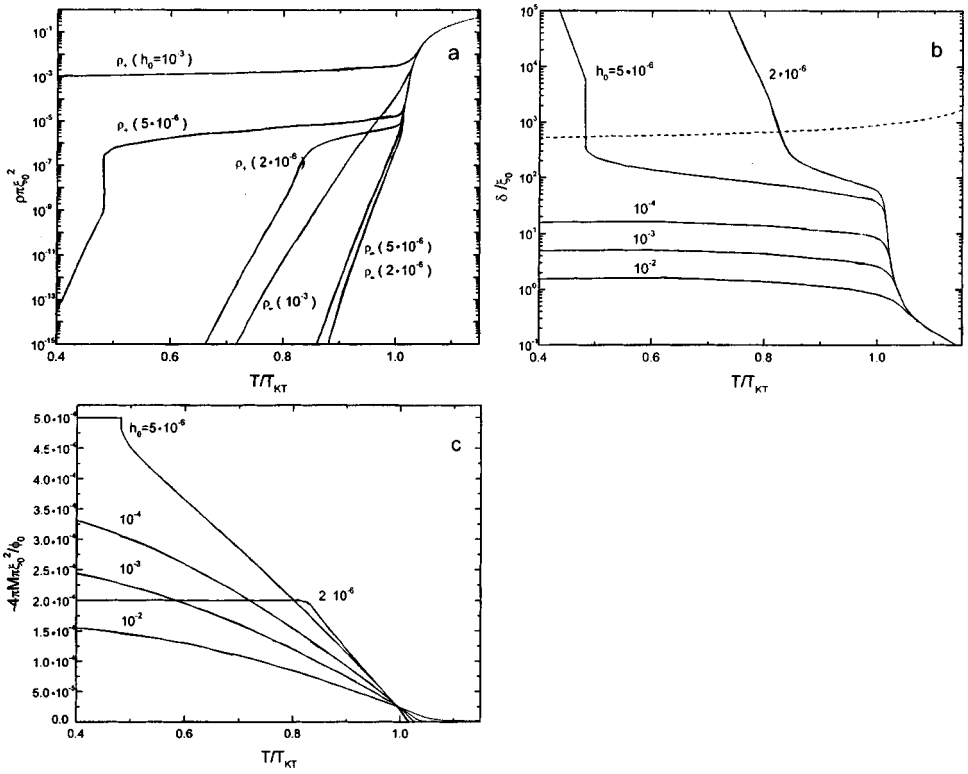

FIG. 1. a) Density of Pearl vortices versus temperature for different values of the external magnetic field. b) Screening length versus temperature. The dashed line shows the temperature dependence of the effective length Λ. c) Magnetic moment of the sample versus the temperature for different values of the external magnetic field.

$$\lambda(T)=\lambda_0/\sqrt{1-T^2/T_{c0}^2}, \quad \xi(T)=\xi_0/\sqrt{1-T^2/T_{c0}^2},$$

where T_{c0} is the superconducting transition temperature. The values of the magnetic field $h_0=H_e\pi\xi_0^2/\phi_0$ presented in the figure approximately correspond to the ratio $H_e/H_{c2}(T=0)$. The equilibrium densities of vortices are shown in the figure as a function of temperature. All possible types of solutions of the equations of equilibrium (7) in a magnetic field are presented here. All solutions exhibit sharp growth of the density of vortices at temperature $T>T_{KT}$. This growth is replaced by an almost horizontal section for n_+ at low temperatures. In sufficiently high fields ($h_0>10^{-5}$) this solution extends essentially to zero temperature. In weaker fields ($h_0<10^{-5}$), as the temperature decreases further, the plateau in the dependence $n_+(T)$ is replaced by a sharp decrease in the density of vortices. Depending on the magnitude of the external field, the solution type can change continuously ($h_0=2\times10^{-6}$) or abruptly ($h_0=5\times10^{-6}$), as was noted in Ref. 9. There are two reasons for this behavior of the solutions — instability of thermally excited vortex dipoles with respect to their dissociation into a gas of free vortices, resulting in a Kosterlitz–Thouless transition, and collective effects in a system of free vortices, manifested as screening of the interaction of the vortices.

Instability appears at temperature T_{KT}. To show this we shall study the asymptotic behavior at extremely high vortex densities $n_+ \approx n_1 \gg n_+ - n_-$ for a potential g. In this case the last three terms in Eq. (6) can be neglected, as can the difference between n_+ and n_-, which we denote by n_0:

$$g \approx 2(1-p)n_0(\ln n_0 - 1) - 2pn_0(\ln 8p - e_0).$$

It is evident that for $p=1$ the coefficient multiplying the logarithm of the density changes sign, which signifies that instability appears for $p<1$. The condition $p=1$ determines the temperature at which instability appears:

$$T_{KT} = \frac{\phi^2}{16\pi^2 \Lambda(T_{KT})}. \tag{9}$$

The appearance of instability at this temperature in thin superconducting films was discussed in Ref. 13.

The flat section of the curve $\rho_+(T)$ is due to collective effects in a system of interacting Pearl vortices. The energy of a Pearl vortex is finite.[14] It depends on the value of the effective length Λ, which is a characteristic length of the magnetic core of a vortex. If the density of vortices in the system is finite, then another characteristic length appears — the Debye screening length

$$\delta = \sqrt{\frac{2\pi\Lambda T}{\phi_0^2(\rho_+ + \rho_-)}}.$$

For $\delta \gg \Lambda$ collective effects do not play a large role in the behavior of a system of vortices. In the opposite limit their role is decisive. The temperature dependence of the screening length is shown in Fig. 1. The dashed line shows $\Lambda(T)$. One can see that the temperatures at which $\delta = \Lambda$ are correlated with the temperatures at which the plateau in the curve $\rho_+(T)$ is replaced by a sharp drop in the density. This means that the low-temperature tails of the curves $\rho_\pm(T)$ are due to the behavior of individual Pearl vortices, while in the high-temperature region we have screened vortices, which are collective formations. The advantage of a collective state of a system of vortices is due to the fact that the energy of a screened Pearl vortex is determined not by the length Λ but rather by the length δ, which is much shorter at this temperature.

These two factors are responsible for the characteristic features of the magnetization of a superconducting film. For high fields and temperatures, where collective effects in a system of Pearl vortices play a decisive role, the magnetization curves (figure) behave just as the curves of reversible magnetization of high-T_c superconductors.[1–3,5] This is natural, since the collective states of screened 2D and Pearl vortices (for $\delta < \Delta$) are qualitatively the same. The temperature T^* at which the magnetization curves intersect in this model depends on the external field. As the field $h_0 \to \infty$, it asymptotically approaches the value T_{KT}.

In these field and temperature ranges, where collective effects are of no consequence, the magnetization of the sample is determined by the edge barrier, which is not considered in our model. As a result, in weak fields low-temperature plateaus appear in the magnetization curves.

In summary, collective effects in a system of magnetic vortices and the Kosterlitz–Thouless instability determine the characteristic features of the reversible magnetization of both bulk layered superconductors and Pearl films.

[a)]e-mail: art@gam.dipt.donetsk.ua

[1] P. H. Kes, C. J. Van der Beek, M. P. Maley *et al.*, Phys. Rev. Lett. **67**, 2383 (1991).
[2] K. Kadowaki, Physica C **185–189**, 2249 (1991).
[3] Q. Li, M. Suenaga, D. K. Finnemore *et al.*, Phys. Rev. **46**, 3195 (1992).
[4] F. Zuo, D. Vacaru, H. M. Duan, A. M. Herman, Phys. Rev. B **7**, 8327 (1993).
[5] Sung-Ik Lee, Mun-Seog Kim, Jim-Nam Park *et al.*, Czech. J. Phys. **46**, 1781 (1996).
[6] L. N. Bulaevskii, M. Ledvij, and V. G. Kogan, Phys. Rev. Lett. **68**, 3773 (1992).
[7] Z. Tezanović, L. Xing, L. N. Bulaevskii *et al.*, Phys. Rev. Lett. **69**, 3563 (1992).
[8] A. Yu. Martynovich and A. N. Artemov, Phys. Rev. B **56**, 14827 (1997).
[9] V. N. Ryzhov and E. E. Tareyeva, Phys. Rev. B **49**, 6162 (1994).
[10] P. G. de Gennes, *Superconductivity of Metals and Alloys*, W. A. Benjamin, Inc., New York, 1966 [Russian translation, Mir, Moscow, 1968].
[11] L. D. Landau and E. M. Lifshitz, *Electrodynamics of Continuous Media*, Pergamon Press, New York [Russian original, Nauka, Moscow, 1982].
[12] R. Balescu, *Equilibrium and Nonequilibrium Statistical Mechanics*, John Wiley and Sons, New York, 1975 [Russian translation, Mir, Moscow, 1978].
[13] M. R. Beasley, J. E. Mooij, and T. P. Orlando, Phys. Rev. Lett. **42**, 1165 (1979).
[14] J. Pearl, Appl. Phys. Lett. **5**, 65 (1964).

Translated by M. E. Alferieff

Synthesis of a bulk crystalline phase of carbon nitride

V. P. Dymont,[a] E. M. Nekrashevich, and I. M. Starchenko
Institute of Solid State Physics and Semiconductors, National Academy of Sciences of Belarus, 220076 Minsk, Belarus

(Submitted 10 August 1998)
Pis'ma Zh. Éksp. Teor. Fiz. **68**, No. 6, 466–468 (25 September 1998)

A crystalline phase, whose lattice parameters are close to those of theoretically predicted carbon nitride, is synthesized by a high-pressure technique from a precursor containing carbon, nitrogen, and hydrogen.
 [S0021-3640(98)00618-5]

PACS numbers: 81.05.Je, 81.20.Zx

The works of Liu and Cohen,[1,2] win which a value of the bulk modulus (427 GPa) comparable to that of diamond (443 GPa) was obtained on the basis of quantum-chemical calculations of the structural and electronic properties of the hypothetical carbon nitride C_3N_4, initiated many attempts to synthesize this substance. A quite complete review of works concerning the synthesis and investigation of the properties of carbon nitride is given in Refs. 3 and 4. Most experimental works concern the production of carbon–nitrogen films and the investigation of their physical properties. As for the synthesis of a bulk crystalline carbon–nitrogen phase, we know of only one work[5] where a crystalline phase, which x-ray diffraction shows to be cubic and different from all of the theoretically predicted crystal structures, was obtained from a mixture of carbon (graphite, amorphous, carbon or C_{60}) and nitrogen at pressure 30 ± 5 GPa and temperature 2000–2500 K.

In the present letter we report the results of synthesis of a bulk carbon–nitrogen phase from a precursor containing carbon, nitrogen, and hydrogen.

The precursor was synthesized in an ammonia solution of sodium acetylenide by an electrochemical process, following a procedure similar to that described in Ref. 6. The result was a substance which consists of a light-brown powder. X-ray diffraction analysis, performed at room temperature using CuK_α radiation, showed that the powder has no crystal structure (Fig. 1a). Figure 2a shows the IR spectrum of the precursor. A number of well-defined absorption bands are observed in the room-temperature spectrum in the region 1000–4000 cm^{-1}. The wide band in the region 3600–3100 cm^{-1} could be due to vibrations of the N—H bond. The absorption band in the region 2800–3000 cm^{-1} is due to C—H vibrations, the shape of this peak showing definitely that sp^3–CH_3 groups make the main contribution. The band at 1700 cm^{-1} can be attributed to vibrations of the double bond C═N, while the band at 1630 cm^{-1} can be attributed to sp^2—C═C vibrations, which are ordinarily IR-inactive. The appearance of this band attests indirectly to the presence of carbon and nitrogen bonds. The band at 1550 cm^{-1} can be attributed

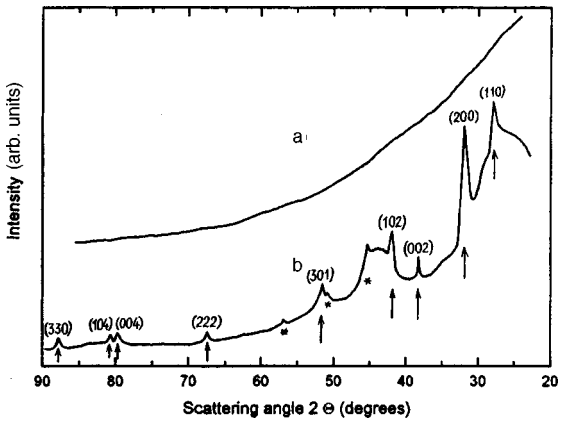

FIG. 1. Room-temperature diffraction pattern obtained in Cu$K\alpha$ radiation: a — for the precursor, b — for the substance synthesized under pressure.

to vibrations of the NH_2 group. The narrow absorption line at 1380 cm^{-1} is most likely due to the presence of CH_3C groups in the material.

It is well known[7] that synthesis under high-pressure conditions could be effective for obtaining carbon nitride. We employed the high-pressure method of synthesis. High pressure was produced in an apparatus of the type using an anvil with a recess against a toroid. Taking into consideration the results of Ref. 8, where the conditions for thermodynamic stability of covalent carbon nitride were estimated, we performed a series of syntheses under comparatively soft conditions — pressures up to 6 GPa and temperatures up to 400 °C. As a result, a black polycrystalline substance was obtained from the precursor. The x-ray diffraction pattern of the synthesized material is presented in Fig. 1b. A series of narrow reflections of a new crystalline phase is observed against a background consisting of two wide lines (half-width about 4°), which on the basis of their angular positions can be attributed to reflections from the {002} and {101} planes of polycrystalline graphite. The set of observed interplanar distances can be described on the basis of

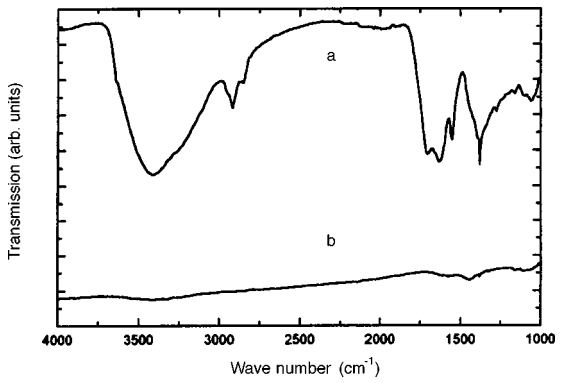

FIG. 2. IR transmission spectra: a — precursor, b — substance synthesized under pressure.

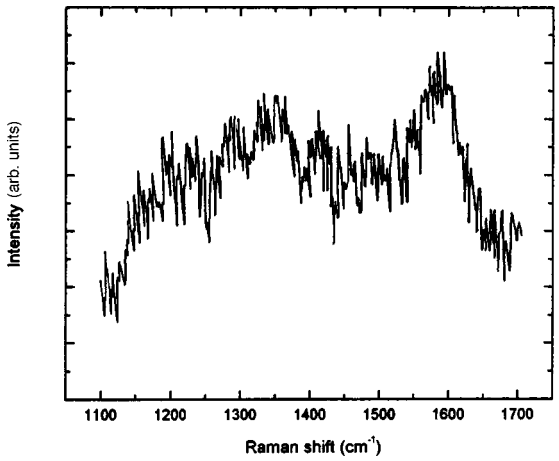

FIG. 3. Raman scattering spectrum of the substance synthesized under pressure.

a hexagonal unit cell with the parameters $a = 6.65$ Å and $c = 4.82$ Å. The computed positions of the reflections are marked by arrows in Fig. 1b. The lines with $d = 2.02$, 1.82, and 1.63 Å, which are not indexed on the basis of a hexagonal cell, could belong to the (206), (400), and (109) reflections of carbyne — a linear allotropic modification of carbon.[9]

The IR spectrum of the synthesized substance has essentially no absorption bands in the range 1000–4000 cm^{-1} (Fig. 2b). This indicates that the synthesis conditions have effected a radical transformation of the ensemble of chemical bonds in the initial substance.

Figure 3 shows the room-temperature Raman scattering spectrum of the synthesized substance at excitation wavelength $\lambda = 514.5$ nm. Very weak bands centered at ~ 1350 and 1600 cm^{-1}, which correspond to scattering from disordered graphite, can be distinguished in the spectrum.

It can be concluded on the basis of x-ray diffraction analysis that the substance obtained consists of a mixture of at least three phases: a poorly ordered graphite phase, a phase which is possibly α-carbyne, and a hexagonal phase whose lattice parameters are quite close to those of hypothetical carbon nitride. Many different crystal structures with different cell parameters and symmetry have been proposed for carbon nitride.[2] For example, hexagonal α-C_3N_4 would have parameters $a = 6.47$ Å and $c = 4.71$ Å, while for hexagonal β-C_4N_3, where some nitrogen atoms are replaced by carbon, $a = 6.45$ Å and $c = 4.80$ Å.[8] The lattice parameters of our hexagonal phase are close to those of β-C_4N_3. The somewhat larger value of the parameter a (the difference is 3%) is most likely due to the characteristic structural features of covalent carbon nitride.

Additional investigations must be performed in order to say anything more definite about the structure and composition of the crystalline phase that we obtained. However, it can be inferred with high probability that we have successfully synthesized crystalline carbon nitride.

[a)]e-mail: ryzkov@ifttp.bas-net.by

[1]A. Y. Liu and M. L. Cohen, Science **245**, 841 (1989).
[2]A. Y. Liu and M. L. Cohen, Phys. Rev. **41**, 10727 (1990).
[3]D. Marton, K. J. Boyd, and J. W. Rabalais, Int. J. Mod. Phys. B **9**, 3527 (1995).
[4]B. L. Korsunskiĭ and V. I. Pepekin, Usp. Khim. **66**, 1003 (1997).
[5]J. H. Nguyen and R. Jeanloz, Mater. Sci. Eng., A **209**, 23 (1996).
[6]V. P. Novikov and V. P. Dymont, Pis'ma Zh. Éksp. Teor. Fiz. **22**, 39 (1996) [Tech. Phys. Lett. **22**, 283 (1996)].
[7]D. M. Teter and R. J. Hemley, Science **271**, 53 (1996).
[8]V. V. Odintsov and V. I. Pepekin, Dokl. Ross. Akad. Nauk **343**, 210 (1995).
[9]T. Hughbanks and Y. Tian, Solid State Commun. **96**, 321 (1995).

Translated by M. E. Alferieff

Investigation of the crystallization of liquid iron under pressure: extrapolation of the melt viscosity into the megabar range

V. V. Brazhkin[a)]

Institute of High-Pressure Physics, Russian Academy of Sciences, 142092 Troitsk, Moscow Region, Russia

(Submitted 11 August 1998)
Pis'ma Zh. Éksp. Teor. Fiz. **68**, No. 6, 469–474 (25 September 1998)

Measurements are made of the average size of the crystallites in Fe samples obtained by rapid quenching from the melt at high pressures up to 95 kbar. The data obtained make it possible to estimate the pressure dependence of the viscosity of the Fe melt. It is found that, contrary to the existing empirical models, the viscosity increases along the melting curve under compression. Extrapolation of the pressure dependences obtained to the P,T conditions corresponding to the Earth's core gives extremely high values of the viscosity, ranging from 10^2 Pa·s up to 10^{11} Pa·s in the outer core, which suggests that the inner core is in a glassy state. The possibility that the lines of vitrification and melting of substances intersect in the megabar range is discussed. © *1998 American Institute of Physics.* [S0021-3640(98)00718-X]

PACS numbers: 61.50.Ks, 64.70.Dv

1. Unlike the case of metals in the crystalline state, reasearch on the properties of liquid metals under high pressure has been extremely fragmentary. This is especially true of the kinetic properties, such as the viscosity and self-diffusion coefficient.[1] At the same time it is difficult to exaggerate the importance of information about these characteristics for a number of metallic melts under high pressures, since a substantial portion of the deep interior of celestial bodies, including the Earth's outer core, is in a liquid metallic state under conditions of high static compression.[2,3]

For liquid metals, reliable data have been obtained only for the viscosity under pressure in Hg up to pressures of 10–12 kbar[4] and for the self-diffusion coefficients of Cs, K, and Na up to pressures of 3–4 kbar.[5] The increase in the viscosity and the decrease in the self-diffusion coefficients in metallic melts under compression are negligible — only several tens of percent under pressures $\sim$10 kbar.[4,5]

Different empirical models are used to describe the viscosity of metallic melts. According to Ref. 1, the viscosity of liquids remains virtually constant along the melting curve. This signifies that the viscosity and diffusion coefficient depend only on the reduced temperature T/T_m, where T_m is the melting temperature. The weak pressure dependence of the self-diffusion coefficient along the melting curve has been proved theoretically only for systems with a homogeneous potential function.[6] On the basis of

the Arrhenius temperature and pressure dependences of the viscosity

$$\eta \sim \exp\left(\frac{E_{\mathrm{act}_0} + PV_{\mathrm{act}}}{kT}\right), \tag{1}$$

where V_{act} is the activation volume, E_{act_0} is the activation energy at normal pressure, the activation volume for liquid metals is very small, $\sim 0.05\, V_{\mathrm{at}}$, where V_{at} is the atomic volume.[1,7]

We note that for other classes of melts — organic liquids and liquid inert gases — the increase in the viscosity with pressure is much larger: 1–3 orders of magnitude for pressure increasing up to 10 kbar and 5–14 orders of magnitude for pressure increasing up to 30–80 kbar.[8–10]

It is perhaps of greatest interest to study the viscosity and solidification of liquid Fe under pressure, since a large portion of the Earth's core apparently consists of a melt based on Fe (the inner core is thought to be crystalline). The viscosity of the melt in the core largely determines the heat and mass transfer and the Earth's magnetic field.[2,3] Different kinds of indirect experiments give extremely diverse values for the estimated viscosity of the outer core, ranging over 14 orders of magnitude — from 10^{-3} to 10^{11} Pa·s.[1]

The viscosity of Fe melts under pressure has not been investigated experimentally. The empirical models examined above[1] predict that the viscosity of liquid iron under the conditions corresponding to the Earth's core should be close to the viscosity of liquid iron at normal pressure $\sim 10^{-2}$ Pa·s,[1] but the validity of extrapolating these models to megabar pressures and over the severalfold change in the density of the melt remain open to question.[7]

Therefore investigations of the viscosity of iron melts under pressure and the construction of appropriate models that describe adequately the viscosity of liquids over a wide range of pressures and densities remain extremely urgent problems.

2. The high melting temperatures of iron (1811 K at $P=0$, ~ 5000 K at $P \sim 3$ Mbar) make it extremely difficult to perform direct measurements of the viscosity of melts under pressure. In the present work we employed the method of estimating the change in viscosity with pressure on the basis of an investigation of the average grain size in samples crystallized at different pressures.[11,12] This method has been used by the present author to investigate Pb, In, and Cu melts under pressure.[11,13] At high rates of cooling $\dot{T} > 10^3$ K/s, the condition of homogeneous nucleation and growth of crystalline grains holds for sufficiently pure melts. The grain size is determined mainly by the diffusion coefficient or viscosity and can be estimated as[12]

$$d \sim \tau U \sim C \Delta T \left(\frac{\Delta T}{T_m}\right)^2 \exp\left(\frac{-E_{\mathrm{act}}}{kT_{\mathrm{cr}}}\right), \tag{2}$$

where τ is the average grain growth time corresponding to the crystallization time; U is the grain growth rate; C depends on the cooling rate, the melting temperature and enthalpy, the surface tension, the specific volume of the solid phase, and the Debye frequency; T_{cr} is the crystallization temperature of the melt; ΔT is the amount of supercooling ($\Delta T = T_m - T_{\mathrm{cr}}$); and, E_{act} is the effective diffusion activation energy, which determines the viscosity. To a first approximation, the relative change of grain size with

pressure in samples crystallized in the P,T region of stability of one phase corresponds to the relative change in the melt viscosity with pressure at the crystallization temperatures (which are close to the melting temperatures):

$$\frac{\eta(P_1)}{\eta(P_2)} \approx \frac{d(P_2)}{d(P_1)}. \tag{3}$$

Therefore the empirical models proposed in Ref. 1 predict that the same grain size in samples crystallized at different pressures.

3. Iron with a purity of 99.99% was used in experiments. Pressure in the 10–95 kbar range was produced in a chamber of the ''toroid'' type. The sample, consisting of a cylinder 2 mm high and 2 mm in diameter pressed from Fe powder, was placed inside an ampul made from a NaCl single crystal. The ends of the sample were in contact with Fe caps having a diameter of 6 mm. The sample was heated and cooled by direct passage of an ac current pulse of duration ~ 0.3 s, with $J \sim 1.5$–2 kA and $U \sim 2$–3 V. The measured average cooling rate of the melt near the melting temperature was, to a high degree of accuracy, the same as the value estimated from the heat conduction equations and equalled $3-5\times 10^3$ K/s. As the pressure increased from 20 to 95 kbar, the average cooling rate increased by only 30–40%. The size and morphology of the crystal grains were investigated on an MBS-10 optical microscope and a Stereoscan MK2 scanning electron microscope. We investigated both cleavage surfaces of the sample, which was cleaved in nitrogen, and polished sections that had been treated in the appropriate etchants. We note that on cooling at pressures $0 < P < 50$ kbar the iron melt crystallizes in the bcc δ phase, while for $P > 50$ kbar it crystallizes in the fcc γ phase. The small changes in volume which accompany phase transformations in solid iron on cooling ($\sim 1\%$ for the γ–α transition and 0.5% for δ–γ) and the high plasticity of the crystals suggest that grain-size reduction did not occur in the solid state. Repeated melting–solidification of the samples did not show an appreciable change in crystallite size, in agreement with the assumption of homogeneous nucleation.

The average radius of the columnar crystals was taken as the grain size. The data obtained are presented in Fig. 1. It is obvious that a large change in grain size (by almost a factor of 3 with a pressure change of 40 kbar) does not correspond to the models examined in Ref. 1.

4. The estimated change in the viscosity of the Fe melt under pressure ranging from 56 to 95 kbar corresponds to an effective activation volume $V_{act} \sim (0.35$–$0.4)V_{at}$. The different level of absolute values of the grain size in iron polycrystals obtained at pressures $P < 50$ kbar and 56 kbar $< P <$ 95 kbar is apparently due to the different values of the surface tension of the melt relative to the δ- and γ-phase crystals. Previous investigations of the viscosity of melts of substances such as Pb, In, and Cu under pressures up to 80 kbar also established pressure dependences of the viscosity that correspond to activation volumes $V_{act} \sim (0.2$–$0.35)V_{at}$.[11,13] It can be inferred that the increase in the effective activation volume for the viscosity of metallic melts from $\sim 0.05\,V_{at}$ at pressures $P < 10$ kbar to $(0.2$–$0.4)V_{at}$ at pressures $P \geqslant 30$ kbar is a quite general phenomenon. In consequence, the empirical models examined in Ref. 1 are incorrect starting at pressures of several tens of kilobars. We note that the effective activation volumes for molecular organic liquids and liquid inert gases under pressure are $(0.2$–$0.4)V_{mol}$, where

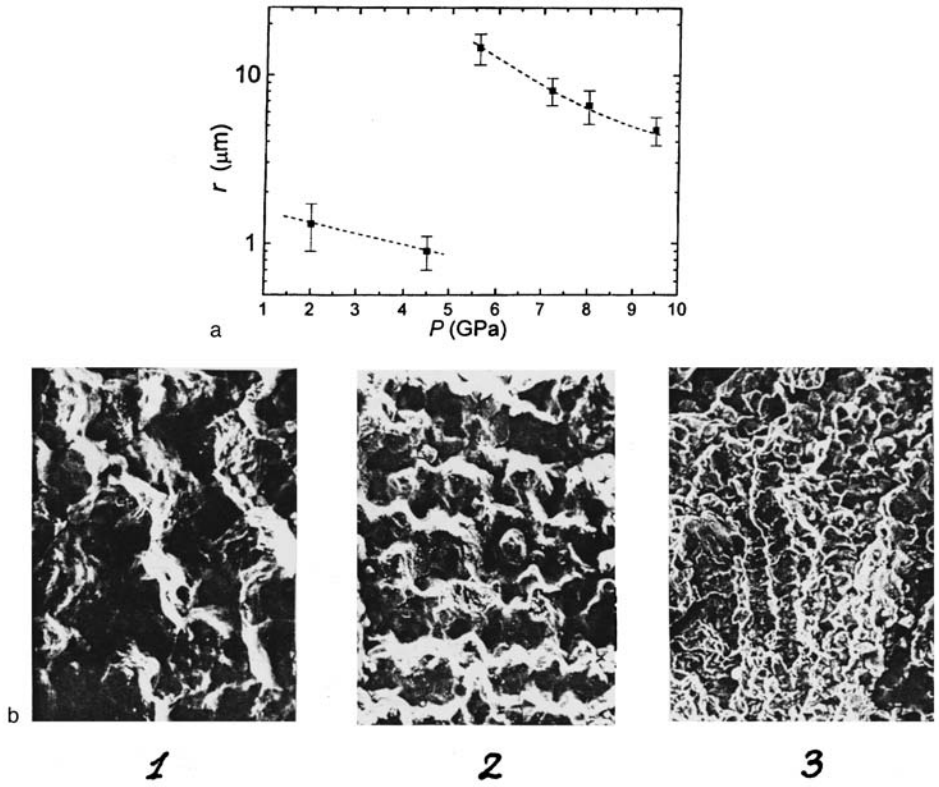

FIG. 1. a) Average grain size in iron samples obtained by rapid cooling from the melt ($\dot{T}\sim 5\times 10^3$ K/s) versus the pressure under which quenching was conducted. b) Photographs (with the same magnification) of cleaved surfaces of Fe samples obtained under different pressures: *1* — 56 kbar, *2* — 72 kbar, *3* — 95 kbar. The size of the fields presented is 190 μm×140 μm.

$V_{\rm mol}$ is the volume of a molecule.[8,9] The effective activation volume for self-diffusion coefficients in crystals under pressure is $(0.3–1)V_{\rm at}$ (Ref. 7), i.e., the activation volume in melts under pressure approaches values characteristic for solids.

Extrapolation of the viscosity of liquid iron to the P,T conditions corresponding to the Earth's core (see Fig. 2) gives $\sim 10^2$ Pa·s near the core–mantle boundary ($P\approx 1.3$ Mbar, $T\approx 4000$ K, melt density $\rho\approx 10.5$ g/cm^3) and 10^8–10^{11} Pa·s near the boundary of the outer and inner cores ($P\sim 3.3$ Mbar, $T\sim 5000$ K, $\rho\approx 13.5$ g/cm^3). The fact that the viscosity reaches $\sim 10^{10}$–10^{11} Pa·s at the boundary of the Earth's inner core signifies that with respect to seismic oscillations with frequency $\nu\geqslant 1$ Hz an iron melt will behave like a solid.[2] The idea that the Earth's core is a viscoelastic body with the viscosity increasing in the inner part up to values corresponding to glass was advanced quite a long time ago.[2] In the light of the estimates presented above there are good reasons to believe that the hypothesis of a glassy state in the Earth's inner core deserves another look. The high values of the viscosity in the Earth's outer core $\sim 10^4$–10^6 Pa·s, which were estimated from data on the damping of seismic waves,[2] were apparently correct and corresponded to an average value between 10^2 Pa·s and 10^{10} Pa·s in the outer core. Such values of the

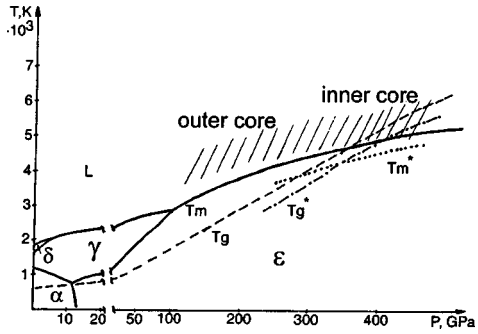

FIG. 2. P,T phase diagram of Fe. The hatched region corresponds to the P,T conditions in the Earth's core. The glass temperature of iron is shown by the dashed line, and the provisional melting temperature T_m^* and glass temperature T_g^* of the material in the Earth's core are shown by the dotted and dot-and-dash lines, respectively.

viscosity can lead to a nonadiabatic temperature distribution in the core. The anomalously high (for crystalline metals) experimentally measured value of the Poisson's ratio of the inner core, ~ 0.44,[2] has a natural explanation on the basis of the hypothesis that the interior zone of the core is in a metallic-glass state. New data on the anisotropy[14] and the precession[15] of the inner core could also find an explanation on the basis of the concept of gradual vitrification of the core during the Earth's evolution and continuing slow convection in the inner core.

We note that on account of the large increase of the viscosity of an Fe melt under compression, rapid cooling ($\sim 10^3$–10^6 K/s) of the melt under pressures $P > 0.5$–1 Mbar should lead to solidification into a nanocrystalline or amorphous state, which admits a direct experimental check.

5. The data obtained do not agree with the assumption that the viscosity of metallic melts is constant along the melting curve. On the basis of an Arrhenius-type pressure dependence the condition of constant viscosity means that $PV_{\rm at}/T = $ const (if we neglect $E_{\rm act_0}$ and assume that $V_{\rm act}$ and $V_{\rm at}$ are proportional quantities). For a large increase in density this condition corresponds to the relation

$$\rho^{3-4}T^{-1} = \text{const}, \tag{4}$$

since $P \sim (\Delta\rho)^{4-5}$ (Ref. 16), where $\Delta\rho$ is the density change under pressure. The condition

$$T_m \sim \rho^{1-1.5} \tag{5}$$

holds along the melting curve of iron in the megabar range.[17] Correspondingly, we have for the viscosity along the melting curve

$$\eta \sim \exp(C_1\rho^{1.5-2.5}) \sim \exp(C_2 P^{0.4-0.7}), \tag{6}$$

where C_1 and C_2 are constants.

The pressure and temperature dependences of the viscosity determine the position of the vitrification line $T_g(P)$ in the T,P plane. It is known that vitrification is determined mainly by the repulsive part of the effective pair potential

$$\rho T_g^{-3/n} = \text{const}, \tag{7}$$

where n is the exponent in the repulsive potential.[18] For Fe the effective pair potential with a repulsive part $\sim 1/r^8$ has been used successfully in a wide range of densities and temperatures.[19] This corresponds to the condition

$$T_g \sim \rho^{8/3}, \tag{8}$$

in good agreement with the condition (4) for lines of constant viscosity. It follows from Eqs. (5) and (8) that at high pressures the curve $T_g(P)$ can intersect the melting curve. For the standard relation for metals under normal pressure $T_g \approx (0.3\text{–}0.4)T_m$, the $T_g(P)$ and $T_m(P)$ curves should intersect when the density of the melt has increased by a factor of 2–2.5, which agrees completely with the estimates presented above for the vitrification of the Earth's inner core. We note that melting is likewise mainly determined by the repulsive potential, but the contribution of the attractive part of the potential to the dependence $T_m(P)$ for metals is very substantial all the way up to megabar pressures,[20] and this leads to the weaker dependence (5).

The intersection of the curves $T_g(P)$ and $T_m(P)$ (see Fig. 2) signifies that vitrification under compression is possible in the P,T region of stability of the melt. An increase of the viscosity of melts to values characteristic for glasses at temperatures $T > T_m$ should lead to extremely long melting times of the corresponding crystals and the possibility of superheating of the crystals right up to the vitrification (glass) temperature during the experimental times.

I thank S. M. Stishov, A. G. Lyapin, and S. V. Popov for many helpful suggestions and fruitful discussions and N. F. Borovikov, N. V. Kalyaev, and P. I. Artemov for assisting in the experiments.

[a)]e-mail: brazhkin@hppi.troitsk.ru

[1] J. P. Poirier, Geophys. J. **92**, 99 (1988).
[2] D. L. Anderson, *Theory of the Earth*, Blackwell Scientific Publications, Boston, 1989.
[3] W. B. Hubbard, *Planetary Interiors*, Van Nostrand Reinhold Company Inc., 1984 [Russian translation, Mir, Moscow, 1987].
[4] P. W. Bridgman, *Collected Experimental Papers*, Harvard University Press, Cambridge, Mass., 1964, Vol. IV, Paper 72, p. 2155.
[5] M. Hsieh and R. A. Swalin, Acta Metall. **22**, 219 (1974).
[6] V. V. Zhakhovskiĭ, Zh. Éksp. Teor. Fiz. **105**, 1615 (1994) [JETP **78**, 871 (1994)].
[7] R. W. Keyes in *Solids Under Pressure*, edited by W. Paul and D. M. Warschauer, McGraw-Hill, New York, 1963, p. 71.
[8] N. J. Trappeniers, P. S. van der Gulik, and H. van den Hooff, Chem. Phys. Lett. **70**, 438 (1980).
[9] P. W. Bridgman, *Collected Experimental Papers*, Harvard University Press, Cambridge, MA, 1964, Vol. VI, Paper 166, p. 3903.
[10] R. G. Munro, G. J. Piermarini, and S. Block, Rev. Phys. Chem. Jpn. **50**, 79 (1980).
[11] V. V. Brazhkin, V. I. Larchev, S. V. Popova, and G. G. Skrotskaya, Phys. Scr. **39**, 338 (1989).
[12] V. V. Brazhkin and S. V. Popova, Rasplavy **4,** 97 (1989).
[13] V. V. Brazhkin and S. V. Popova, Rasplavy **1**, 10 (1990).
[14] V. V. Kuznetsov, Usp. Fiz. Nauk **167**, 1001 (1997).
[15] X. Song and P. G. Richards, Nature (London) **382**, 221 (1996).
[16] M. W. Gunian and D. J. Steinberg, J. Phys. Chem. Solids **35**, 1501 (1974).
[17] R. Boehler, Nature (London) **363**, 534 (1993).

[18] A. Tolle, H. Schober, J. Wuttke *et al.*, Phys. Rev. Lett. **80**, 2374 (1998).
[19] J. M. Wills and W. A. Harrison, Phys. Rev. B **28**, 4363 (1983).
[20] S. M. Stishov, Usp. Fiz. Nauk **114**, 3 (1974) [Sov. Phys. Usp. **17**, 625 (1975)].

Translated by M. E. Alferieff

Collective effects accompanying magnetization of two-dimensional lattices of nanosize magnetic particles

S. A. Gusev, L. A. Mazo, I. M. Nefedov, Yu. N. Nozdrin, M. V. Sapozhnikov, L. V. Sukhodoev, and A. A. Fraerman[a)]
Institute of Microstructure Physics, Russian Academy of Sciences, 603600 Nizhniĭ Novgorod, Russia

(Submitted 8 May 1998; resubmitted 11 August 1998)
Pis'ma Zh. Éksp. Teor. Fiz. **68**, No. 6, 475–479 (25 September 1998)

Collective effects arising in a two-dimensional lattice of nanosize magnetic particles as a result of the dipole interparticle interaction are investigated by Hall magnetometry. The experimental system consists of 10^5 permalloy particles having a diameter of ~ 40 nm and a height of ~ 40 nm and forming a lattice with a rectangular unit cell (90 nm $\times$ 180 nm). We attribute the characteristic features observed in the magnetization curves to quasi-one-dimensionality of the experimental lattice of particles and to the formation of solitons in chains of dipoles.
 [S0021-3640(98)00818-4]

PACS numbers: 75.70.−i, 75.50.Tt, 75.30.−m

One reason for the collective behavior of a system of single-domain magnetic particles is their dipole interaction. In the case of ordered lattices of nanosize particles this interaction produces long-range order in the orientation of the magnetic moments of the particles, the type of order being determined by the lattice symmetry.[1] The possibility of the existence of a temperature-induced phase transition in a two-dimensional system of superparamagnetic particles interacting by dipole forces was pointed out in Ref. 2, for example. Since the interaction energy of the particles is proportional to their squared magnetic moment, the superparamagnetic phase transition temperature should be quite high. This temperature can be controlled by varying the particle size and the interparticle distance. Such a phase transition may have been detected in self-organized irregular lattices of nanosize magnetic particles.[3,4]

In our work we investigated the effects of a dipole interaction in regular two-dimensional lattices of single-domain particles with controllable parameters. It was observed that the magnetization curves (the shapes of the hysteresis loops) depend on the orientation of the external magnetic field relative to the axes of the particle lattice and on the temperature. For a square lattice there is no magnetization hysteresis.

Two-dimensional lattices of nanosize magnetic particles were produced from permalloy films (Ni_3Fe) by electronic lithography. The films were laser deposited on a substrate. Exposure of the electronic resist and investigation of the morphology of the lattices obtained were conducted in a JEM-2000EX electron microscope. Patterns were produced using C_{60} fullerene films as negative electron resists and Ti films as transmitting

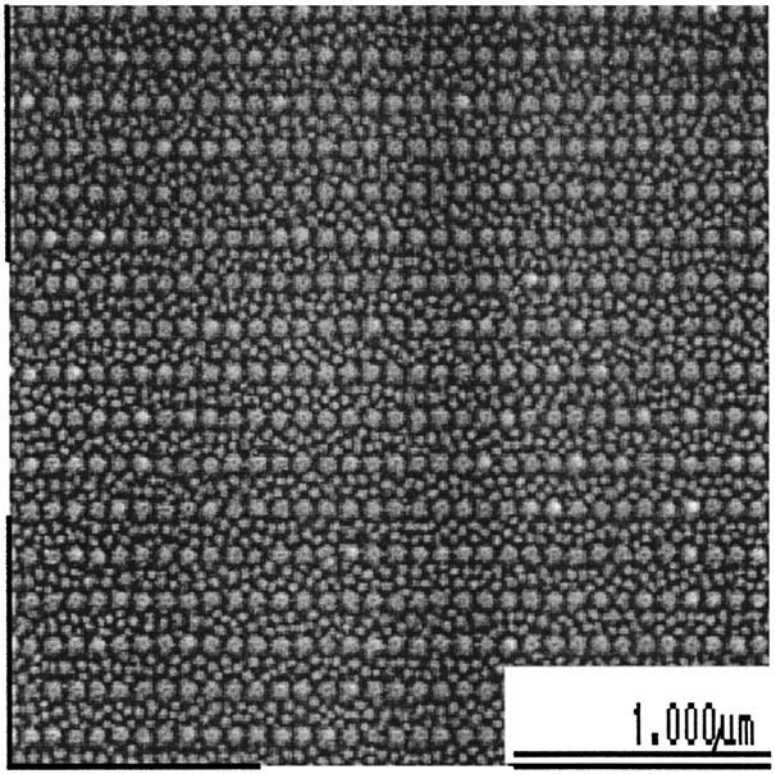

FIG. 1. Secondary-electron image of a lattice of nanosize magnetic particles. The image was obtained in a scanning electron microscope: a periodic lattice of 40–50 nm size permalloy particles can be seen against a background consisting of 10 nm irregularities of the substrate (result of ion etching).

layers. Plasma-chemical etching of the Ti layers was performed in a CF_2Cl_2 atmosphere, while ion etching in an Ar atmosphere was used to transfer a figure to the permalloy film. This method makes it possible to produce two-dimensional lattices consisting of cylindrically shaped particles ranging from 15 to 100 nm in diameter and from 10 to 50 nm in height, which is determined by the thickness of the initial Ni_3Fe film.[5] A system containing approximately 10^5 particles with diameters $\sim 40-50$ nm and heights ~ 45 nm, forming a lattice with a 90 nm$\times$180 nm rectangular unit cell (Fig. 1), was prepared for the magnetic measurements. Existing data show permalloy particles of this size to be single-domain.[6,7]

Just as in Ref. 8, a difference scheme, consisting of two semiconductor (InSb) Hall sensors with common potential contacts and independent current contacts was used to investigate the magnetic properties. The size of the working zone of the sensors was 50×100 μm and the thickness was ~ 10 μm. The Hall bridges were manufactured by the Scientific and Industrial Association ''Sensor'' (St. Petersburg). The system investigated was produced in the working zone of one of the sensors. The method developed makes it possible to measure the magnetic moment component perpendicular to the sample plane to within ~ 0.1 G in an up to 10 kOe external field in a wide temperature

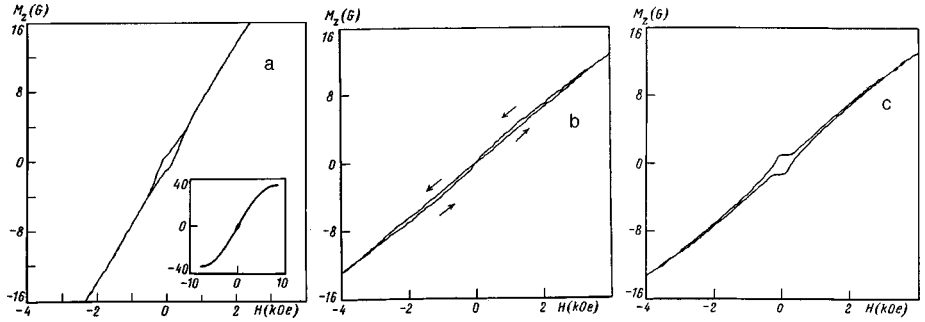

FIG. 2. a) M_z versus the magnetic field applied in the direction $\theta=0°$. Inset: Magnetization curve up to saturation fields. b) M_z versus the magnetic field applied in the direction $\theta=45°$, $\varphi=0°$. c) M_z versus the magnetic field applied in the direction $\theta=45°$, $\varphi=90°$.

range. It follows from the symmetry of the system and the anisotropic character of the dipole interaction that the easy axis lies in the plane of the sample and is parallel to the shortest lattice vector. This anisotropy should be manifested as hysteresis when the sample is magnetized in the indicated direction.

We shall characterize the direction of the external field by two angles θ and φ, where θ is the angle measured from the normal to the sample (z axis) and φ is the azimuthal angle measured from the axis directed parallel to the particle chains (x axis). Since the method employed makes it possible to measure only the perpendicular component of the magnetic moment, to investigate anisotropy in the sample plane we performed measurements for three orientations of the external field: 1) $\theta=0$; 2) $\theta=\pi/4$, $\varphi=0$; 3) $\theta=\pi/4$, $\varphi=\pi/2$. The magnetization curves obtained at $T=4.2$ K are presented in Fig. 2. The hysteresis in Fig. 2b is qualitatively identical to expectations and attests to the existence of an easy axis parallel to the shortest lattice vector. The existence of a remanent magnetic moment for magnetization in the geometries 1 and 3 was unexpected. The dependence of the magnetization curves on the orientation of the field relative to the lattice axes cannot be explained by the properties of an individual particle and is a manifestation of the collective behavior of the particles.

The remanent magnetization could be due to the formation of nonuniform states (solitons) in the experimental system, which is close to being quasi-one-dimensional. Indeed, our calculations of the Fourier components of the dipole tensor show that the interparticle interaction energy in the chains is approximately an order of magnitude greater than the interchain interaction energy. When a field is applied in the geometries 1 and 3, two equilibrium states with the same energy and different sign of the x component of the magnetic moment exist in the dipole chain, and therefore domain formation is possible. An analytical determination of the structure of the domain wall encounters substantial difficulties even for an isolated dipole chain. For this reason, we solved the problem numerically, using the system of relaxation equations[9]

$$\frac{\partial M_i(\overline{r})}{\partial t}=-\frac{\partial E}{\partial M_i(\overline{r})}, \quad i=x,y,z,$$

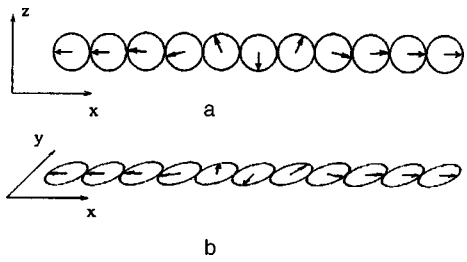

FIG. 3. View of a soliton in a dipole chain: a) for $H_0=9$, $K=3$, b) for $H_0=0$, $K=0$.

$$E=\frac{1}{2}\sum_{\bar{r}\neq\bar{r}'} D_{ik}(\bar{r}-\bar{r}')M_i(\bar{r})M_k(\bar{r}')-H_{0i}\sum_{\bar{r}} M_i(\bar{r})-\frac{1}{2}K\sum_{\bar{r}} M_z^2(\bar{r}), \tag{1}$$

$$D_{ik}(\bar{r})=\frac{\delta_{ik}}{r^3}-\frac{3r_ir_k}{r^5},$$

where $M_i(\bar{r})$ is the ith component of the magnetic moment of a particle located at the point with radius vector $\bar{r}$, $|\bar{M}(\bar{r})|=1$, $\bar{H}_0$ is the external magnetic field, and K is the single-particle anisotropy constant. The initial conditions for solving the system (1) were chosen in the form $M_z(\bar{r},0)=1$. No conditions were imposed at the boundary of the sample. The form of a domain wall (soliton) in a dipole chain for $H_0=0$ and different values of the single-particle anisotropy constant K is presented in Fig. 3. We note that a soliton possesses antiferromagnetic structure and its total zero-field magnetization in the case $K=0$ is zero. A necessary condition for a soliton to possess a magnetic moment is that single-particle anisotropy must be present. In this case the total magnetic moment of a soliton can reach the value of the magnetic moment of a particle. Specifically, for $K=3$ the total magnetization is 0.8. The calculations performed suggest the following mechanism for the appearance of a remanent magnetization with the external field orientation perpendicular to the particle chains (in the geometries 1 and 3). Since the system is quasi-one-dimensional in fields close to the saturation value, the soliton energy is low and thermally induced formation of solitons is possible. As the field decreases in magnitude, the soliton energy increases and the characteristic size of solitons decreases. This leads to soliton pinning associated with the discreteness of the lattice. Therefore the remanent magnetization is due to the presence of ''frozen-in'' solitons which are produced in high fields. A necessary condition for the existence of remanent magnetization is the presence of a perpendicular anisotropy for the particles comprising the lattice. The hypothesis advanced above is confirmed indirectly by our measurements of the magnetization curves of a particle lattice with a square unit cell, showing no remanent magnetization for any orientation of the external field. Numerical modeling likewise shows no solitons and no remanent magnetization in a square lattice. The question of whether or not the system studied undergoes a transition into a superparamagnetic state can be solved by investigating the temperature dependence of the observed collective effects. The qualitative changes occurring in the magnetization curve of a sample with a rectangular unit cell as the sample temperature increases up to 77 K attest to the existence of such a dependence (Fig. 4). We believe that from the fundamental standpoint the results

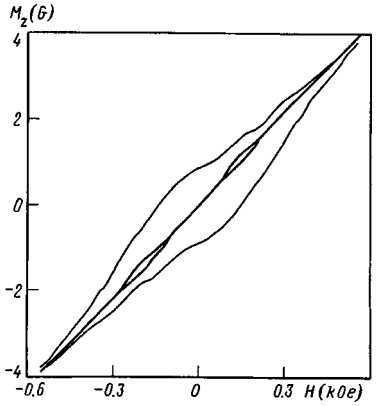

FIG. 4. Variation of the shape of the magnetization curve ($\theta = 0°$) with temperature increasing from 4.2 K (fine line) to 77 K (heavy line).

obtained are of great interest as an example of the behavior of a classical two-dimensional magnetic system with a precisely known interaction. The samples themselves and the technology for producing them and for performing the measurements could be helpful for ultrahigh-density magnetic recording media which are currently being widely developed.

We thank A. A. Andronov, S. V. Gaponov, and N. N. Salashchenko for some stimulating discussions and for assistance. This work was performed as part of Project 98-02-16183 of the Russian Fund for Fundamental Research and the program ''Physics of Solid-State Nanostructures.''

[a)]e-mail: andr@ipm.sci-nnov.ru

[1] V. M. Rozenbaum, V. M. Ogenko, and A. A. Chuĭko, Usp. Fiz. Nauk **161**, 79 (1991) [Sov. Phys. Usp. **34**, 883 (1991)].
[2] S. Morup, P. H. Christensen, J. Franck *et al.*, J. Magn. Magn. Mater. **40**, 163 (1983).
[3] A. Sugawara and M. R. Scheinfein, Phys. Rev. B **56**, R8499 (1997).
[4] J. Hauschild, H. J. Elmers, and U. Gradmann, Phys. Rev. B **57**, R677 (1998).
[5] S. A. Gusev, E. B. Kluenkov, L. A. Mazo *et al.*, *Abstracts of IWFAC'97*, St. Petersburg, 1997, p. 296.
[6] A. A. Bukharaev, D. V. Ovchinnikov, N. I. Nurgazizov *et al.*, *Proceedings of the Working Conference on ''Probe Microscopy''*, Nizhniĭ Novgorod, 1998.
[7] S. A. Nepeĭko, *Physical Properties of Small Metallic Particles*, Naukova Dumka, Kiev, 1985.
[8] A. D. Kent, S. von Molnar, S. Gider, and D. D. Awschalom, J. Appl. Phys. **76**, 6656 (1994).
[9] P. I. Belobrov, R. S. Gekht, and V. A. Ignatchenko, Zh. Éksp. Teor. Fiz. **84**, 1097 (1983) [Sov. Phys. JETP **57**, 636 (1983)].

Translated by M. E. Alferieff

Quasielastic magnetic scattering of neutrons by heavy-fermion systems

A. S. Mishchenko
Kurchatov Institute Russian Science Center, 123182 Moscow, Russia

(Submitted 12 August 1998)
Pis'ma Zh. Éksp. Teor. Fiz. **68**, No. 6, 480–485 (25 September 1998)

A theory of quasielastic scattering by a spin liquid with resonating valence bonds is constructed. It is demonstrated that the dependence of the scattering cross section of the spin liquid on the energy transfer has the same shape as the quasielastic peak observed experimentally in heavy-fermion systems. It is shown that a consequence of fact that the excitations of the spin-liquid state obey Fermi statistics is that the total quasielastic scattering cross section oscillates as a function of the momentum transfer. © *1998 American Institute of Physics.*
[S0021-3640(98)00918-9]

PACS numbers: 75.25.+z, 75.20.Hr

1. Ever since the idea of describing a state with heavy fermions on the basis of the formalism of a spin liquid of the resonating valence bond (RVB) type was advanced in a number of works,[1–3] discussions of the adequacy of the proposed model have continued unabated. Despite the fact that RVBs are a quite fruitful idea for describing both the thermodynamic properties[4] and the low-energy spectral response[5] of heavy-fermion systems, an unequivocal proof of the existence of RVB-type correlations is still lacking. The main problem impeding the identification of a spin liquid is the lack of a decisive experiment that would make it possible to accept or reject the quite well-developed concept of RVBs.

The main feature of a state with RVBs is that at low temperatures a system of localized spins undergoes a transformation into a half-filled spin-excitation band whose width T^* is of the order of the Kondo temperature T_K.[3,6,7] The main property that distinguishes a correlated RVB state is that the spin-liquid excitations obey Fermi statistics. The change from Boltzmann statistics characteristic for a system of localized spins to Fermi statistics in the spin-liquid state is the circumstance whose detailed study could reveal the properties that are characteristic of only a strongly correlated state with RVBs.

In the present letter a theory of the quasielastic magnetic scattering of neutrons by a spin liquid is proposed and it is shown that on account of the Fermi statistics of spin excitations in systems with RVBs the total quasielastic scattering cross section oscillates as a function of the transferred momentum κ.

2. The basic Hamiltonian describing a state with heavy fermions is the Anderson lattice Hamiltonian for f ions which are hybridized with the conduction electrons. The canonical Coqblin–Schrieffer transformation[8,9] takes hybridization into account in sec-

ond order, and the effective Hamiltonian describing the lower doublet $\sigma=\pm$ of the state of the crystal field assumes the form of an exchange interaction $I^{\sigma\sigma'}_{\mathbf{mm}'}$ between the spin states at different sites $\mathbf{m}=\mathbf{l}$, $\boldsymbol{\xi}$ ($\mathbf{l}$ is the vector of the unit cells and $\boldsymbol{\xi}$ is a basis vector):

$$H_{ex}=\sum_{\mathbf{mm}'}^{\mathbf{m}\neq\mathbf{m}'}\sum_{\sigma\sigma'} I^{\sigma\sigma'}_{\mathbf{mm}'} f^{\dagger}_{\mathbf{m}\sigma} f_{\mathbf{m}\sigma'} f^{\dagger}_{\mathbf{m}'\sigma'} f_{\mathbf{m}'\sigma}. \tag{1}$$

The operators $f^{\dagger}_{\mathbf{m}\sigma}(f_{\mathbf{m}\sigma})$ are Fermi operators creating (annihilating) states with spin σ at site $\mathbf{m}$ and satisfy the constraint $\Sigma_\sigma f^{\dagger}_{\mathbf{m}\sigma} f_{\mathbf{m}\sigma}=1$.

The state with RVBs that arises at low temperatures is characterized in the mean-field approximation by the appearance of anomalous intersite averages $\langle f^{\dagger}_{\mathbf{m}\sigma} f_{\mathbf{m}'\sigma}\rangle$. As a result, the spin-liquid state is determined by the effective Hamiltonian

$$H^{\mathrm{eff}}_{ex}=\sum_{\mathbf{mm}'}^{\mathbf{m}\neq\mathbf{m}'}\sum_{\sigma} A_{\mathbf{mm}'} f^{\dagger}_{\mathbf{m}\sigma} f_{\mathbf{m}'\sigma}, \tag{2}$$

which describes the spectrum of uncharged Fermi excitations in the spin subsystem. The constants $A_{\mathbf{mm}'}$ are determined by the values of the exchange integrals and the anomalous averages.[5] The chemical potential μ is determined from the global constraint for N sites $N^{-1}\Sigma_{\mathbf{m}}\Sigma_\sigma\langle f^{\dagger}_{\mathbf{m}\sigma} f_{\mathbf{m}\sigma}\rangle=1$ and therefore a state with RVBs is described by a half-filled Fermi-particle band which has width $\sim T^*$ and whose spectrum is formally similar to the band spectrum in the tight-binding approximation. With the eigenvectors $\Xi^{\lambda}_{\xi\sigma}$ the eigenstates $|\lambda\rangle$ of the Hamiltonian (2) can be represented as a superposition[5]

$$|\lambda\rangle=\sum_{\mathbf{l}\xi\sigma}\exp(i\mathbf{l}\cdot\mathbf{k}_\lambda)\Xi^{\lambda}_{\xi\sigma}\varphi(\mathbf{r}-\mathbf{l}-\boldsymbol{\xi})|\sigma\rangle, \tag{3}$$

where $\varphi(\mathbf{r}-\mathbf{l}-\boldsymbol{\xi})$ are the spatial wave functions of localized f electrons, $|\sigma\rangle$ is the spin component, and $\mathbf{k}_\lambda$ is the wave vector of the state $|\lambda\rangle$. At temperature T the statistical population density of the states $|\lambda\rangle$ with energies ε_λ is determined by the occupation numbers $n_\lambda=\{1+\exp[(\varepsilon_\lambda-\mu)/T]\}^{-1}$.

3. The standard formula for the scattering function for magnetic scattering of neutrons[10] by a single magnetic ion with momentum transfer $\boldsymbol{\kappa}$ and energy loss $\hbar\omega$ is expressed in terms of the matrix elements of the operator $\hat{\mathbf{Q}}=\Sigma_{\mathbf{l}\xi}\exp\{i\boldsymbol{\kappa}\cdot(\mathbf{l}+\boldsymbol{\xi})\}\hat{\mathbf{J}}$ and the Cartesian coordinates of the unit vectors $\hat{\boldsymbol{\kappa}}_\alpha=\boldsymbol{\kappa}_\alpha/|\boldsymbol{\kappa}|$:

$$S(\boldsymbol{\kappa},\hbar\omega)=b^2N^{-1}\sum_{\alpha\beta}^{xyz}(\delta_{\alpha\beta}-\hat{\boldsymbol{\kappa}}_\alpha\cdot\hat{\boldsymbol{\kappa}}_\beta)\sum_{\lambda\lambda'}\Omega_{\lambda,\lambda'}\langle\lambda|\hat{Q}^{\dagger}_\alpha|\lambda'\rangle\langle\lambda'|\hat{Q}_\beta|\lambda\rangle\delta(\hbar\omega-\varepsilon_{\lambda'}+\varepsilon_\lambda) \tag{4}$$

(b is the magnetic scattering length[10] and $\hat{\mathbf{J}}$ is the total magnetic moment operator). The statistical function $\Omega_{\lambda,\lambda'}$ in the case of scattering by local states of the crystal field depends only on the occupation of the initial states λ and is determined by Boltzmann statistics. In the case of the Fermi statistics characteristic of a spin liquid the occupation of the final states also plays a role. As a result, $\Omega_{\lambda,\lambda'}$ assumes the form

$$\Omega_{\lambda,\lambda'}=n_\lambda(1-n_{\lambda'}). \tag{5}$$

Substituting the eigenstates (3) into expression (4) and, since the spatial wave functions of the f electrons are strongly localized, neglecting the off-diagonal (with respect to site) matrix elements of the operator $\hat{\mathbf{J}}$ we find that the neutron scattering function of a spin liquid is given by

$$S_{sl}(\boldsymbol{\kappa},\hbar\omega)=B(\kappa)\sum_{\alpha\beta}^{xyz}(\delta_{\alpha\beta}-\hat{\boldsymbol{\kappa}}_{\alpha}\cdot\hat{\boldsymbol{\kappa}}_{\beta})\sum_{\lambda\lambda'}\Omega_{\lambda,\lambda'}\Theta^{\alpha\beta}_{\lambda\lambda'}(\boldsymbol{\kappa})\,\delta(\hbar\omega-\varepsilon_{\lambda'}+\varepsilon_{\lambda}), \tag{6}$$

where

$$\Theta^{\alpha\beta}_{\lambda\lambda'}(\boldsymbol{\kappa})=I^{\lambda\lambda'}_{\alpha}(\boldsymbol{\kappa})(I^{\lambda\lambda'}_{\beta}(\boldsymbol{\kappa}))^{*}, \tag{7}$$

$$I^{\lambda\lambda'}_{\alpha}(\boldsymbol{\kappa})=\sum_{\boldsymbol{\xi}}\exp(-i\boldsymbol{\kappa}\cdot\boldsymbol{\xi})\sum_{\sigma\sigma'}(\Xi^{\lambda}_{\xi\sigma})^{*}\Xi^{\lambda'}_{\xi\sigma'}\langle\sigma|\hat{J}_{\alpha}|\sigma'\rangle. \tag{8}$$

In the formulas presented above $B(\kappa)=b^2(g_JF(\kappa)/2)^2$, where g_J is the Landé factor and $F(\boldsymbol{\kappa})$ is the magnetic form factor of the ion.

4. It should be noted first that the dependence of the scattering function (6) on the energy transfer $\hbar\omega$ and the temperature is virtually indistinguishable from that observed in heavy-fermion compounds,[11] where this dependence is ordinarily interpreted on the basis of the phenomenological expression $S_{ph}(\hbar\omega,T)=[1-\exp(-\hbar\omega/T)]^{-1}\hbar\omega/[(\Gamma(T)^2+(\hbar\omega)^2]$. A characteristic feature of the neutron response of systems with heavy fermions is the nonzero width $\Gamma(T)$ of the quasielastic peak at zero temperature.[11]

For quantitative analysis we shall examine a symmetric spin band of width $2T^*$ with a constant density of states $\mathcal{D}(\varepsilon)=1$ if $\varepsilon\in[-T^*,T^*]$ and $\mathcal{D}(\varepsilon)=0$ elsewhere. The chemical potential in a spin band with this shape is zero. Averaging the scattering function (6) over angles (which corresponds to the case of scattering by a polycrystal), we obtain the expression

$$S_{sl}(\kappa,\hbar\omega)=R(\kappa)\int_{-T^*}^{T^*}d\varepsilon\,\mathcal{D}(\varepsilon+\hbar\omega)n(\varepsilon)(1-n(\varepsilon+\hbar\omega)), \tag{9}$$

where the dependence on the modulus of the momentum transfer is incorporated into the separate factor $R(\kappa)$. The dependence of the cross section on the momentum transfer will be examined separately. We shall focus our attention on the dependence of the scattering function on the energy transfer, which for the model density of states adopted has the form

$$S_{sl}(\kappa,\hbar\omega)=\frac{R(\kappa)}{2}T\exp\left(\frac{\hbar\omega}{2T}\right)\sinh^{-1}\left(\frac{|\hbar\omega|}{2T}\right)\ln\left\{\frac{1+\cosh[T^*/T]}{1+\cosh[(T^*-|\hbar\omega|)/T]}\right\}. \tag{10}$$

The curves presented in Fig. 1 agree qualitatively with the experimentally observed response in heavy-fermion systems, and for $\hbar\omega<T^*$ they are virtually indistinguishable from the Lorentz function $S_{ph}(\hbar\omega,T)$ weighted with the detailed-balance factor. The fitting a phenomenological function $S_{ph}(\hbar\omega,T)$ to $S_{sl}(\hbar\omega,T)$, as is done in practice when analyzing experimental data, gives $\Gamma(T=0)\sim T^*$. We note that taking account of the damping of the excitations of the spin liquid and examining less singular density of

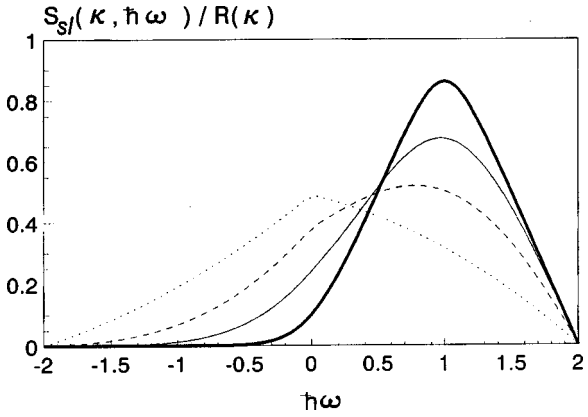

FIG. 1. Scattering function for a spin liquid with a band of width $T^*=1$ versus the energy transfer for $T=0.1$ (thick solid line), $T=0.25$ (thin solid line), $T=0.5$ (dashed line), and $T=2$ (dotted line).

states $\mathcal{D}(\varepsilon)$ removes the restriction of the energy transfer $\hbar\omega$ to the interval $[-2T^*,2T^*]$ and smooths the kinks in the energy dependence of the cross section at zero energy transfer (see Fig. 1).

5. The finite width obtained for the quasielastic peak in the spin-liquid model at zero temperature cannot be a decisive argument in favor of the existence of a state with RVBs, since various different models lead to the same result.[12,13] A more striking consequence of Fermi statistics, which can serve as a decisive test, is the dependence of the quasielastic cross section on the momentum transfer.

To demonstrate this consequence of the Fermi statistics, we shall consider a two-sublattice system where the intersublattice interaction dominates, i.e., $A_{\mathbf{l},\xi,\mathbf{l}'\xi'}=\delta_{\mathbf{ll}'}T^*/2$ for $\xi\neq\xi'$ and is negligibly small for $\xi=\xi'$. (Numerical calculations show that this approximation does not affect the character of the effects considered below and serves only for convenience in performing analytical calculations.) In this case the fourfold degeneracy of the states in each unit cell is partially removed and the system of eigenstates consists of two twofold degenerate levels with energies $\pm T^*/2$ and chemical potential $\mu=0$. For definiteness, we shall assume that the basis vector $\boldsymbol{\xi}$ is directed along the z axis and that the distance between the ions is d.

To calculate the dependence on the momentum transfer it is convenient to introduce the function

$$S_{sl}^{qe}(\boldsymbol{\kappa})=\int_{-T^*}^{T^*} d(\hbar\omega)S_{sl}(\boldsymbol{\kappa},\hbar\omega), \tag{11}$$

corresponding to the quasielastic scattering cross section integrated over the energy transfer. In the final expression for the scattering function

$$S_{sl}^{qe}(\boldsymbol{\kappa})=(B(\kappa)/2)\sum_{\alpha\beta}(\delta_{\alpha\beta}-\hat{\boldsymbol{\kappa}}_\alpha\cdot\hat{\boldsymbol{\kappa}}_\beta)T^{\alpha\beta}D(\boldsymbol{\kappa},T), \tag{12}$$

where

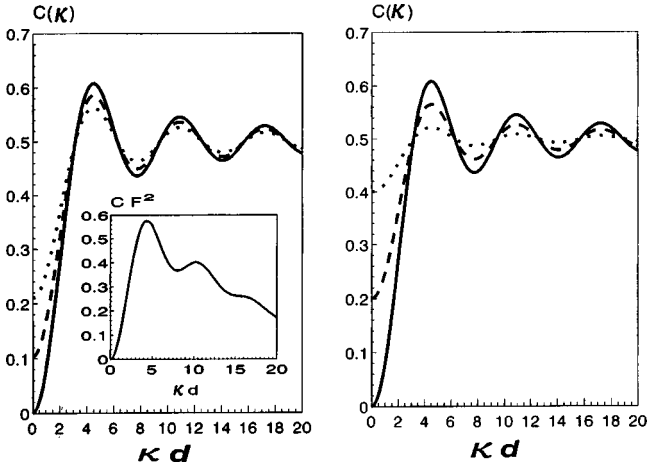

FIG. 2. $C(\kappa)=S_{sl}^{\mathrm{tot}}(\kappa)/S^{\mathrm{tot}}(\kappa)$ versus the modulus κ of the momentum transfer for $T^*=1$ and $\eta=0$: a) in a perfect lattice at temperatures $T=0$ (solid line), $T=0.7$ (dashed line), and $T=1.0$ (dotted line); b) at zero temperature for $\Lambda=1$ (solid line), $\Lambda=0.6$ (dashed line), and $\Lambda=0.2$ (dotted line). Inset: Scattering function taking into account the form factor of the ion Ce^{3+} for interionic distance $d=4$ Å.

$$T^{\alpha\beta}=\sum_{\sigma\sigma'}\langle\sigma|\hat{J}_\alpha|\sigma'\rangle\langle\sigma'|\hat{J}_\beta|\sigma\rangle, \tag{13}$$

Fermi statistics leads to the appearance of an additional factor

$$D(\boldsymbol{\kappa},T)=\{1-\tanh^2(T^*/T)\cos(\boldsymbol{\kappa}\cdot\mathbf{d})\}/2, \tag{14}$$

which is identically equal to 1 in the case of Boltzmann statistics. At sufficiently low temperatures $T<T^*$ the factor $D(\boldsymbol{\kappa},T)$ causes the scattering cross section to oscillate with period $\kappa_p=2\pi/(d\cos[\widehat{\boldsymbol{\kappa}\cdot\mathbf{d}}])$. An important consequence for experimental verification is that the period of the oscillations depends on the direction of the momentum transfer.

To acquire a good statistical sample of experimental data it is most convenient to perform measurements on polycrystalline samples. The results of such measurements are determined by the scattering function $S_{sl}^{\mathrm{tot}}(\kappa)$ obtained by integrating expression (12) over angles. To demonstrate the influence of Fermi statistics we segregate into a separate factor the standard scattering function $S^{\mathrm{tot}}(\kappa)$, whose dependence on the momentum transfer is determined only by the squared magnetic form factor $F(\kappa)$. The integration over angles does not completely suppress the oscillations:

$$S_{sl}^{\mathrm{tot}}(\kappa)=(S^{\mathrm{tot}}(\kappa)/2)\{1-\tanh^2(T^*/T)[(1+\eta/2)\sin(\kappa d)/\kappa d-3\eta\Phi(\kappa d)/2]\} \tag{15}$$

($\eta=(T^{xx}+T^{yy}-2T^{xx})/(T^{xx}+T^{yy}+T^{xx})$ is a measure of the axial one-site scattering anisotropy). Their character is determined by the factor $\sin(\kappa d)/\kappa d$ and by the function $\Phi(x)=(\sin(x)-x\cos(x))x^{-3}$. For sufficiently large values of the momentum transfer $\kappa d \gg 1$ the function $\Phi(\kappa d)$ is much less than the factor $\sin(\kappa d)/\kappa d$. The effect is slightly suppressed with increasing temperature (see Fig. 2a), since even at temperature $\sim T^*$, which is sufficient for destroying the spin-liquid state, the amplitude of the oscillations is still large. It should be noted that the period of the oscillations which arise only in the

case that the excitations obey Fermi statistics is determined by the scattering between interacting ions and is not related with the characteristic features of the Fermi surface of the spin liquid. The characteristic distance between magnetic ions in compounds with heavy fermions is $d \sim 4$ Å. Therefore, despite the intensity dropoff associated with the magnetic form factor $F(\kappa)$ and described by the law $F^2(\kappa)$, the first several periods of the oscillations can be distinguished experimentally (see inset in Fig. 2a).

6. The imperfection of the crystal lattice has a much stronger effect on the suppression of the oscillations. In the simplest case, if scattering coherence is not destroyed altogether because of the absence of one of the magnetic atoms of the basis, the influence of lattice imperfection is expressed as a somewhat different environment around different basis ions. A change in the environment produces a change in the wave functions of the crystal field and, in consequence, a change in the matrix elements of the magnetic operator, which are different for sites 1 and 2: $\langle\sigma|\hat{J}^{\alpha}|\sigma'\rangle_1 \neq \langle\sigma|\hat{J}^{\alpha}|\sigma'\rangle_2$. Although the expressions for the scattering function were obtained in the general case, we present the less complicated formulas for isotropically scattering ions (the directions x, y, and z are equivalent, and we shall drop the Cartesian indices in what follows). Site nonequivalence can be characterized by the quantity

$$U = \left\{ \sum_{\sigma\sigma'} |\langle\sigma|\hat{J}|\sigma'\rangle_1 - \langle\sigma|\hat{J}|\sigma'\rangle_2|^2 \right\} \left\{ \sum_{\sigma\sigma'} |\langle\sigma|\hat{J}|\sigma'\rangle_1 + \langle\sigma|\hat{J}|\sigma'\rangle_2|^2 \right\}^{-1}. \tag{16}$$

The effect of a lattice imperfection on the scattering function

$$S_{sl}^{\mathrm{tot}}(\kappa) = (S^{\mathrm{tot}}(\kappa)/2)\{1 - \Lambda \tanh^2(T^*/T)\sin(\kappa d)/(\kappa d)\} \tag{17}$$

is determined by the quantity $\Lambda = (1-U)/(1+U)$, which equals 1 in a perfect lattice and zero in the case of complete site nonequivalence. Figure 2b demonstrates the influence of lattice imperfection on the suppression of the oscillations.

7. In summary, although the dependence of the cross section of quasielastic magnetic scattering of neutrons by a spin liquid on the energy transfer is essentially indistinguishable from scattering by a spin which relaxes as a result of Kondo processes, the oscillatory dependence of the cross section on the momentum transfer is unique to a spin liquid. It should be noted that in the case of sufficiently soft crystal-field splittings $\Delta_{CF} \sim T^*$ the terms of the Hamiltonian (1) which are off-diagonal with respect to the levels of the crystal field also lead to oscillations of the inelastic scattering cross section. Oscillations of the differential inelastic scattering cross section have been observed experimentally[14] in the Kondo semimetal CeNiSn and can be quantitatively explained on the basis of the spin-liquid approach.[5] However, since many characteristics which are measured in experiments on neutron scattering by periodic systems demonstrate oscillatory behavior (for example, oscillations of the width of the neutron scattering peak in a paramagnet[15,16]), it is important to study properties which uniquely related with a spin liquid. As we have shown in the present letter, the oscillations of the total quasielastic scattering cross section are a direct consequence of the Fermi statistics of excitations in a state with resonating valence bonds. For this reason, the experimental observation of the predicted effect can serve as a substantial argument support of the concept of spin-liquid correlations in heavy-fermion systems.

I am deeply grateful to P. A. Alekseev, K. A. Kikoin, and V. N. Lazukov for critical discussions. This work was supported by the Russian Fund for Fundamental Research (Project 98-02-16730).

[1] G. Baskaran, Z. Zou, and P. W. Anderson, Solid State Commun. **63**, 973 (1987).
[2] P. Coleman and N. Andrei, J. Phys.: Condens. Matter **1**, 4057 (1989).
[3] K. A. Kikoin, M. N. Kiselev, and A. S. Mishchenko, Zh. Éksp. Teor. Fiz. **112**, 729 (1997) [JETP **85**, 399 (1997)].
[4] K. A. Kikoin, M. N. Kiselev, and A. S. Mishchenko, Czech. J. Phys. **46**, 1899 (1996).
[5] Yu. Kagan, K. A. Kikoin, and A. S. Mishchenko, Phys. Rev. B **55**, 12348 (1997).
[6] D. R. Grempel and M. Lavagna, Solid State Commun. **83**, 595 (1992).
[7] T. Tanamoto, H. Kohno, and H. Fukuyama, J. Phys. Soc. Jpn. **62**, 617 (1993).
[8] B. Coqblin and J. R. Schrieffer, Phys. Rev. **185**, 847 (1969).
[9] B. Cornut and B. Coqblin, Phys. Rev. B **5**, 4541 (1972).
[10] W. Marshall and S. W. Lovesey, *Theory of Thermal Neutron Scattering*, Clarendon Press, Oxford, 1971.
[11] P. Fulde and M. Lowenhaupt, Adv. Phys. **34**, 589 (1985).
[12] N. E. Bickers, D. L. Cox, and J. H. Wilkins, Phys. Rev. B **36**, 2036 (1987).
[13] M. N. Kiselev and A. S. Mishchenko, Zh. Éksp. Teor. Fiz. **113**, 1843 (1998) [JETP **86**, 1008 (1998)].
[14] T. Sato, H. Kadowaki, H. Yoshizawa *et al.*, J. Phys.: Condens. Matter **7**, 8009 (1995).
[15] P. G. De Gennes, J. Phys. Chem. Solids **4**, 223 (1958).
[16] A. J. Neville, B. D. Rainford, D. T. Adroja, and H. Schober, Physica B **223–224**, 271 (1996).

Translated by M. E. Alferieff

Direct STM observation of electronic structure modification of naphthacenequinone molecules due to photoisomerization

A. I. Oreshkin, V. I. Panov, and S. I. Vasil'ev
Chair of Quantum Radiophysics, Moscow State University, 119899 Moscow, Russia

N. I. Koroteev and S. A. Magnitskii
International Laser Center, Moscow State University, 119899 Moscow, Russia

(Submitted 6 August 1998)
Pis'ma Zh. Éksp. Teor. Fiz. **68**, No. 6, 486–490 (25 September 1998)

Light-induced conformational transformations of the naphthacenequinone (NQ) molecules are observed by scanning tunneling microscopy (STM). NQ molecules packed in a Langmuir–Blodgett (LB) film are shown to form stable ordered structures on a surface of highly oriented pyrolytic graphite (HOPG). The local density of electronic states is found to exhibit the distinct peak which is characteristic of two-dimensional conductivity. An additional subband of empty electronic states is found for NQ molecules in form *A* but not in form *B*. The constant-height STM images of individual molecules in form *A* demonstrate an additional structure that is indicative of a conformational transition of the NQ molecules. This transition involves the transfer of the phenoxy group from one oxygen to another. © *1998 American Institute of Physics.* [S0021-3640(98)01018-4]

PACS numbers: 73.61.Ph, 73.50.−h, 73.20.Dx

1. Photochromic molecules have been attracting sizable and steady interest due to their capability of reversibly changing their absorption and fluorescence spectra under irradiation at different wavelengths. In view of the development of a new generation of ultrahigh-density three-dimensional optical data storage based on the use of photochromic molecules, it is important to clarify the fundamental mechanisms that lead to modification of the basic characteristics of photochromic molecules (especially when organized in Langmuir–Blodgett (LB) films) under exposure to light. The properties of photochromic molecules embedded either into polymeric matrices or other media (liquid crystals, solutions, etc.) depend substantially on their environment. The LB technique enables one to produce photochromic molecular structures packed with ultrahigh density on the surface of a substrate. LB films are typical two-dimensional (single layer films) or three-dimensional (multilayer films) ordered assemblies. Evidently, one expects that photochromic molecules incorporated in highly ordered LB films should exhibit behavior that is not typical for free molecules or solutions. However, very little is known about the physical aspects of photochromic reactions in LB films.

Photochromic compounds deposited on a substrate by the (Langmuir–Sheffer) tech-

nique are an interesting and attractive object for investigations by different methods. The optical properties of molecular layers of spiropyrans and the photochromic reaction kinetics of spiropyran molecules in LB layers on stearic acid were investigated in Refs. 1–3. The possibility of photochromic reaction in LB films of diarylethenes and salicylideneanilines has been demonstrated.[4,5] Similar results are presented in Refs. 6 and 7.

For particular molecules photoisomeric changes can be observed by means of precision methods based on scanning probe microscopy, e.g., scanning tunnel microscopy/spectroscopy (STM/STS), scanning force microscopy (SFM), etc. These methods in principle allow one to study with atomic resolution the electronic properties[8,9] and topology of particular molecules on a substrate surface and their changes brought about by external optical irradiation. The major advantage of STM methods is their high resolution (they are capable of resolving details much smaller than an optical wavelength). Recently, the possibility of the direct STM real-space analysis of the shapes of molecules has been demonstrated.[10] The authors have identified two different conformations of the Cu-tetra (3,5 di-t-butylphenyl) porphyrin (Cu-TBPP) molecule deposited on a metal substrate in two metastable forms characterized by different shapes of the molecules. Up till now, however, there have been no direct STM observations of reversible modification of molecular structure under optical radiation.

In this paper we have for the first time, to the best of our knowledge, demonstrated the direct STM registration of a photochromic reaction in LB films under exposure to light. The direct reaction (form $A \rightarrow$ form B) of naphtcenequinone (NQ) molecules ordered in LB films is caused by 400 nm light, and the reverse reaction (form $B \rightarrow$ form A) is initiated by 480 nm light. The conformational transformations of individual molecules in a LB layer were observed before and after the direct photoreaction. Our main findings are as follows:

1) A distinct peak is found in the tunnel local density of electronic states of 6-phenoxi-5, 12-naphthacenequinone molecules[11] ordered in LB films. Such a peak is inherent in both the A and B forms and is indicative of a two-dimensional (2D) character of the conductivity of the film. The shape of the differential conductivity curves is shown to be significantly modified after direct photoisomerization;

2) for molecules in the A form the additional subband in the range of unoccupied electronic states of LB films is detected;

3) the tunnel current flowing through an individual molecule falls from ~ 0.1 nA to ~ 0.04 nA when the molecule undergoes the transition from the A to the B form;

4) the constant-height images of individual molecule in the A form exhibit an additional fine structure that points to the conformational transition of the molecules from the A to the B form. This transition involves the transfer of the phenoxy group from one oxygen atom to another and probably leads to the shutdown of some of the tunneling channels.

2. To study the electronic properties of NQ molecules and their possible conformational modifications during photochemical reactions we used the STM and STS techniques. Molecules were deposited on a highly oriented pyrolytic graphite (HOPG) substrate using the Langmuir–Sheffer technique to form different numbers of ordered molecular layers. The expected modification of the NQ molecular structure in the transition from the *para* form (form A) to the *ana* form (form B) and back is shown in Fig.

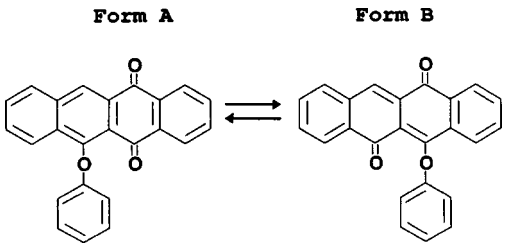

FIG. 1. Schematic structure of two conformational forms (A and B) of 6 – phenoxi–5, 12–naphthacenequinone molecules which occurs during the photocoloration ($A \rightarrow B$) and photobleaching ($B \rightarrow A$) reactions.

1. Variations of molecular properties in multilayer thin films caused by light irradiation change the initial density of electronic states which is detected in our STM and STS experiments.

The photochemical reaction was initiated by light passed through an interference filter with the transmission maximum at 400 nm for the direct reaction ($A \rightarrow B$) and at 480 nm for the reverse reaction ($B \rightarrow A$). We used an incandescent lamp as a light source. After the filtering, the light transpored through a multimode optical fiber was used to illuminate the STM tunneling junction. The typical light intensity on the sample was about 1 mW/cm^2. This scheme allowed us to follow the changes of electronic properties of NQ molecules in the processes of forward and backward phototransitions by means of STM and STS methods *in situ*.

The LB film was deposited on the HOPG substrate at a pressure of 5 mN/m. The average transfer coefficient $\langle k \rangle$ was equal to 0.84.

All the measurements were performed using a home-built STM with atomic resolution and a maximum scan range $5 \times 5\ \mu$m under ambient conditions. STM tips were mechanically cut from PtIr or Au wires. We used the STM to obtain constant-current (topographic) as well as constant-height images. Spectroscopic data [$I(V)$ and hardware $dI/dV(V)$] were then acquired at the chosen point of the surface.[12]

We have found that LB films of NQ molecules (from 1 to 40 monolayers) are capable of forming stable ordered structures on a HOPG surface. The area occupied by each molecule is of the order of 20–23 Å^2, which is in good agreement with the value 27 Å^2 obtained from the $\pi - S$ isotherm at the deposition pressure. The distance between molecular rows is about 5.8–6.0 Å and that between molecules within a row is 3.8–4.0 Å.

The tunneling conductivity curves measured for LB films with different number of layers always had a peak in the vicinity of zero bias voltage. In the tight-binding approximation this points to a 2D character[13] of the conductivity of LB films and to the existence of a long-range interaction between molecules (see Fig. 2a).

Another set of experimental data is concerned with investigations of the behavior of the tunneling conductivity during photoreactions. Substantial variation in the local density of electronic states (LDOS) for direct photoreaction has been observed for a three-layer LB film. It is found that the shape of the differential conductivity curve is significantly modified during photoisomerization. The upper graph in Fig. 2b shows a strong

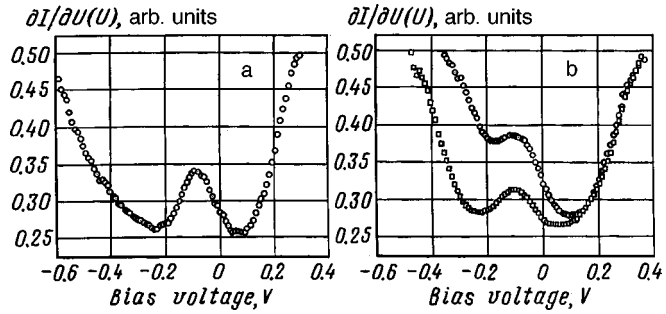

FIG. 2. a: Dependence of the differential conductivity of a LB film on the tunneling voltage (3 monolayers). The LB film was under exposure to natural light for a few days. b: Dependence of the differential conductivity of a LB film on the tunneling voltage (3 monolayers) before and after the direct photoreaction; ○ — *A* form; □ — *B* form.

asymmetry of the curve for form *A*. There is an additional contribution to LDOS at $U_t < 0$ as compared to form *B*, while at $U_t > 0$ the dependence of the conductivity of the LB films is rather similar for the *A* and *B* forms. This additional contribution points to the origination of an additional subband in the range of empty electronic states.

We have also studied the STM current images of individual molecules in NQ LB films. STM constant-height images of a three-layer LB film corresponding to the *A* and *B* forms of NQ are presented in Fig. 3. Images (a) and (b) represent the selected site of the surface before and after direct photoreaction. Both pictures were taken under the same tunneling conditions: $U_t = -150$ mV; $I_t = 0.4$ nA. In these experiments we found that the STM current images of every molecule in the LB layer are noticeably different for forms *A* and *B*. These distinctions are clearly seen from Fig. 4, which shows cross sections of the images from Fig. 3, taken along the *1–1′* direction. As can be seen from Fig. 4, the constant-height STM image of 6-phenoxi-5,12-naphthacenequinone molecules in form *A* has an amplitude of ~ 0.1 nA, while the current amplitude for molecules in form *B* is ~ 0.04 nA. Besides, the STM current image of molecules in form *A* possesses an additional fine structure (see the peak shifted to the edge of the image of the molecule). This

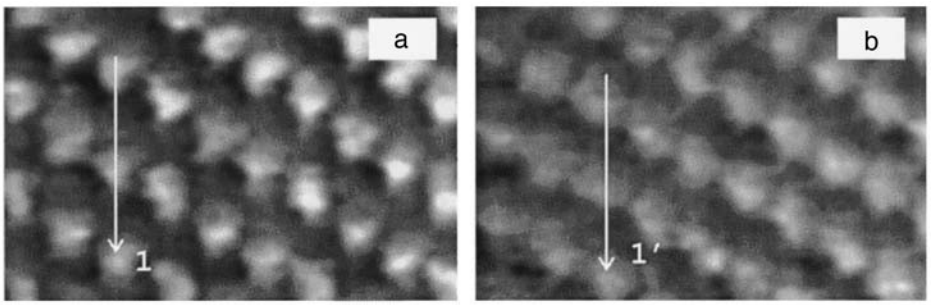

FIG. 3. STM current images of the same portion of 3-layer naphthacenequinone LB films. a: form *A*, $I_t(x,y)$: 3.4 nm×2.2 nm×0.14 nA, b: form *B*, $I_t(x,y)$: 3.3 nm×2.5 nm×0.08 nA.

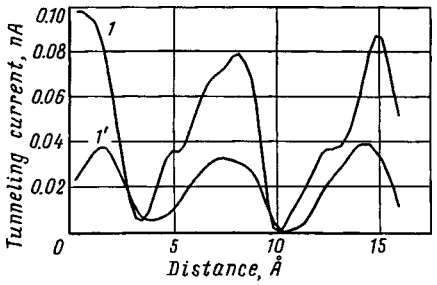

FIG. 4. STM current image cross-sections according to arrows in Fig. 3. Curves *1, 1′* correspond to the directions *1, 1′* in Fig. 3. .

peculiarity is connected either with a topological conformational transition of molecule or with the occurrence of an additional tunneling channel after molecular conformation.

The direct ($A \rightarrow B$) and reverse ($B \rightarrow A$) transitions of molecules caused by changing of the light frequency can be understood by analyzing the behavior of a driven nonlinear oscillator. The driven nonlinear oscillator model has been successfully used to describe the molecular vibrational spectrum in an external radiation field.[14] One can use a double-well potential with the simplest nonlinearity $\sim \gamma X^4$, where X is the configuration parameter. According to the semiclassical approach based on a quasi-energy formalism there are two stable states (1 and 2) for the driven oscillator in each well A and B, if the radiation frequency ν is close enough to the unperturbed molecular frequency ν_0. The most probable state 1 or 2 (with low and high energy) is determined by the parameter $\beta = \gamma J/(\nu - \nu_0)^3$, where J is the intensity of the external light, γ is the nonlinearity, which can be slightly different for wells A and B, and ν_0 is the unperturbed molecular frequency, which can also differ for wells A and B. If β is greater than a critical value, the driven nonlinear oscillator occupies the high-energy state 2. For light at wavelength $\lambda_1 = 400$ nm the parameter β is greater than the critical value for well A but smaller than the critical value for well B. Thus a direct conformational transition $A \rightarrow B$ occurs from the high-energy state 2 in well A to the low-energy state 1 in well B. Changing the wavelength of the light from $\lambda_1 = 400$ nm to $\lambda_2 = 480$ nm changes the value of parameter β. Now $\beta > \beta_c$ for well B (the high-energy state 2 is occupied in well B) and $\beta < \beta_c$ for well A. The reverse conformational transition $B \rightarrow A$ occurs from the high-energy state in well B to the low-energy state in well A. An analytical expression for the occupation numbers of the nonlinear oscillator in each well A and B can be obtained from the system of kinetic equations in the quasi-energy formalism and will be published elsewhere. In our opinion, the observed transition is due to oxygen bonding transfer, which gives rise to an additional tunneling channel and, in the ordered molecular system of a LB film, to an additional subband.

3. We have demonstrated the direct observation by STM/STS methods of the changes in the differential conductivity of NQ LB films as a result of a photochemical reaction. The unusual behavior of the differential conductivity of the molecular film is probably due to an additional subband in the range of unoccupied electronic states of the sample as a result of the photoreaction and can be referred to as conformational modification of naphthacenequinone molecules. A distinction in the constant-height STM im-

ages of individual NQ molecules in the different forms has been found which bears witness to the conformation transition during photoisomerization.

The authors would like to thank Dr. N. S. Maslova and Dr. S. V. Savinov for valuable discussions. We are grateful to Dr. N. T. Sokolyuk for molecular synthesis and to Dr. I. V. Myagkov for sample preparation. This work was financially supported by Memory Devices Inc. of the Constellation Group GmbH (Austria), by the Russian Ministry of Research (Surface Atomic Structures, Grant 95-1.22; Micro- and Nanoelectronics, Project 214/68/2-3) and the Russian Fund for Fundamental Research (RFFR), Grants 96-0219640a and 96-03-32867.

[1] T. Minami, N. Tamai, T. Yamazaki *et al.*, J. Phys. Chem. **95**, 3988 (1991).
[2] V. M. Anisimov, A. M. Vinogradov, E. I. Kuznetsov *et al.*, Div. Chem. Sci. **40,** 1783 (1991).
[3] A. Miyata, Yu. Unuma, and Yo. Higashigaki, Bull. Chem. Soc. Jpn. **64**, 1719 (1991).
[4] S. Abe, A. Sugai, I. Yamazaki *et al.*, Chem. Lett. 69 (1995).
[5] S. Kawamura, T. Tsutsui, S. Saito *et al.*, J. Am. Chem. Soc. **110**, 509 (1988).
[6] M. Tamura and A. Sekiya, Bull. Chem. Soc. Jpn. **66**, 1356 (1993).
[7] A. Yabe, Y. Kawabata, H. Niino *et al.*, Chem. Lett. 1 (1988).
[8] Supriyo Datta, Weidong Tian, Seunghum Hong *et al.*, Phys. Rev. Lett. **79**, 2530 (1997).
[9] U. During, O. Zuger, B. Michel *et al.*, Phys. Rev. B **48**, 1711 (1993).
[10] T. A. Jung, R. R. Schlitter, and J. K. Gimzevski, Nature (London) **386**, 696 (1997).
[11] N. I. Koroteev, S. A. Magnitskii, V. V. Shubin *et al.*, Jpn. J. Appl. Phys., Part 1 **36**, part 1, no. 1B, 424 (1997).
[12] S. I. Vasil'ev, Yu. N. Moiseev, A. I. Oreshkin *et al.*, Instrum. Exp. Tech. **37**, No.2, path 2, 153 (1994).
[13] N. S. Maslova, Yu. N. Moiseev, S. V. Savinov *et al.*, JETP Lett. **58**, 524 (1993).
[14] N. S. Maslova, JETP Lett. **91**, 913 (1986).

Published in English in the original Russian journal. Edited by Steve Torstveit.

Superconductivity in the presence of fermion condensation

V. R. Shaginyan

St. Petersburg Nuclear Physics Institute Russian Academy of Sciences, 188350 Gatchina, Russia

(Submitted 17 August 1998)
Pis'ma Zh. Éksp. Teor. Fiz. **68**, No. 6, 491–496 (25 September 1998)

Fermion condensation (FC) is studied within the density functional theory. FC can fulfill the role of a boundary, separating the region of strongly interacting electron liquid from the region of strongly correlated electron liquid. Consideration of the superconductivity in the presence of FC shows that, under certain circumstances, at temperatures above T_c the superconductivity vanishes and the superconducting gap smoothly transforms into a pseudogap. The pseudogap occupies only a part of the Fermi surface, and one that shrinks with increasing temperature and vanishes at $T=T^*$, and the single-particle excitations of the gapped area of the Fermi surface have a width $\gamma\sim(T-T_c)$.
 [S0021-3640(98)01118-9]

PACS numbers: 74.20.Mn, 74.70.Tx, 74.72.Jt

Recently a powerful method was developed for measuring the electronic structure close to the Fermi level.[1] As a result, a plateau adjacent to the Fermi level has been observed in the electronic spectra of a number strongly correlated metals. For example, it has been shown that optimally doped high-temperature superconductors exhibit an anomalous normal state.[1] The spectra of Sr_2RuO_4 or $YBa_2Cu_4O_{7-\delta}$ (YBCO), for instance, contain very smooth segments on the Fermi surface. It is a remarkable thing that these spectra have not been reproduced in theoretical calculations.[2] It has been shown that such peculiarities of the electronic spectra can be understood within the framework of the theory of fermion condensation (FC), which was predicted in Ref. 3 and is associated with the rearrangement of the single-particle degrees of freedom in strongly correlated Fermi systems. The main feature of FC is the appearance of a plateau in the single-particle excitation spectrum at the Fermi level.[3–5] On the other hand, quite unusual behavior has been observed[6–9] in underdoped high-temperature superconductors, which indicates a pseudogap above T_c. As we shall see, such behavior can be also clarified within the concept of fermion condensation.

It has been demonstrated that the onset of the density-wave instability in a Fermi system can be preceded by the FC phase transition; thus FC can take place if the effective coupling constant is sufficiently strong.[10] This makes one think that FC is a rather widespread phenomenon inherent to strongly correlated Fermi systems. For example, FC can arise in such an unusual system as fermions locked in vortex cores in a superfluid Fermi

liquid.[11] On the other hand, it has been demonstrated that the charge-density wave instability takes place in three-dimensional[12] and two-dimensional electron liquids.[13] Thus, the electronic systems of some strongly correlated metals are suitable places to look for FC.[14]

Now let us outline the key points of the FC theory.[5,15] FC is related to a new class of solutions of the Fermi-liquid-theory equation[16]

$$\frac{\delta(F-\mu N)}{\delta n(p,T)}=\varepsilon(p,T)-\mu(T)-T\ln\frac{1-n(p,T)}{n(p,T)}=0, \tag{1}$$

for the quasiparticle distribution function $n(p,T)$, depending on the momentum p and temperature T. Here F is the free energy, μ is the chemical potential, and $\varepsilon(p,T)=\delta E/\delta n(p,T)$ is the quasiparticle energy, which, like the energy E and the other thermodynamic functions, is a functional of $n(p,T)$. Equation (1) is usually rewritten in the form of the Fermi–Dirac distribution

$$n(p,T)=\left\{1+\exp\left[\frac{(\varepsilon(p,T)-\mu)}{T}\right]\right\}^{-1}. \tag{2}$$

In homogeneous matter, the standard solution $n_F(p,T=0)=\theta(p_F-p)$, with p_F being the Fermi momentum, is obtained assuming that the effective mass,

$$\frac{1}{M^*}=\left.\frac{d\varepsilon(p,T=0)}{pdp}\right|_{p=p_F}, \tag{3}$$

is positive and finite at the Fermi momentum p_F. As a result, the T-dependent corrections to M^*, to the quasiparticle energy, and to other quantities start with the T^2 terms. But this solution of Eq. (1) is not the only one. There exist ''anomalous'' solutions[3,11] of Eq. (1) associated with a so-called fermion condensation.[3] Being continuous within a region in p, such a solution $n(p)$ admits a finite limit for the logarithm in Eq. (1) at $T\to 0$, yielding

$$\varepsilon(p)=\frac{\delta E}{\delta n(p)}=\mu, \quad p_i\leqslant p\leqslant p_f. \tag{4}$$

Thus, within the region $p_i<p<p_f$ the solution $n(p)$ deviates from the Fermi step function $n_F(p)$ in such a way that the energy $\varepsilon(p)$ stays constant, while outside this region $n(p)$ coincides with $n_F(p)$. We see that the occupation numbers $n(p)$ become variational parameters: the solution $n(p)$ emerges if the energy E is lowered by alteration of the occupation numbers. New solutions, as it is seen from Eq. (1), possess at low T a shape of the spectrum $\varepsilon(p,T)$ which is linear in T (Ref. 14):

$$\varepsilon(p,T)-\mu(T)\sim T\ll T_f, \tag{5}$$

within the interval occupied by the fermion condensate. If $T\ll T_f$ it follows from Eqs. (1) and (5) that

$$M^*\sim N(0)\sim\frac{1}{T}, \tag{6}$$

with $N(0)$ being the density of states at the Fermi level. Here T_f is the quasi-FC phase transition temperature above which FC effects become insignificant.[15] The quasiparticle

formalism is applicable to this problem, since the damping of the condensate states is small compared to their energy. This condition obviously holds for superfluid systems, but it is also true for a normal system.[15]

In this letter the influence of FC on the superconducting phase transition is considered on the basis of the density functional theory, including a study of the pseudogap.

We start with a general consideration of the superconductivity in the presence of FC. In the density functional theory of superconductivity, there exists a unique functional $F(T)$ of two densities, namely, the normal density of an electron system ρ and the anomalous density κ. In atomic units, the functional $F[\rho,\kappa]$ is given by[17]

$$F[\rho,\kappa]=T_s[\rho,\kappa]-TS_s[\rho,\kappa]+\int \frac{\rho(\mathbf{r}_1)\rho(\mathbf{r}_2)}{|\mathbf{r}_1-\mathbf{r}_2|}d^3\mathbf{r}_1 d^3\mathbf{r}_2+F_{xc}[\rho,\kappa]$$
$$-\int \kappa^*(\mathbf{r}_1,\mathbf{r}_2)V(\mathbf{r}_1,\mathbf{r}_2,\mathbf{r}_3,\mathbf{r}_4)\kappa(\mathbf{r}_3,\mathbf{r}_4)d^3\mathbf{r}_1 d^3\mathbf{r}_2 d^3\mathbf{r}_3 d^3\mathbf{r}_4$$
$$=E[\rho,\kappa]-TS_s[\rho,\kappa]. \tag{7}$$

Here $T_s[\rho,\kappa]$ and $S_s[\rho,\kappa]$ stand for the kinetic energy and the entropy of a noninteracting system, while $F_{xc}[\rho(\mathbf{r}),\kappa(\mathbf{r}_1,\mathbf{r}_2)]$ is the exchange-correlation free-energy functional, and V is a pairing interaction. The third and fifth terms on the right-hand side of (7) are the Hartree terms due to the Coulomb forces and the pairing interaction, respectively. We suppose V to be sufficiently weak, like the model BCS interaction.[18] The last equality in Eq. (7) can be regarded as the definition of E. For the densities ρ and κ one can employ quite general forms,

$$\rho(\mathbf{r}_1)=\sum_n [|\phi_n(\mathbf{r}_1)|^2|v_n|^2(1-f_n)+|\phi_{-n}(\mathbf{r}_1)|^2|u_n|^2 f_n], \tag{8}$$

$$\kappa(\mathbf{r}_1,\mathbf{r}_2)=\frac{1}{2}\sum_n [\phi_n^*(\mathbf{r}_1)\phi_{-n}(\mathbf{r}_2)+\phi_n^*(\mathbf{r}_2)\phi_{-n}(\mathbf{r}_1)]v_n^* u_n(1-2f_n), \tag{9}$$

with the coefficients v_n and u_n obeying the conditions $|v_n|^2+|u_n|^2=1$. Here n denotes the quantum numbers such as the momentum p in the case of homogeneous matter or the crystal momentum and the band index in the solid state. For the sake of simplicity, we omit the spin variables. Since we are going to take a fresh look at Eq. (4), we set $T=0$. Minimization of F with respect to ϕ_n leads to the eigenfunction problem,

$$\left(-\frac{\nabla^2}{2}+\int \frac{\rho(\mathbf{r}_2)}{|\mathbf{r}_1-\mathbf{r}_2|}d^3\mathbf{r}_2\right)\phi_m(\mathbf{r}_1)+\int v_{xc}(\mathbf{r}_1,\mathbf{r}_2)\phi_m(\mathbf{r}_2)d^3\mathbf{r}_2=\varepsilon_m\phi_m(\mathbf{r}_1), \tag{10}$$

with v_{xc} being a nonlocal potential.[19] In the case of a homogeneous system the functions ϕ_m are plain waves, $|v_p|^2=n_p$, and Eq. (10) reduces to $p^2/2+v(p)=\varepsilon(p)$. Taking into account Eq. (10), one can also infer that $\delta E/\delta|v_l|^2=\varepsilon_l$. If V were zero, ε_l would represent the real single-particle excitation spectra of the system. The energy ε_l is perturbed by the BCS correlations, but, in fact, this perturbation is small. It is convenient to take $v_l=\cos\theta_l$; $u_l=\sin\theta_l$, while minimization with respect to θ_l yields

$$\frac{\delta F[\rho_1,\kappa]}{\delta\theta_l}=(\varepsilon_l-\mu)\tan 2\theta_l+\Delta_l=0. \tag{11}$$

The gap Δ_l is given by

$$\Delta_l = -\int \frac{\delta F[\rho_1, \kappa]}{\delta \kappa(\mathbf{r}_1, \mathbf{r}_2)} \phi_l^*(\mathbf{r}_1)\phi_{-l}(\mathbf{r}_2) d^3\mathbf{r}_1 d^3\mathbf{r}_2 . \tag{12}$$

We shall now give further proof of Eq. (4), deduced at $T=0$. Consider Eq. (11) in the limit $V=0$. In this case $\Delta_l=0$, and Eq. (11) can be written as

$$(\varepsilon_l - \mu)\tan 2\theta_l = 0. \tag{13}$$

Equation (13) requires that

$$\varepsilon_l - \mu = 0, \quad \text{if} \quad |v_l|^2 \neq 0,1. \tag{14}$$

Therefore, the fermion condensation solution is a new solution of the old equations. On the other hand, it is seen from Eq. (14) that the standard Kohn–Sham scheme for the single-particle equations is no longer valid beyond the point of the FC phase transition, since the quasiparticle occupation numbers $|v_l|^2$ become variational parameters, minimizing the total energy. In the homogeneous limit Eq. (14) takes form of Eq. (4).

FC involves the unbounded growth of the density of states when $T \to 0$; see Eq. (6). As a result, FC serves as a source for new phase transitions which lift the degeneracy of the spectrum. We are going to analyze the situation when the superconductivity wins the competition with the other phase transitions. Now let us switch on the interaction V. Then, as follows from Eqs. (7) and (12), $\Delta \sim V$ when V is sufficiently small,[3,15] while in the BCS case Δ, given by Eq. (12), is exponentially small. Inserting the result $\Delta \sim V$ into Eq. (7), one finds that the pairing correction $\delta E_s(T=0)$ to the ground state energy at $T=0$ is given by $\delta E_s(T=0) \sim \Delta$.[15] This result differs drastically from the ordinary BCS result $\delta E_s \sim \Delta^2$. In response to this, a substantial increase of the critical magnetic field for the destruction of superconductivity can be expected. Above the critical temperature the system under consideration is in its anomalous normal state, Eq. (5) is valid, and one can observe the smooth segments of the spectra at the Fermi level.[9]

Now we focus our attention on an investigation of the pseudogap which is formed above T_c in underdoped high-temperature superconductors.[6–9] Let us consider a 2D liquid on a simple square lattice which has a superconducting state with a d-wave symmetry of the order parameter κ. We assume that the long-range component $V_{lr}(\mathbf{q})$ of the particle–particle interaction $V_{pp}(\mathbf{q})$ is large and repulsive and has a radius q_{lr} such that $p_F/q_{lr} \sim 1$. The short-range component $V_{sr}(\mathbf{q})$ is relatively small and attractive, with a radius $p_F/q_{sr} \gg 1$ (Ref. 20). As a result, the low-temperature gap Δ, in accordance with the d-wave symmetry, is given by,[20,21]

$$\Delta(\phi) \simeq \Delta_1 \cos 2\phi = \Delta_1(x^2 - y^2), \tag{15}$$

with Δ_1 being the maximal gap. At finite temperatures Eq. (12) for the gap can be written as

$$\Delta(p,\phi) = -\int_0^{2\pi} V_{pp}(p,\phi,p_1,\phi_1)\kappa(p_1,\phi_1)\tanh\frac{E(p_1,\phi_1)}{2T}\frac{p_1 dp_1 d\phi_1}{4\pi^2}, \tag{16}$$

with p being the absolute value of the momentum, while ϕ is the angle. It is also suggested that FC arises near the van Hove singularities and that the different areas of FC overlap slightly.[14] It follows from the chosen interaction V_{pp} and Eq. (15) that Δ will change sign,

$$\Delta\left(\frac{\pi}{4}+\phi\right)=-\Delta\left(\frac{\pi}{4}-\phi\right), \tag{17}$$

vanishing at $\pi/4$. Thus, Δ can be expanded in Taylor series around $\pi/4$, $p\approx p_F$:

$$\Delta(p,\theta)=a\,\theta-b\,\theta^3, \tag{18}$$

with θ being reckoned from $\pi/4$. Hereafter we shall consider the solutions of Eq. (16) on the interval $0<\theta<\pi/4$. We recast Eq. (16), setting $p\approx p_F$ and separating out the contribution I_{lr} which comes from V_{lr}, while the contribution related to V_{sr} is denoted by I_{sr}. At small angles the contribution I_{lr} can be approximated by $I_{lr}=\theta A+\theta^3 B$. The quantities A and B are independent of T if $T\leqslant T^*\ll T_f$ since they are defined by an integral running over the regions occupied by FC. This finding is consistent with the experimental results which show that Δ_1 is essentially T-independent.[9] Thus one has for Δ,

$$\Delta(\theta)=I_{sr}+I_{lr}=-\int_0^{2\pi}V_{sr}(\theta,p,\phi)\kappa(p,\phi)\tanh\frac{E(p,\phi)}{2T}\frac{pdpd\phi}{4\pi^2}+\theta A+\theta^3 B. \tag{19}$$

In Eq. (19) the variable p was omitted. It is seen from Eq. (19) that the function of FC is to produce the free term $\theta A+\theta^3 B$. We shall show that at $T\geqslant T_c$ the solution of Eq. (19) has the second node at $\theta_c(T)$ in the vicinity of the first node $\pi/4$. To show this, let us simplify Eq. (19) to an algebraic equation. The quantity $I_{sr}\sim(V_0/T)\theta$, since $\tanh(E/2T)\sim E/2T$ if $T\approx T_c$, while $V_0\sim V_{sr}$ is a constant. Upon dividing both part of Eq. (19) by $\kappa(\theta)$, one gets

$$E(\theta)=-\left(\frac{V_0}{T}-A_1-\theta^2 B_1\right)|\theta|, \tag{20}$$

with A_1, B_1 being new constants. The quantity A_1 is negative, and it is inferred from the condition that Eq. (16) has the only solution $\Delta\equiv 0$ when $V_{sr}=0$, while B_1 is positive. The factor in brackets on the right-hand side of Eq. (20) changes its sign at some temperature $T=T_c\approx V_0/A_1$. On the other hand, the excitation energy $E(\theta)$ must be positive, and as a result the gap has to reverse its sign on the interval Ω $[0<\theta<\theta_c]$, with $\Delta(\theta_c)=\Delta(0)=0$. It is seen from Eq. (20) that the angle θ_c is related to $T>T_c$ by the equation

$$T\approx\frac{V_0}{(A_1+B_1\theta_c^2)}. \tag{21}$$

Our estimates of the maximal gap Δ_0 in the range Ω show that $\Delta_0\sim 10^{-3}\Delta_1$. Thus we can conclude that the gap in the range Ω can be destroyed by the strong antiferromagnetic correlations that exist in underdoped superconductors.[22,23] Then it is believed that impurities can easily destroy Δ in the area under consideration. Now one can conclude from Eq. (20) that T_c is the temperature at which the superconductivity vanishes, while

the gap, which is also referred to as a pseudogap, persists outside the region. It is seen from Eq. (21) that $\theta_c \sim \sqrt{(T-T_c)/T_c}$, and so one can expect that the pseudogap dies out as the temperature T^* is approached.

Now consider the quasiparticle excitations at the Fermi level. At temperatures $T<T_c$ they are typical excitations of the superconducting state. At $T>T_c$ in the range Ω we have normal quasiparticle excitations with a width γ. The other part of the Fermi level is occupied by the BCS-like excitations with a finite energy of excitation, given by the gap $\Delta(\phi)$, while both type of excitations have widths of the same order of magnitude. Let us estimate γ. If the entire Fermi level were occupied by the normal state, the width would be $\gamma \sim N(0)^3 T^2/\alpha^2$, with a density of states $N(0) \sim 1/T$ and a dielectric constant $\alpha \sim N(0)$. Thus one has $\gamma \sim T$ (Ref. 15). But in our case only part of the Fermi level, the region within Ω, belongs to the normal excitations. Therefore, the number of states allowed for quasiparticles and for quasiholes are proportional to θ_c, and thus the factor T^2 is replaced by $T^2\theta_c^2$. Taking these factors into account, one gets $\gamma \sim \theta_c^2 T \sim T(T-T_c)/T_c \sim (T-T_c)$, since we consider only small angles. Here we have omitted the small contribution coming from the BCS-like excitations, and that is why the width γ vanishes at $T=T_c$. Thus, we can conclude that above T_c the superconducting gap smoothly transforms into the pseudogap. The excitations of the gapped area of the Fermi surface have the same width $\gamma \sim (T-T_c)$, and the region occupied by the pseudogap shrinks with increasing temperature. These results are in good agreement with the experimental facts.[6–9]

A few remarks are in order at this point. Based on the foregoing arguments, we can conclude that BCS-type approach is fruitful for consideration of underdoped samples. It is worth noting that Δ_1 scales with T^* rather than with T_c (Ref. 7), since T^* determines the existence of nontrivial solutions of Eq. (16), while T_c is related to the emergence of the new nodes of the gap. Then, the peak was observed in inelastic neutron scattering from single crystals of optimally doped YBCO and of underdoped samples, at temperatures below T_c, while the broad maximum above T_c exists in underdoped samples.[21] An explanation of this peak, based on the ideas of the BCS theory, was given in Ref. 24. One can recognize that the same explanation holds for the broad maximum in underdoped samples above T_c.

In summary, we have considered FC within the density functional theory. The FC phase transition manifests itself when the effective coupling constant is sufficiently large. FC can fulfill the role of a boundary, separating the region of strongly interacting electron liquid from the region of strongly correlated electron liquid. We have also considered the superconductivity in the presence of FC. As a result, we were led to the conclusion that under certain circumstances, at temperatures above T_c, the superconducting gap smoothly transforms into a pseudogap. The pseudogap occupies only a part of the Fermi surface, one which shrinks with increasing temperature and vanishes at $T=T^*$, while the single-particle excitations of the gapped area of the Fermi surface have a width $\gamma \sim (T-T_c)$.

This research was funded in part by the Russian Fund for Fundamental Research under Grant 98-02-16170. The work has benefited from discussions with V. Belincher, M. de Llano, V. A. Khodel, and G. E. Volovik.

[1] Z.-X. Shen and D. S. Dessau, Phys. Rep. **253**, 1 (1995).
[2] D. J. Singh, Phys. Rev. B **54**, 13311 (1996).
[3] V. A. Khodel and V. R. Shaginyan, JETP Lett. **51**, 553 (1990).
[4] G. E. Volovik, JETP Lett. **53**, 208 (1991).
[5] V. A. Khodel, V. R. Shaginyan, and V. V. Khodel, Phys. Rep. **249**, 1 (1994).
[6] H. Ding *et al.*, Nature (London) **382**, 51 (1996).
[7] H. Ding *et al.*, http://xxx.lanl.gov/abs/cond-mat/9712100 (9 Dec. 1997).
[8] M. R. Norman *et al.*, http://xxx.lanl.gov/abs/cond-mat/9710163 (15 Oct. 1997).
[9] M. R. Norman *et al.*, http://xxx.lanl.gov/abs/cond-mat/9711232 (21 Nov. 1997).
[10] V. A. Khodel, V. R. Shaginyan, and M. V. Zverev, JETP Lett. **65**, 253 (1997).
[11] G. E. Volovik, JETP Lett. **63**, 763 (1996).
[12] M. Levy and J. P. Perdew, Phys. Rev. **48**, 11638 (1993).
[13] L. Świerkowski, D. Neilson, and J. Szymański, Phys. Rev. Lett. **67**, 240 (1991).
[14] V. A. Khodel, J. W. Clark, and V. R. Shaginyan, Solid State Commun. **96**, 353 (1995).
[15] J. Dukelsky, V. A. Khodel, P. Schuck, and V. R. Shaginyan, Z. Phys. **102**, 245 (1997).
[16] L. D. Landau, Zh. Éksp. Teor. **30**, 1058 (1956) [Sov. Phys. JETP **3**, 920 (1956)].
[17] L. N. Oliveira, E. K. U. Gross, and W. Kohn, Phys. Rev. Lett. **60**, 2430 (1988).
[18] J. Bardeen, L. N. Cooper, and J. R. Schrieffer, Phys. Rev. **108**, 1175 (1957).
[19] V. R. Shaginyan, Proceedings of CMT22, in press (1997).
[20] D. J. Scalapino *et al.*, Phys. Rev. B **34**, 8190 (1986); D. J. Scalapino, Phys. Rep. **250**, 329 (1995).
[21] A. A. Abrikosov, Physica C **222**, 191 (1994).
[22] J. Schmalian, D. Pines, and B. Stojkovic, Phys. Rev. Lett. **80**, 3839 (1998).
[23] I. A. Privorotsky, Zh. Eksp. Teor. Fiz. **43**, 2255 (1962) [Sov. Phys. JETP **16**, 1593 (1963).
[24] A. A. Abrikosov, Phys. Rev. B **57**, 8656 (1998).

Published in English in the original Russian journal. Edited by Steve Torstveit.

Logarithmic temperature dependence of the conductivity of the two-dimensional metal

V. M. Pudalov
Institute for High Pressure Physics, 142092 Troitsk, Moscow Region, Russia; Lebedev Research Center in Physics, 117924 Moscow, Russia

G. Brunthaler, A. Prinz, and G. Bauer
Institut für Halbleiterphysik, Johannes Kepler Universität, Linz, A-4040, Austria

(Submitted 17 August 1998)
Pis'ma Zh. Éksp. Teor. Fiz. **68**, No. 6, 497–501 (25 September 1998)

We report on the first observation and studies of a weak delocalizing logarithmic temperature dependence of the conductivity, which causes the conductivity of the 2D metal to increase as T decreases down to 16 mK. The prefactor of the logarithmic dependence is found to decrease gradually with density, to vanish at a critical density $n_{c,2}\sim 2\times 10^{12}$ cm^{-2}, and then to have the opposite sign at $n>n_{c,2}$. The second critical density sets the upper limit on the existence region of the 2D metal, whereas the conductivity at the critical point, $G_{c,2}\sim 120\,e^2/h$, sets an upper (low-temperature) limit on its conductivity.
 [S0021-3640(98)01218-3]

PACS numbers: 73.61.At, 73.40.Qv, 73.50.Dn

Recently, a metal–insulator transition and a metallic state have been observed in the strongly interacting two-dimensional (2D) carrier systems in Si-MOS structures[1] and later confirmed on *n*-Si-MOS (Refs. 2), *n*- and *p*-Si/SiGe (Refs. 3,4), and *p*-GaAs/AlGaAs structures.[5,6] This finding is in apparent contradiction to the commonly accepted one-parameter scaling theory (OPST)[7] for noninteracting particles and has initiated a debate over the nature of the 2D metal.[8–14]

Among the properties of the 2D metallic state, a striking exponential dependence of the resistance was found to exist over the whole range of metallic densities, $n>n_{c,1}\sim 10^{11}$ cm^{-2}, at temperatures $T\ll E_F$ (Refs. 12,15):

$$\rho=\rho_0+\rho_1\,\exp(-(T_0/T)^p), \tag{1}$$

where $p\approx 1$, and T_0 is sample- and density-dependent. The above empirical law has recently been given a theoretical interpretation.[10,16]

Since the above temperature dependence is reminiscent of the quasi-classical contribution of two scattering processes, there was not much evidence for a quantum origin of the phenomena in total. Moreover, it was earlier discussed[17] that the resistivity of the 2D gas may decrease $\propto(T/E_F)$ as T decreases, due to the temperature dependence of the screening length and, hence, of the random potential. Another classical argument invoked earlier[18] is related to valley multiplicity, which may result in additional intervalley scat-

tering of the electrons. The present studies were performed in order to verify whether or not the 2D metal has something in common with a quantum theoretical picture that is currently being intensively studied.

We have made ac measurements of the conductivity on two different, high-mobility *n*-Si-MOS structures at low dissipated power, with high precision, and at low temperatures $T \ll E_F$. In this paper we present experimental data which reveal, for the first time, a weak logarithmic temperature dependence of the conductivity, which persists down to 16 mK and gives a positive contribution to the conductivity in the range from $G \approx 10$ up to $G = 120$ (throughout the paper conductivity is given in units of e^2/h, and the resistivity $\rho = 1/G$). Our data confirm that the 2D metallic state, once it is formed by increasing the carrier density n above $n_{c,1}$, remains stable as $T \to 0$. We have found the upper critical density $n_{c,2}$ at which the delocalizing logarithmic temperature dependence vanishes and gives way to the localizing one. It is not clear so far whether this point is an attractive focus or a critical point, but in any case it provides a finite conductivity value as the temperature decreases or the density increases.

We studied the resistivity of two Si-MOS samples, with peak mobilities, $\mu = 41{,}000$ cm^2/V·s (Si-15a) at $T = 0.3$ K and $\mu = 19{,}600$ (Si-43). Measurements were taken by a 4-terminal ac technique in the temperature range from 0.28 K to 15 K, by precise sweeping of the temperature over about 5 h, and from 0.016 K to 3 K (for a few temperature points).

As described by Eq. (1), the exponential drop saturates at low temperatures. In order to reveal a weak quantum correction to the conductivity and to separate it from the strong exponential dependence (1), measurements have to be performed at $T \ll T_0$, in the range of the apparent saturation of the exponential temperature dependence, Eq. (1). This can be achieved most effectively in the limit of high carrier density (high T_0 and high G) and low temperatures. The typical results measured in this extreme regime are represented in Fig. 1 for a few carrier densities.

The solid curves in Fig. 1 represent the empirical exponential function, $G \sim [\rho_0 + \rho_1 \exp(-T_0/T)]^{-1}$, where the data were fitted with three parameters, ρ_1, ρ_2, and T_0 (Refs. 12,15). This function saturates below a certain temperature, T^*, whereas the measured temperature dependence of G crosses over to a weak dependence, which is linear on a $\ln T$ scale, $\delta G = C_T \ln(T/T^*)$.

For both samples, over a wide range of density, $\sim 1 \times 10^{11}$ to $\sim 20 \times 10^{11}$, this logarithmic dependence has a negative prefactor, i.e. it is delocalizing, thus driving the system to higher conductivity as temperature decreases. At relatively low G and low n (as shown in Fig. 1a), the prefactor, $C_T = -0.4 \pm 0.1$, is of the order of the typical value u_v/π (Ref. 19), where $u_v \sim (2-1)$ is due to the contribution of two valleys in (100) Si-MOS structures. At even lower density, close to $n_{c,1}$, the derivative $d\rho/dT$ remains positive down to 16 mK, however, the strong exponential dependence in Eq. (1) does not permit the revelation of a weak logarithmic dependence in the limited temperature range.

As the density increases, the prefactor C_T gradually decreases and nearly vanishes at $n = 23.7 \times 10^{11}$ cm^{-2}, which corresponds to $G_{c,2} = 120.5$. Figure 2 shows a typical density dependence of C_T for the sample Si-43. At $n = n_{c,2} \approx 25 \times 10^{11}$ cm^{-2} the prefactor crosses the abscissa and further, at $n > n_{c,2}$, has opposite sign. The positive logarithmic prefactor indicates a weakly localized state in the limit of low temperatures, whereas at

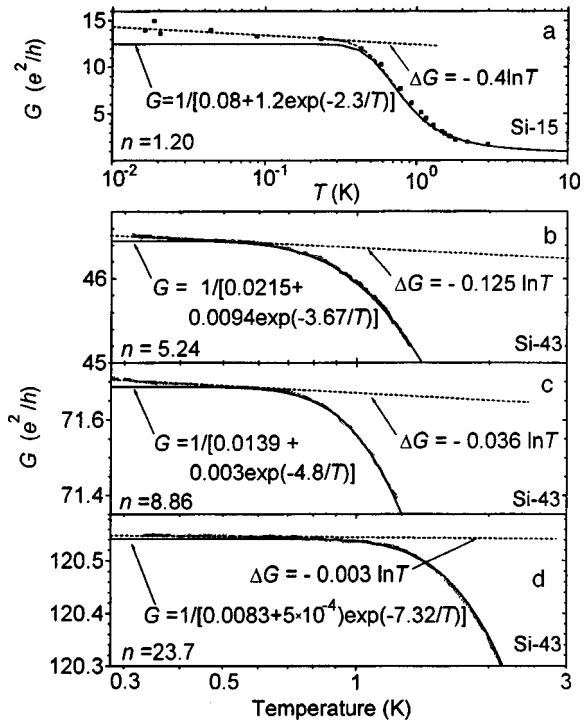

FIG. 1. Temperature dependence of the conductivity in the low temperature limit: a — for Si-15a at low electron density, and b, c, d — for Si-43 in a wide range of electron densities (indicated in units of 10^{11} cm^{-2}). To provide the required signal/noise ratio, every data point was averaged over 0.5 to 2 minutes. The solid curves show the best fits by the exponential dependence of Eq. (1), and the dashed curves show the logarithmic temperature dependence.

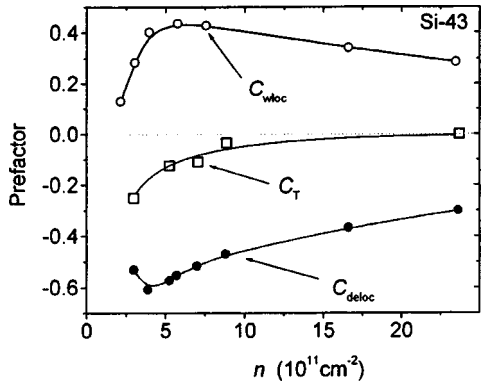

FIG. 2. Density dependence of the logarithmic temperature prefactors: (i) the total prefactor of the zero-field temperature dependence $C_T(n)$ (square symbols), (ii) the prefactor for the localizing term $C_{\mathrm{wloc}}(n)$ (open circles), and (iii) the purely delocalizing term, $C_{\mathrm{deloc}}(n)$ (full circles).

$T>T^*$ the derivative $d\rho/dT$ remains positive. A similar dependence of C_T was found for the sample Si-15, with $G_{c,2}\approx 122$.

At first sight, the positive sign of C_T is consistent with the recent calculations of the quantum corrections for a 2D noninteracting chiral system[13,14] as well as consistent with the spin–orbit scattering model.[19] However, the strong reduction of the prefactor C_T with density has no correlation with the relevant spin–orbit and disorder parameters[13] $\Delta\tau$ and $k_F l$: both of them remain much greater than 1 up to the density $n_{c,2}$ at which C_T vanishes. We therefore presume that the observed weak delocalization is related to electron–electron interaction.[20] The existence of the 2D metallic state in the limited range of densities from $n_{c,1}=0.8$ to $n_{c,2}=25\times 10^{11}$ cm^{-2}, or correspondingly, from $r_s=10$ to 1.8, is, evidently, in agreement with a consideration based on the Coulomb interaction.[20,11]

The measurements performed on both samples have revealed qualitatively similar temperature and density dependence of the conductivity, shown in Figs. 1 and 2. However, the magnitude of the prefactor C_T was different, with the difference increasing from $\sim 10\%$ at high density to a factor of 1.5 at low density, which is beyond the error limit. The prefactor C_T may roughly be represented by a sum of two large prefactors having opposite signs (see e.g., Eq. (2.104) in Ref. 20), both of which are disorder-dependent:

$$C_T = C_{\rm deloc} + C_{\rm wloc}. \tag{2}$$

Here the positive $C_{\rm wloc}$ is due to the single-particle quantum interference (''backscattering''), and the negative $C_{\rm deloc}$ is an interaction contribution.

Motivated by this interpretation, we have also measured the negative magnetoresistance in the perpendicular magnetic field.[21] This effect is known to be due to suppression of the single-electron quantum interference by the magnetic field. Analysis of the $R(H)$ data thus yields the ''localizing'' term in the logarithmic temperature dependence,[22] $C_{\rm wloc}\ln T$ (where $C_{\rm wloc}>0$). The localizing prefactor shown in Fig. 2 has a peak value $C_{\rm wloc}\approx 0.4$ at a density $n=5\times 10^{11}$ cm^{-2}; it decays sharply (by 2 times) as the density decreases to $n_{c,1}$, and it decreases gradually with increasing density. The difference of the total and localizing corrections, $C_{\rm deloc}=C_T-C_{\rm wloc}$, shown in Fig. 2, represents thus an estimate for the purely delocalizing quantum correction;[20] it decays with density $\propto n^{-0.48}$ at $n>3\times 10^{11}$ cm^{-2}.

With these results, the overall temperature dependence of the resistivity given by Eq. (1) should be generalized as follows:

$$\rho=\begin{cases}\rho_0+\rho_1\,\exp(-(T_0/T)^p) & \text{at } T>T^*,\\ \rho_0-\rho_0^2 C_T\,\ln(T/T^*) & \text{at } T<T^*,\end{cases} \tag{3}$$

where T^* is the sample and density-dependent crossover temperature, varying from $T^*=0$ at $n=n_{c,1}\approx 0.8\times 10^{11}$ cm^{-2} to $T^*\approx 1$ K at $n=10\times 10^{11}$ cm^{-2}.

Equation (3) corresponds to a non-universal, density-dependent scaling function $\beta=d\ln G/d\ln L$ (Ref. 16), rising with G in proportion to $\ln(G/G_{c,1})$ at $T>T^*$ and at $G>G_{c,1}\sim 1$, and gradually falling with G roughly $\propto(C_T/G)$ at $T<T^*$ and at $G_{c,2}>G\gg 1$. Here the parameters $G_{c,1}$, $G_{c,2}$, T^*, and C_T are all density-dependent,[15] and β equals zero at two points, $n=n_{c,1}$ and $n_{c,2}$.

In summary, we have observed the persistence of the metallic state in the conductivity range up to $G=120$ and at temperatures down to 16 mK. Experimentally, a weak

logarithmic temperature dependence of the conductivity was found, which increases the conductivity of the 2D metal as T decreases. The pronounced logarithmic temperature dependence provides strong evidence for the quantum origin of the 2D metallic state that emerges as temperature decreases. We have found the second critical density $n_{c,2}$ at which the delocalizing logarithmic correction vanishes and hence the conductivity stops growing, $d \ln G/d \ln L=0$. The interpretation of this point either as an attractive stable focus or as a second critical point requires additional studies. In any case, the existence of this point provides a nonzero value of the conductivity as T decreases to zero or as the density grows.

V. P. acknowledges discussions with M. Baranov, V. Kravtsov, A. Mirlin, and I. Suslov. This work was supported by RFBR (97-02-17378), by the programs on ''Physics of Solid-State Nanostructures'' and ''Statistical Physics,'' by INTAS, by NWO, and by FWF Vienna, ÖNB and GME Austria.

[1] S. V. Kravchenko, G. V. Kravchenko, and J. E. Furneaux *et al.*, Phys. Rev. B **50**, 8039 (1994); S. V. Kravchenko, W. E. Mason, G. E. Bowker *et al.*, Phys. Rev. B **51**, 7038 (1995).
[2] D. Popović, A. B. Fowler, and S. Washburn, Phys. Rev. Lett. **79**, 1543 (1997); K. P. Li, D. Popović, S. Washburn, in *Proceedings EP2DS-12*, Tokyo (1997).
[3] P. T. Coleridge, R. L. Williams, Y. Feng, and P. Zawadzki, Phys. Rev. B **56**, R12764 (1997); M. D'Iorio, D. Brown, and H. Lafontain, http://xxx.lanl.gov/abs/cond-mat/9708201.
[4] K. Ismail, J. O. Chu, D. Popović *et al.*, http://xxx.lanl.gov/abs/cond-mat/9707061.
[5] Y. Hanein, U. Meirav, D. Shahar *et al.*, Phys. Rev. Lett. **80**, 1288 (1998).
[6] M. Y. Simmons, A. R. Hamilton, M. Pepper *et al.*, Phys. Rev. Lett. **80**, 1292 (1998).
[7] E. Abrahams, P. W. Anderson, D. C. Licciardello, and T. V. Ramakrishnan, Phys. Rev. Lett. **42**, 673 (1979).
[8] P. Phillips and Y. Wan, http://xxx.lanl.gov/abs/cond-mat/9704200; P. Phillips, Y. Wan, I. Martin *et al.*, http://xxx.lanl.gov/abs/cond-mat/9709168; D. Belitz and T. R. Kirkpatrick, http://xxx.lanl.gov/abs/cond-mat/9705023; S. Chakravarty, L. Yin, and E. Abrahams, Phys. Rev. B **58**, R559 (1998); C. Castellani, C. diCastro, and P. A. Lee, Phys. Rev. B **57**, R9381 (1998).
[9] V. Dobrosavljević, E. Abrahams, E. Miranda, and S. Chakravarty, Phys. Rev. Lett. **79**, 455 (1997).
[10] Song He and X. C. Xie, Phys. Rev. Lett. **80**, 3324 (1998).
[11] S. Ckhakravarty, S. Kivelson, C. Nayak, and K. Völker, http://xxx.lanl.gov/abs/cond-mat/9805383.
[12] V. M. Pudalov, http://xxx.lanl.gov/abs/cond-mat/9707076v2; JETP Lett. **66**, 170 (1997).
[13] M. A. Skvortsov, http://xxx.lanl.gov/abs/cond-mat/9712135; JETP Lett. **66**, 133 (1998).
[14] Y. Lyanda-Geller, Phys. Rev. Lett. **80**, 4273 (1998).
[15] V. M. Pudalov, G. Brunthaler, A. Prinz, and G. Bauer, JETP Lett. **68**, 415 (1998).
[16] V. M. Pudalov, G. Brunthaler, A. Prinz, and G. Bauer, in *Proceedings of the 10th Winter School ''Frontiers in Condensed Matter Physics,''* Mauterndorf, 1998; Physica E 2 Oct. (1998), in press.
[17] F. Stern, Phys. Rev. Lett. **44**, 1469 (1980); A. Gold and V. T. Dolgopolov, Phys. Rev. B **33**, 1076 (1986).
[18] S. S. Murzin, S. I. Dorozhkin, G. Landwehr, and A. C. Gossard, in *Proceedings ICPS-23* (Berlin), 1996, p. 2187.
[19] S. Hikami, A. I. Larkin, and Y. Nagaoka, Prog. Theor. Phys. **63**, 707 (1980).
[20] A. M. Finkel'stein, Z. Phys. B **56**, 189 (1984); Sov. Sci. Rev., Sect. A – Physics Reviews, edited by I. M. Khalatnikov, **14**, 3 (1990).
[21] V. M. Pudalov, G. Brunthaler, A. Prinz, and G. Bauer, JETP Lett. **65**, 932 (1997).
[22] H. Fukuyama, in *Electron-Electron Interactions in Disordered Systems*, edited by A. L. Efros and M. Pollak, North-Holland, 1985.

Published in English in the original Russian journal. Edited by Steve Torstveit.

Properties of activated states of oxygen and carbon atoms during diffusion in α-Ti

V. B. Vykhodets[a)]
Institute of Metal Physics, Urals Branch of the Russian Academy of Sciences, 620219 Ekaterinburg, Russia

A. Ya. Fishman
Institute of Metallurgy, Urals Branch of the Russian Academy of Sciences, 620066 Ekaterinburg, Russia

(Submitted 18 August 1998)
Pis'ma Zh. Éksp. Teor. Fiz. **68**, No. 6, 502–506 (25 September 1998)

Activated energy states of interstitial atoms in α-Ti crystals are investigated. Previous precision experiments on the anisotropy of the diffusion coefficients D_{zz}/D_{xx} in this system revealed that $d(D_{zz}/D_{xx})/dT$ has different signs for oxygen and carbon. It is shown that the anomalous positive sign of the effect for carbon atoms is due to the presence of a double-well potential for a diffusing atom at the saddle points. © *1998 American Institute of Physics.* [S0021-3640(98)01318-8]

PACS numbers: 66.30.Jt

1. The highest accuracy achieved to date in measuring diffusion coefficients and other diffusion parameters for the atoms of light elements in solids has been achieved in investigations of the anisotropy of the diffusion coefficients D_{zz}/D_{xx} of tagged ^{18}O oxygen atoms[1] and ^{14}C carbon atoms[2] in the hcp titanium lattice. The most important result of these experiments is the observation that the sign of $d(D_{zz}/D_{xx})/dT$ is different for oxygen and carbon (Fig. 1). The temperature dependence of the diffusion anisotropy D_{zz}/D_{xx} in the systems studied arises only in the presence of a deviation of the hcp lattice from the ideal lattice (for which $c/a=\sqrt{8/3}$), in which case two kinds of saddle points for the migration of interstitial impurity atoms appear in the crystal.[3] The fact that the oxygen and carbon atoms respond differently to these small deviations ($|c/a-\sqrt{8/3}|\ll 1$) shows that the character of their activated states is different. Thus the characteristic structural features of a nonideal hcp crystal provide a unique opportunity for studying these diffusion states.

The main problem of the present work is to explain the anomalous positive sign of the quantity $d(D_{zz}/D_{xx})/dT$ for carbon. It will be shown that the effect is due to the degeneracy of the energy levels of the impurity atoms in the activated state. In the past, such detailed information about the energy states of atoms at the saddle points could not be obtained by means of diffusion measurements.

2. To solve the problem posed, we identified the hopping mechanism, i.e., we determined the coordinates of the equilibrium and saddle points during the migration of carbon atoms. For this purpose we examined the various expressions for D_{zz}/D_{xx} ob-

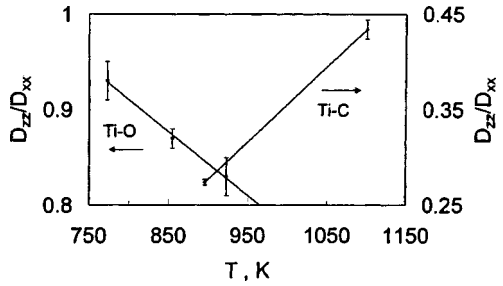

FIG. 1. Temperature dependence of the anisotropy D_{zz}/D_{xx} of the diffusion coefficients for oxygen and carbon in α-Ti.

tained in the random walk theory for all the possible mechanisms of atomic hops between nearest equilibrium positions of the interstitial atoms. The choice of the hopping mechanism that is realized was determined by the value of the ratio $\Gamma^0_{ik}/\Gamma^0_{ij}$ of the preexponential factors in the hopping frequencies Γ_{ik} between different equilibrium positions of interstitial atoms. According to existing diffusion theories, these ratios cannot differ much from 1.

It turned out that there is only one mechanism of atomic hopping that satisfies the indicated criterion. For this mechanism, both the octahedral and tetrahedral interstitial sites are equilibrium positions of carbon atoms in the α-Ti lattice. The ratio of preexponential factors of the hopping frequencies for the other mechanisms considered differed severalfold from 1, so that the results for them are not presented.

The anisotropy of the diffusion coefficients for the established hopping mechanism is described by the expression[4]

$$D_{zz}/D_{xx}=(1/4)(c/a)^2\{\Gamma_{OO}/\Gamma_{OT}+[2/3+\Gamma_{TO}/\Gamma_{TT}]^{-1}\}, \tag{1}$$

where c and a are the parameters of the hcp lattice and the indices O and T denote the octahedral and tetrahedral interstitial sites. The following temperature dependence was assumed for the hopping frequencies:

$$\Gamma_{ik}=\Gamma^0_{ik}\exp\{-\Delta E_{ik}/(k_BT\}, \tag{2}$$

where ΔE_{ik} is the energy parameter of the potential barrier, k_B is Boltzmann's constant, and T is the absolute temperature.

For the atomic hopping mechanism realized in a nonideal hcp lattice, the potential energy profile for an interstitial atom is as shown in Fig. 2. The saddle points S_1 and S_2 are located at the centers of the faces of the octahedra and tetrahedra forming the interstitial sites.[3] One can see that atomic hops between interstitial sites of the same kind occur with the participation of the saddle points S_2, while atomic hops between interstitial sites of different kinds occur through S_1. For the indicated form of the profile, the hopping frequencies in expression (1) are related as

$$\Gamma_{TO}/\Gamma_{TT}=\Gamma_{OT}/\Gamma_{OO}. \tag{3}$$

In the case $c/a=(8/3)^{1/2}$ the potential energies $E(S_1)$ and $E(S_2)$ are the same, and the anisotropy of the diffusion coefficients is temperature-independent.

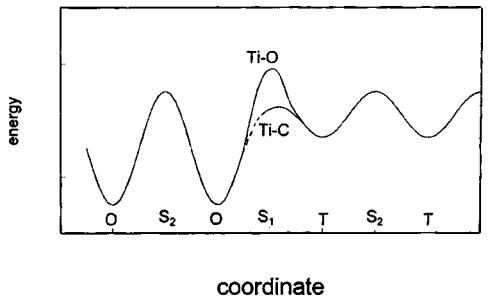

FIG. 2. Potential energy profile for interstitial atoms in a nonideal hcp crystal.

The results of an analysis of the experimental data on the anisotropy of the diffusion coefficients of carbon in α-Ti are presented in Table I.

We note that Zener's theory[5] has proven to be the most successful of the existing theories of the pre-exponential factors of diffusion coefficients. In our case it gives for $\Gamma^0_{OT}/\Gamma^0_{OO}$ values ranging from 1.0 to 1.6. The ratio $\Gamma^0_{OT}/\Gamma^0_{OO}$ presented in the table lies in this range.

The hopping mechanism for oxygen atoms in α-Ti was identified in Ref. 6. The mechanism is similar to that established here for carbon atoms from the standpoint of the types of saddle points through which interstitial atoms migrate. Localization of oxygen atoms in tetrahedral interstitial sites was not observed.

3. The foregoing analysis of the anisotropy of the diffusion coefficients made it possible to express the variations of D_{zz}/D_{xx} with temperature in terms of the difference $E(S_1)-E(S_2)$ of the potential energies of the diffusing atoms at different types of saddle points. The values obtained for $E(S_1)-E(S_2)$ were 0.057 eV for oxygen atoms and -0.208 eV for carbon atoms. This difference is depicted schematically in Fig. 2.

The packing of the Ti atoms at the saddle points S_1 is closer than the packing at S_2. This makes it possible to anticipate which impurity, carbon or oxygen, will have a positive sign of the parameter $E(S_1)-E(S_2)$. This result follows from the standard elastic model of diffusion potential barriers. The difference $E(S_1)-E(S_2)$ should be greatest for carbon atoms, since carbon atoms stretch the α-Ti lattice more strongly on dissolution than do oxygen atoms.[7] Similar results can be obtained by using different models of the pair interactions Ti–Ti, Ti–C, and Ti–O, if it is assumed that repulsive

TABLE I. Experimental[2] and computational data used to identify the hopping mechanism for carbon in α-Ti.

T, K	D_{zz}/D_{xx}	Γ_{OT}/Γ_{OO} or Γ_{TO}/Γ_{TT}	$E(S_1)-E(S_2)$, eV	$\Gamma^0_{OT}/\Gamma^0_{OO}$ or $\Gamma^0_{TO}/\Gamma^0_{TT}$
856	0.274 ± 0.003	0.1386		
1100	0.434 ± 0.009	0.2144	-0.208	1.45 ± 0.15

forces dominate at distances corresponding to the position of an interstitial atom at a saddle point.

On this basis, the fact that the signs of the quantities $d(D_{zz}/D_{xx})/dT$ and $E(S_1)-E(S_2)$ are different for carbon and oxygen atoms is an unexpected result.[b)] It requires a revision of the viewpoints concerning the nature of the activated state during diffusion of interstitial atoms, at least for carbon atoms.

Let us consider this question in greater detail. In an elastic model of the potential barrier for the diffusion of interstitial atoms it is ordinarily assumed that the energy of an impurity in the lattice is proportional to the squared difference $D-d$ of the diameter D of the interstitial atom and the diameter d of the corresponding cavity (or passage in the case of a saddle point) (see, for example, Refs. 3 and 8). As a result, a decrease in the size of the passage increases the elastic energy of the impurity. If it is assumed that the change in the parameter d is due to the deviation of the packing of α-Ti from the ideal packing, then the difference of the energies $E(S_1)$ and $E(S_2)$ of the activated states is

$$E(S_1)-E(S_2)\cong -2E(S_1)\Delta d/(D-d)=-2\epsilon E(S_1)d/(D-d)>0, \tag{4}$$

where Δd is the change in the passage diameter d, while the corresponding deformation ϵ is proportional to $\{c/a-(8/3)^{1/2}\}$ and is negative.

When the energy state of an interstitial impurity in the position S_1 is nondegenerate, such an effect, which is linear in $\{c/a-(8/3)^{1/2}\}$, can be due only to the fully symmetric (A_1) deformation $\epsilon\equiv\epsilon(A_1)$. In Eq. (4) the quantity $-2E(S_1)d/(D-d)$, where $E(S_1)\cong 2$ eV,[2] plays the role of the interaction parameter $V(A_1)$ $(V(A_1)<0)$ of the impurity with the indicated deformation in the excited state.[2] The effect of changes in the shape of the cavity (and not its size) on the energy $E(S_1)$ is of second-order and can be neglected.

A completely different situation obtains in the case of energy degeneracy of activated states of diffusing atoms. An additional linear interaction of the degenerate term with incompletely symmetric deformations appears. This results in splitting of the impurity level and decreases the energy of the impurity. If the hcp lattice deviates from an ideal lattice, such deformations arise as a result of a change induced in the symmetry of the environment of the saddle point by the titanium atoms. This effect occurs at the saddle point S_1, where the three matrix atoms closest to this position form an isosceles triangle. The nearest-neighbor environment of the saddle point S_2 is represented by an equilateral triangle.

Since only twofold degeneracy (E term) is possible in positions with trigonal symmetry, the corresponding decrease of the energy can be described by the expression

$$\Delta E(S_1)=-(k_BT)\ln\{2\ \cosh[V(E)\epsilon_1/k_BT]\}\cong -|V(E)\epsilon_1|,\quad |V(E)\epsilon_1|>k_BT, \tag{5}$$

where $V(E)$ is an interaction constant describing the interaction of the degenerate term with the incompletely symmetric deformation ϵ_1.

As a result, the total effect for $E(S_1)-E(S_2)$, which is proportional to $\{c/a-(8/3)^{1/2}\}$, can be negative:

$$E(S_1)-E(S_2)\cong V(A_1)\epsilon-|V(E)\epsilon_1|. \tag{6}$$

We note that for the particular symmetry of the environment of the saddle point S_1 considered here, the deformations ϵ_1 and ϵ are the same. For $|V(A_1)/V(E)|<1$ the difference $E(S_1)-E(S_2)$ is negative and, correspondingly, $d(D_{zz}/D_{xx})/dT$ is positive. This condition is not exotic for Jahn–Teller states.

In summary, the assumption that energy degeneracy is possible in an activated state can eliminate the previously noted disagreement between the experimental data and theory.

We shall now briefly discuss the possible reasons why structural differences could arise between the activated states of carbon and oxygen atoms. It is simplest to examine excited localized states of impurities in a crystal field. The impurity $2p$ levels in a trigonal crystal field split into a doublet and singlet. For the lowest singlet state the energy of the p^2(C) configuration is twofold degenerate, while the energy of the configuration p^4(O) is nondegenerate. In contrast, for the lowest doublet the configuration p^4(O) is degenerate and the configuration p^2(C) is nondegenerate. In consequence, if the interaction of the degenerate term with deformations is strong, the sign of the quantities $d(D_{zz}/D_{xx})/dT$ for carbon and oxygen should be different irrespective of the character of the splitting of the p levels by a trigonal field. A positive sign of $d(D_{zz}/D_{xx})/dT$ for carbon atoms requires a lower energy in the singlet p state.

4. This investigation has established that there is a substantial difference between the activated energy states of carbon and oxygen in α-Ti. It was shown that the decrease of the potential energy observed for carbon atoms at saddle points with the closest packing of the environment is most likely due to the Jahn–Teller effect. It was found that the results of diffusion measurements ordinarily make it possible to determine only the values of the energy difference of the diffusing atom in the saddle and equilibrium positions.

This work was supported by the Russian Fund for Fundamental Research under Grant 96-03-32106.

[a)]e-mail: vykhod@imp.uran.ru

[b)]The difficulties that arise formally can be overcome by assuming that the volume of the system decreases when a carbon atom hops from an equilibrium position to a saddle point. For all its artificiality, this hypothesis in principle can be checked by means of experiments studying the influence of hydrostatic pressure on the diffusion coefficients of interstitial atoms.

[1] V. V. Vykhodets, S. M. Klotsman, and T. E. Kurennykh, Dokl. Akad. Nauk SSSR **302,** 1357 (1988) [Sov. Phys. Dokl. **33**, 748 (1988)].
[2] Chr. Minkwitz and Chr. Herzig, Defect Diffus. Forum **143–147**, 61 (1997).
[3] Y. A. Bertin, J. Parisot, and J. L. Gacougnolle, J. Less-Common Met. **69**, 121 (1980).
[4] S. Ishioka and M. Koiwa, Philos. Mag. A **52**, 267 (1985).
[5] P. Shewmon, *Diffusion in Solids*, Ohio State University, 1989.
[6] V. B. Vykhodets and T. E. Kurennykh, Fiz. Met. Metalloved. **78**, 116 (1994).
[7] E. Fromm and E. Gerbracholt, *Gase und Kohlenstoff in Metallen*, Springer-Verlag, Berlin, 1976.
[8] J. D. Eshelby, Solid State Phys. **3**, 79 (1956).

Translated by M. E. Alferieff

Vortex structure in the presence of tilted columnar defects

A. Buzdin

Université Bordeaux I, Centre de Physique Théorique et Modélisation, Rue du Solarium, 33174 Gradignan Cedex, France

(Submitted 19 August 1998)
Pis'ma Zh. Éksp. Teor. Fiz. **68**, No. 6, 507–511 (25 September 1998)

It is argued that vortices in layered superconductors will be trapped by tilted columnar defects even when the external magnetic field is oriented along the **c** axis. For such tilted, trapped vortices the interaction at long distances becomes attractive in some directions. This must result in the formation of vortex chains with an intervortex distance of the order of the London penetration depth. © *1998 American Institute of Physics.* [S0021-3640(98)01418-2]

PACS numbers: 61.80.Jh, 74.76.Bz, 74.62.Dh, 74.80.Dm

The defects produced by ion irradiation are columnar damage tracks with thickness of the order of $2R \sim 50-100$ Å. These columnar defects (CDs) have a dramatic effect on the vortex pinning and can increase the critical current many times over.[1,2] Investigation of the properties of superconductors with CDs has attracted much attention recently. In high-T_c superconducting oxides it is possible to introduce the tilted columnar defects by controlling the orientation of a heavy ion beam (see, e.g., Ref. 3 and references cited therein).

In the present paper, we consider theoretically the behavior of vortices in layered superconductors with parallel CDs which are tilted slightly with respect to the **c** axis in an external field directed parallel to the **c** axis. In view of the very high degree of anisotropy of high-T_c superconductors (like Bi-2212 or Tl-2201 for example) we may neglect the Josephson interaction between layers and consider only the electromagnetic one. A vortex line in a highly anisotropic quasi-2D superconductor is in fact a chain of pancake vortices.[4,5] For a vortex line parallel to the **c** axis the situation is the same as in the standard case, and the vortex energy per unit length is given by the classic formula $E_v=(\phi_0/4\pi\lambda)^2(\ln(\lambda/\xi)+0.12)$,[6] where for a layered superconductor $\lambda^{-2}=d_0/\lambda_\parallel^2 d$, with d_0 its thickness, d the distance between superconducting layers, and $\lambda_\parallel$ the in-plane London penetration depth of a single layer. When a vortex is on a CD (the direction of which coincides with the **c** axis) the only difference in the vortex energy calculation is that the cutoff is at the CD radius R rather than at ξ (see, e.g., Refs. 7,8), i.e., the vortex energy is $E_v^{\mathrm{CD}}=(\phi_0/4\pi\lambda)^2\ln(\lambda/R)$ and the pinning energy (per unit length) may be estimated as $E_{\mathrm{pin}}=(\phi_0/4\pi\lambda)^2\ln(\lambda/\xi)$.

This large pinning energy (comparable with the vortex energy itself) may stabilize the orientation of the vortex along the tilted CDs and not along the vertical magnetic

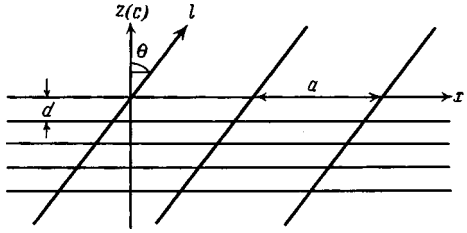

FIG. 1.

field. To find out for what angles θ between the CD axis **l** and the **c** axis a vortex prefers to be oriented along CD, we need to calculate the energy of a tilted vortex in the framework of an electromagnetic coupling model. The general expression for the energy of an arbitrary configuration of pancake vortices has been derived in Ref. 4:

$$E=\frac{1}{8\pi\lambda_{\rm eff}}\sum_n\int\frac{d^2\mathbf{k}}{(2\pi)^2}\Bigg\{|\mathbf{\Phi}_n(\mathbf{k})|^2-\mathbf{\Phi}_n(-\mathbf{k})\sum_m\mathbf{\Phi}_m(\mathbf{k})\times\frac{\sinh(kd)}{2\lambda_{\rm eff}k}\frac{(G_k-\sqrt{G_k^2-1})^{|n-m|}}{\sqrt{G_k^2-1}}\Bigg\},\tag{1}$$

where $\lambda_{\rm eff}=\lambda_\parallel^2/d_0$, $\mathbf{\Phi}_n(\mathbf{k})$ is the Fourier transform of the total London vector of the nth layer $\mathbf{\Phi}_n(\rho)=\Sigma_\alpha\mathbf{\Phi}_L(\rho-\mathbf{R}_{n,\alpha})$, the summation is performed over all pancakes α in the nth layer, $\mathbf{\Phi}_L(\mathbf{k})=i\phi_0(\mathbf{k}\times\mathbf{z})/k^2$, and the function $G_k=\cosh(kd)+\sinh(kd)/2\lambda_{\rm eff}k$.

Let us choose an **x** axis in the plane defined by the the **z(c)** axis and the CD axis **l** (see Fig. 1); then the vector $\mathbf{\Phi}_n(\mathbf{k})$ is given by $\mathbf{\Phi}_n(\mathbf{k})=\exp[-ind(\mathbf{k}\cdot\hat{\mathbf{x}})\tan\theta]\mathbf{\Phi}_L(\mathbf{k})$. Performing the summation over m in formula (1), we obtain the energy of the vortex segment between two adjacent layers:

$$E_s(\theta)=\frac{d}{8\pi\lambda^2}\int\frac{d^2\mathbf{k}}{(2\pi)^2}|\mathbf{\Phi}_L(\mathbf{k})|^2\left(1-\frac{\sinh(kd)}{2\lambda_{\rm eff}k}\frac{1}{G_k-\cos((\mathbf{k}\cdot\hat{\mathbf{x}})d\,\tan\,\theta)}\right).\tag{2}$$

As the main contribution to the integral (2) comes from the region of small wave vectors $k\ll d^{-1}$, we may use the expansion of G_k for small k and finally obtain a very convenient expression for the energy difference for tilted and perpendicular vortices:

$$E_s(\theta)-E_s(0)=\frac{d\phi_0^2}{8\pi\lambda^2}\int\frac{d^2\mathbf{k}}{(2\pi)^2}\left(\frac{1}{(1/\lambda^2)(k^2/(k^2+k_x^2\,\tan^2\theta))+k^2}-\frac{1}{1/\lambda^2+k^2}\right)$$
$$=d\left(\frac{\phi_0}{4\pi\lambda}\right)^2\ln\left(\frac{1+\cos\,\theta}{2\,\cos\,\theta}\right).\tag{3}$$

Naturally the energy of the tilted vortex is larger than the perpendicular one, and it is only the additional pinning energy (when the vortex axis coincides with the CD axis) which could stabilize it. For the tilted CD, superconductivity is destroyed in an elliptical region on the (**a**,**b**) plane with semiaxes R and $R/\cos\theta$, and, accordingly, the energy of a perpendicular vortex with such an elliptic core is $E_s^{\rm el}=d(\phi_0/4\pi\lambda)^2\ln(2\lambda\cos\theta/R($1

$+\cos\theta)$).[8] Taking this into account, we see that the decrease of the energy due to a larger core surface compensates its tilt-related increase, and finally the total energy of the vortex on the tilted columnar defect is

$$E_s^{\mathrm{CD}}(\theta)=d\left(\frac{\phi_0}{4\pi\lambda}\right)^2\ln\left(\frac{\lambda}{R}\right) \tag{4}$$

and does not depend on θ. Comparing this with the energy of a perpendicular vortex (which does not benefit from pinning along the whole length of a CD), we conclude that a vortex will prefer to be always oriented along a CD. In fact, for large values of θ the CD may not be elliptical in the (**a**,**b**) plane, and the above-mentioned compensation will disappear. In practice, however, for $\theta<60°$, the vortices would penetrate along a CD when the magnetic field is parallel to the **c** axis.

The condition for a single vortex to penetrate into a sample is $E_s^{\mathrm{CD}}-\phi_0 Hd/4\pi=0$; this gives us the first critical field

$$H_{c1}=\frac{\phi_0^2}{4\pi\lambda^2}\ln\left(\frac{\lambda}{R}\right), \tag{5}$$

which is smaller than the critical field for a vortex oriented along the **c** axis, $H_{c1}^0=(\phi_0^2/4\pi\lambda^2)\ln(\lambda/\xi)$.

The previous analysis is certainly applicable for well-separated vortices, when it is possible to neglect any intervortex interaction. This case corresponds to a field close to H_{c1} and a very low concentration of CDs. On the other hand, the situation when the interaction between tilted vortices comes into play is very special and may qualitatively change the process of vortex penetration. In fact, in the framework of an anisotropic London model, an attraction between the tilted vortices appears in the (**c**,**l**) plane.[9–11] Such attraction decreases exponentially at long distances and leads to the formation of vortex chains,[9] as has been observed subsequently in experiment (see, e.g., Ref. 12 and references cited therein). An anisotropic London model is not appropriate for extremely quasi-2D compounds like Bi-2212; then the question of the tilted vortex interaction must be treated in the framework of a quasi-2D model with an electromagnetic interaction.

With the help of the general expression (1) one may demonstrate that, as in the case of an anisotropic London model,[9] the attraction between two tilted vortices is maximal in the (**c**,**l**) plane, and at long distance the interaction energy varies as

$$E_{\mathrm{int}}\sim-\sin^2(\theta)/D^2,$$

where D is the distance between the vortex lines. Such a long-range attraction is quite different from the exponentially decreasing attraction in the London model.[9–11] If the sample contains many CDs available for vortex occupation, then vortices will occupy CDs forming a chain in the (**c**,**l**) plane. The first critical field will correspond to the appearance of the vortex chain, not a single vortex.

To calculate the characteristics of such a vortex chain we may write with the help of (1)–(3) the energy of vortex in chain as:

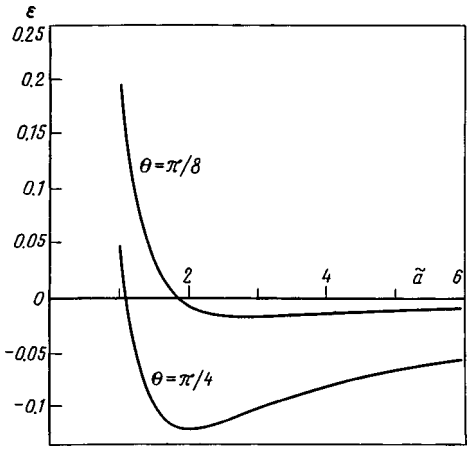

FIG. 2.

$$E_s^{\rm chain}(\theta)=\frac{d}{8\pi\lambda^2}\int\frac{dk_y}{(2\pi)}\frac{1}{a}\sum_{k_x=2\pi n/a}\left\{|\mathbf{\Phi}_L(\mathbf{k})|^2\left(1-\frac{1}{1+\lambda^2k^2+\lambda^2k_x^2\,\tan^2\theta}\right)\right\}, \tag{6}$$

where a is the distance between adjacent vortices in the $(\mathbf{x},\mathbf{y})$ plane (see Fig. 1).

To avoid all the cutoff-related complications, it is convenient to calculate the difference of the energy of the vortex in a chain and in a solitary state:

$$E_s^{\rm chain}(\theta)-E_s^{\rm CD}(\theta)=\frac{d\phi_0^2}{8\pi\lambda^2}\left\{\frac{1}{a}\sum_{k_x=2\pi n/a}\int\frac{dq}{(2\pi)}K(q,Q)-\int\frac{dqdQ}{(2\pi)^2}K(q,Q)\right\}, \tag{7}$$

where $Q=k_x$, $q=k_y$, and the function

$$K(q,Q)=\left(1-\frac{1}{1+\lambda^2(Q^2+q^2)+\lambda^2Q^2\,\tan^2\theta}\right)\frac{1}{(Q^2+q^2)}. \tag{8}$$

Performing summation and integration over Q in (7) we finally obtain

$$E_s^{\rm chain}(\theta)-E_s^{\rm CD}(\theta)=\frac{d\phi_0^2}{8\pi\lambda^2}\int_0^\infty\frac{du}{(2\pi)}\left\{\frac{1-\coth(u\tilde a)}{1-u^2\,\tan^2\theta}u\,\tan^2\theta\right.$$
$$\left.+\frac{1}{\cos\,\theta\sqrt{1+u^2}}\,\frac{\coth(\tilde a\,\cos\,\theta\sqrt{1+u^2})-1}{1-u^2\,\tan^2\theta}\right\}, \tag{9}$$

where $\tilde a=a/(2\lambda)$ and for $a\gg\lambda$

$$E_{\rm int}(\theta)=E_s^{\rm chain}(\theta)-E_s^{\rm CD}(\theta)=-\frac{d\phi_0^2}{4\pi^2a^2}\,\tan^2\theta\int_0^\infty[\coth(u)-1]u\,du, \tag{10}$$

i.e., at long distances there is always an attraction between the vortices located on the tilted CDs.

The interaction energy as a function of distance $\tilde a$ is presented in Fig. 2 for several

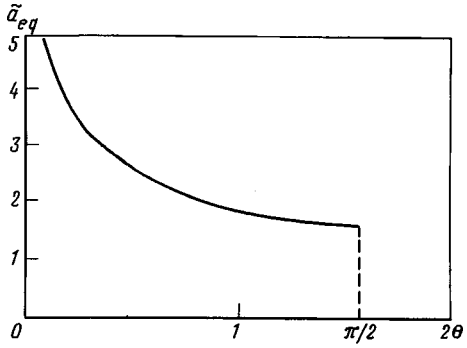

FIG. 3.

tilting angles θ: at short distances the vortices repel each other, while at long distances the interaction becomes attractive, and the minimum of $E_{\rm int}$ corresponds to the equilibrium distance between the vortices in a chain. This equilibrium distance $\tilde{a}_{\rm eq}$ as a function of angle θ is presented in Fig. 3, and we see that it is rather large, $a_{\rm eq}\sim(3-8)\lambda$ (note that at angles θ very close to $\pi/2$ even the weak Josephson interlayer interaction must be taken into account, and our model is no longer valid). For typical concentrations of CDs (fluence $B_\Phi\sim(1-3)$T), the mean distance between them is much smaller than $a_{\rm eq}$, and at low fields the vortices could freely choose the CD to be at, thus forming the vortex chains.

In conclusion we stress that in the presence of tilted CDs, in low magnetic fields oriented along the **c** axis, the vortices prefer to be trapped by CDs, thus giving rise to a magnetization perpendicular to the external field, i.e., a torque. The first critical field will correspond to the appearance of a vortex chain and not a single vortex. The vortex lattice at low field will correspond to well-separated vortex chains, and an increase of the field will cause a decrease of the distance between chains while leaving the intervortex distance within a chain basically the same and equal to $a_{\rm eq}$. It might be interesting to perform magnetization and/or torque measurements, as well as decoration experiments on samples of high-T_c superconductors with tilted columnar defects.

The help of T. Chameeva and C. Meyers in preparation of the manuscript is appreciated.

[1] W. Gerhauser, G. Ries, H. W. Neumüller *et al.*, Phys. Rev. Lett. **68**, 879 (1992).
[2] L. Civale, A. D. Marwick, T. K. Worthington *et al.*, Phys. Rev. Lett. **67**, 648 (1991).
[3] S. Hebert, V. Hardy, G. Villard *et al.*, Phys. Rev. B **57**, 649 (1998).
[4] A. Buzdin and D. Feinberg, J. Phys. (France) **51**, 1971 (1990).
[5] J. Clem, Phys. Rev. B **43**, 7837 (1991).
[6] A. A. Abrikosov, *Fundamentals of Theory of Metals*, North-Holland, Amsterdam, 1988.
[7] A. Buzdin, Phys. Rev. B **47**, 11416 (1996).
[8] A. I. Buzdin and M. Daumens, Physica C **294**, 257 (1998).
[9] A. I. Buzdin and A. Yu. Simonov, JETP Lett. **51**, 191 (1990).
[10] V. G. Kogan, N. Nahagawa, and S. L. Thiemann, Phys. Rev. B **42**, 2631 (1990).
[11] A. M. Grishin, A. Yu. Martynovich, and S. V. Yampol'skii, Zh. Éksp. Teor. Fiz. **97**, 1930 (1990) [Sov. Phys. JETP **70**, 1089 (1990)].
[12] I. V. Grigorieva, J. W. Steeds, G. Balakrishnan, and D. McPaul, Phys. Rev. B **51**, 3765 (1995).

Published in English in the original Russian journal. Edited by Steve Torstveit.